Separation of Touching Grain Kernels in an Image by Ellipse Fitting and Morphological Transform Algorithm

A Thesis
Submitted to the Faculty of Graduate Studies
The University of Manitoba
in partial fulfilment of the requirements for the degree of

Doctor of Philosophy

by

Gong Zhang

Department of Bisosytems Engineering
University of Manitoba
Winnipeg, Canada
R3T 5V6

THE UNIVERSITY OF MANITOBA

FACULTY OF GRADUATE STUDIES

*****

COPYRIGHT PERMISSION

Separation of Touching Grain Kernels in an Image by Ellipse Fitting and Morphological Transform Algorithm

BY

Gong Zhang

A Thesis/Practicum submitted to the Faculty of Graduate Studies of The University of Manitoba in partial fulfillment of the requirement of the degree

Of

DOCTOR OF PHILOSOPHY

ABSTRACT

An ellipse fitting algorithm was developed to separate touching grain kernels in images. The algorithm randomly tracks the edge of touching kernels to find the sample points for fitted ellipses. The fitted ellipses were generated by a direct least squares ellipse fitting method. Then, clustering was used to identify the best representative ellipse for each kernel of the touching instance. With representative ellipses, touching grain kernel images were separated by morphology transform.

Typical touching kernel patterns of four grain types namely barley, Canada Western Amber Durum (CWAD) wheat, Canada Western Red Spring (CWRS) wheat and oats, obtained from composite samples from several growing locations across the Western Canadian prairies, were used to test this algorithm. The accuracies of separation were: 92.4%(barley), 96.1%(CWAD), 94.8%(oats), and 97.3% (CWRS wheat).

The kernels used for the touching grains images were separated physically to create non-touching instances and another set of kernels images were acquired. Morphological features namely area, perimeter, maximum radius, minimum radius, mean radius, major axis, minor axis, shape moment, Fourier transform, major length, and minor length were extracted, from images of physically separated kernels and software separated kernels, to test the effectiveness of the ellipse fitting algorithm. To decide if the difference between two kinds of features was significant, the large sample Z test of hypotheses was employed. Except for Fourier descriptor 1 of barley and CWAD, software

separation did not change the values of morphological features within the tolerance limits of the measurement system.

To assess the classification capability after software separation, the morphological features extracted from physically separated kernels were used as training and basic testing data sets, and the features from software separated kernels were used as production testing data sets. A back-propagation neural network was employed for grain type classification with morphological features as inputs. Compared to 97.1% of correctly classifying rate about physically separated grain kernels, the mean classification accuracy for all the software separated grain types was 96.6%. The morphological features of software separated kernels were not distorted during software separation and can be successfully used in grain type classification.

ACKNOWLEDGEMENTS

With a deep sense of gratitude, I wish to express my sincere thanks to my supervisor, Dr. D.S. Jayas for his encouragement, support, understanding and providing critical comments whenever necessary throughout the course of this study. My appreciation also goes to Dr. N.D.G. White, Dr. S.J. Symons, and Dr. E. Shwedyk for their valuable suggestions and for serving on my advisory committee.

My sincere thanks are due to Dr. P.Shatadal and Dr. N.S. Shashidhar for their works to guide me into this topic. Special thanks are due to Messrs. Dale Bourns, Jerry Woods, Matt McDonald, and Jack Putnam for their technical assistance in setting up the imaging system. Special thanks are due to Dr. Maohua Wang and Dr. Qiang Zhang for their guidance to let me into this exciting research area of Biosystems Engineeing.

This project was funded by the Natural Sciences and Engineering Research Council of Canada (NSERC) and the Canada Research Chairs Program. Many thanks are due to both organizations for the financial support and the Industry Services Division of the Canadian Grain Commission for their assistance in sample acquisition.

I also thank Chitra Karunakaran, Jitendra Paliwal and other friends for all their help and cooperation.

I also want to thank my parents, who taught me the value of hard work by their own example. I would like to share this moment of happiness with them. They rendered me enormous support during the whole tenure of my research.

Finally. I wish to record my sincere appreciation and thanks to my wife, Yanqing Xiu, for her invaluable support, patience and encouragement throughout my study years. Without her support, I would never have completed my present work.

TABLE OF CONTENTS

LIST OF FIGURES

LIST OF TABLES

LISTS OF SYMBOLS

1. Sets.

A, x	Subsets of Z^2
A_x	The *translation* of a set A by a vector x
$\hat{A}$	The reflection of a set A
$A \oplus B$	Dilation of the object *A* by the structuring element *B*
$A \ominus B$	Erosion of the object A by a structuring element B
$A \circ B$	Opening of the object A by a structuring element B
$A \bullet B$	Closing of the object A by a structuring element B
$A \otimes B$	Hit-or-miss transform of a set *A* by *B*= (B_1, B_2)

2. Ellipse fitting.

A	2 by 2 real symmetric matrix
x	The coordinate vector
z	The center of the ellipse
a	Short axis
b	Long axis
θ	Orientation of the major axis from the x-axis
w	Bookstein constraint
C	Direct least Square Constraint matrix
S	The scatter matrix of the size 6 x 6
ω	The set of touching object pixels
ε	The set of pixels of the fitted ellipse

$z_j(k)$	Cluster center of K initial clusters of ellipses

3. Morphological features.

m_{pq}	The general spatial moments of different orders
η_{pq}	The normalized central moments
$f(k)$	The Fourier sequence of coordinates
$F(u)$	Fourier descriptors

1. INTRODUCTION

The total grain and oil seeds production in Canada exceeds 59 Mt (million tonnes) per year (Canada Grains Council 2002). Of this production, nearly 70% is exported. Because grains must be exported according to the buyer's specifications, the grain quality monitoring is very important. Currently, grains are graded manually by comparing samples with pre-defined standards. In the current Canadian grading system, grains are graded on the five factors established by the Canadian Grain Commission: test weight, varietal purity, soundness, vitreousness, and maximum limit of foreign material. The latter four factors are determined visually by trained personnel. These people can be influenced by individual experience and human fatigue. Human visual inspection is prone to errors in applying the numerous grading criteria consistently (Kohler 1991, Jayas et al. 1999).

Machine vision is a technology in which a camera is used to acquire images of given objects and a computer is used to analyze the images with the objectives of performing a pre-defined task. Therefore, machine vision is based on several distinct but related techniques, such as image processing, pattern recognition, artificial intelligence, and neural networks. Machine vision systems (MVS) can be used to determine external features of objects such as colour, size, and shape (Zayas et al. 1989; Tao et al. 1995; Shatadal et al. 1995a, b; Luo et al. 1999a, b; Majumdar and Jayas 2000a, b). Because agricultural objects are of variable shape, colour, and texture, it is very challenging to apply machine vision technology to inspect agricultural products (Tillet 1990). Recently,

researchers in agriculture have been showing more interest in using digital image processing and pattern recognition techniques for quality determination. Machine vision systems offer flexibility in application and are being assessed for their suitability as substitutes for human visual inspection. Moreover, their potential for speed, consistency and cost savings make such systems very attractive. There are several areas of application of machine vision in agriculture such as guidance of equipment, inspection of products, and grading and packaging of products. Much research work has already been reported to help automate sorting and grading of various agricultural products into quality classes using computer vision. For example, machine vision can be used for: sorting tomatoes by size, shape, colour and defects; separating apples by amount of bruising and grading by colour, shape and defects; sorting potatoes by size and shape; separation of peaches and prunes by surface defects (Sarkar 1986; Miller and Delwiche 1989; Tang et al. 1990).

During grain-handling, information on grain type and grain quality is required at several stages to determine the next stage of handling operations. Currently, the process of manually analyzing samples is subjective and is influenced by human factors and working conditions. If a machine vision system could identify the contents of a grain sample quickly and with a high accuracy, it should allow automated systems for grain handling and grain quality monitoring. For example, a machine vision system could be used to collect information on grain types and contamination to automatically decide the type of grain cleaning device and operating parameters. This would help increased cleaning throughput and recovery of salvageable grains. When grains are unloaded at the terminal

grain elevator, MVS could also identify the contents of rail cars to ensure grains of the similar quality and type are binned correctly.

To develop a MVS for a given application in the grain industry, algorithms about image enhancement, features extraction, and classifiers should be developed, tested, and optimized. Substantial work dealing with the use of different features for classification of different grains has been reported in the literature (Zayas et al. 1985, 1986; Neuman et al. 1987; Symons and Fulcher 1988 a,b; Keefe 1992; Barker et al. 1992a, b, c, d; Sapirstein and Kohler 1995; Luo et al. 1999a, 1999b; Paliwal et al. 1999, Majumdar and Jayas 2000a, b, c, d). One of the constraints of these studies was that grain feature extraction algorithms required all kernels to be non-touching. This was necessary because the clusters of touching kernels made the feature extraction of an individual kernel impossible. For most of these studies, grain kernels were manually positioned in a non touching manner for algorithm development. In practice, a grain sample presentation device, such as a vibrating bed, may be used to present the grain kernels in a single-kernel deep layer. But these devices for presenting singular kernels still can not separate all touching kernels. Crowe et al. (1997) used a sample presentation system, a vibratory feeder and flat conveyor, to evaluate the images of grains. With flow-rates near 60 g/min, about 90% of all kernels were presented as individual kernels. The majority of touching kernels appeared in groups of 2, and less than 4% of all kernels appeared in groups of 3 or 4. Therefore, it is necessary to develop a software-disconnecting algorithm to_separate touching grain kernel images to solve this problem. Also, such an algorithm should focus on separating two or three touching kernels,

because multiple kernel touching instances can be eliminated by using mechanical systems (Crowe et al. 1997).

Shatadal et al. (1995a,b) developed a mathematical morphology-based algorithm to disconnect conjoint kernel regions in an image of touching grains. They used up to 50 touching kernels in an image for separation; this, along with the method used for separation, made the separation process very slow. The algorithm was successful in disconnecting 95% wheat, 94% barley, 89% rye, and 79% oat conjoint kernel regions. Because this algorithm is based on a complicated mathematical morphology, it is computationally very demanding, and is not suitable for real-time processing. This method needs to be improved for practical application. Sharshidar et al. (1997) developed an ellipse fitting algorithm for separating touching grain kernel images. This algorithm focused on finding the representative ellipses for individual kernels in the group of touching kernels. Because the fitted ellipses were smooth, the information of the kernel boundary was not captured, making it impossible to extract detailed kernel boundary morphological information. This will cause the loss of morphological information during separation.

The main objectives of this research were to:

- develop and implement an ellipse fitting algorithm to separate the touching grain kernel regions in images and test the effectiveness of the algorithm on different cereal grains, e.g., Canada Western Red Spring (CWRS) wheat, Canada Western Amber Durum (CWAD) wheat, barley, and oats with 2 or 3 touching instances;
- test the integrity of the features after software separation of kernels;

- test the discriminating ability of morphological features of software separated kernels for the classification of different cereal grains, e.g., CWRS wheat, CWAD wheat, barley, and oats.

2. REVIEW OF LITERATURE

2.1 Background

Machine vision had been used in the classification of agricultural products (e.g., Ghazanfari et al. 1998, Ng et al. 1998). The main difficulty in developing machine vision systems for applications in the agri-food industry is the variation in size, shape, colour, and texture of these biological entities (Tillet 1990, Sarkar 1986). Determining the potential of using morphological, colour and textural features for classifying different species, grades, damage of agricultural products with pattern recognition techniques has been the main focus of the reported research. Work has also focused on sample presentation systems and related image processing algorithms (Casady and Paulsen 1988, Jayas et al. 1999). This chapter briefly reviews the research in applying machine vision to the grain industry. A brief introduction to the fundamentals of ellipse fitting is also included.

2.2 Grain Classification Features

Some quantitative information from an image is extracted by image processing and analysis algorithms as "features". These features are used as inputs to some classification algorithm to categorize the objects in the image. Grain classification can be done by using the morphological, colour, textural, or a combination of these features. A detailed review of features extraction and an MVS system has been given by Karunakaran et al. (2001).

2.2.1 Morphological Features

Morphological features of an object are characteristics of its profile and physical structure. These characteristics can be represented by the boundary, region, moment, and structure representation of the object. Shape of a grain kernel was first estimated by Segerlind and Weinberg (1972) using a Fourier series expansion of the radial distance from the center of gravity to the periphery of kernels. The grain kernel profile was traced on a grid paper. The classifying accuracy in separation of oats from barley, and wheat from rye based on extracted shape features was 99%.

Zayas et al. (1986) used several morphological features to differentiate among individual kernels of different American wheat classes and varieties. For different wheat classes and varieties, the average percentages of correctly classified kernels were 77% and 85%, respectively. They used mainly pair-wise discriminations. The work was limited to a single kernel per image frame and it was necessary to immobilize kernels in a fixed orientation prior to analysis.

Neuman et al. (1987) studied the objective classification of Canadian wheat cultivars based on kernel morphology. They used 576 kernels of pedigree seed of 14 wheat varieties for analysis. Using transmitted light, silhouette images of whole wheat kernels were captured to determine spatial size, shape parameters and Fourier descriptors. Hard red spring (HRS) and CWAD wheat kernels were the most easily differentiated groups while there was considerable overlap between hard red winter (HRW) and soft white spring (SWS) wheat classes. Correct classifications for discriminating varieties within classes ranged from 15 to 96%.

Sapirstein et al. (1987) used the technique of Neuman et al. (1987) for classification of HRS wheat, barley, rye, and oats. For a sample size of 580 grains, the classification error was 1%, but for a large sample with randomly selected kernels, the discrimination of the cereals was not satisfactory, as the identification accuracy for rye was low (Sapirstein and Bushuk 1989). For a sample size of 1400 kernels, the classification accuracies for HRS wheat, barley, oats, and rye were 98.4, 93.7, 98.0, and 78.3%, respectively. A substantial improvement in cereal grain discrimination was achieved when the morphology-based discrimination model was supplemented with mean kernel reflectance. The classification accuracies of HRS wheat, barley, oats, and rye using reflectance and morphological features were 99.2, 95.7, 95.3 and 98.3%, respectively.

Symons and Fulcher (1988a, b) conducted studies similar to Neuman et al. (1987) for Eastern Canadian wheat classes and varieties. For a sample size of 225 grains, 94% of soft white winter (SWW) and 64% of HRS wheat originating from Europe (HRS E) were correctly classified using a 4-way classification among SWW, HRW, HRS E, and HRS originating from Western Canada (HRS W). Neuman et al. (1987) found no confusion between HRS wheat and HRW wheat classes. Such diversity or range in results points to the need for a large database to develop a robust classifier. Symons and Fulcher (1988a) also experienced inadequacy of morphological features extracted from 'plan' view for discriminating among different varieties of a wheat class. For three varieties of SWW, correct classification was less than 60%. In a subsequent study, Symons and Fulcher (1988b) used some additional features (i.e., bran tissue features,

and total bran thickness that were measured at five different locations in a wheat kernel from 'cut' transverse sections) to aid in classification among different varieties of SWW wheat. Though the classifying errors were up to 20%, considering this algorithm was to identify the grain type and not to identify the foreign materials, the classifying result was still considered as satisfactory.

Barker et al. (1992a, b, c, d) used different sets of features for discriminating among kernels of eight Australian wheat cultivars. The features were ray (i.e., radial distance from the center) parameters, slice and aspect ratio parameters, Fourier descriptors, and Chebychev coefficient. The overall classification errors obtained were from 35 to 48%. Because of its high error rate, this method was not practical.

Keefe (1992) constructed a semi-automatic image analyzer for classification of wheat grains. It takes 33 primary measurements for each grain and an additional 36 derived parameters from primary measurements for analysis. Twenty varieties of wheat from the United Kingdom were tested using the instrument. To acquire an image, each grain kernel was placed manually in a fixed orientation. For a sample size of 50 grains, the total time from receiving the sample to having the data ready for statistical analysis was approximately 5 min. The overall identification error was 32.9-65.8%.

Sapirstein and Kohler (1995) suggested a new approach to objective wheat grading based on a new set of grading factors. These factors were based on variability of size, shape, and reflectance features of kernels in a sample. Such a system can be easily administered by machine vision based grading. Cargo (grain being shipped out of terminal elevators) samples of CWRS wheat grades

1, 2 and 3 were successfully classified using the mean and variance of the features as quantitative classification variables. For incoming grain samples, however, only grades 1 and 3 could be successfully discriminated from each other.

A morphological features extraction based algorithm for classifying individual kernels of CWRS wheat, CWAD wheat, barley, oats, and rye was developed by Majumdar and Jayas. (2000a). It took 23 extracted morphological features for discriminant analysis. The classification accuracies of single grain kernels using the 10 most significant morphology features were 98.9, 93.7, 96.8, 99.9, and 81.6%, respectively for CWRS wheat, CWAD wheat, barley, oats, and rye. When the training data set was tested on this morphology features model, the classification accuracies of CWRS wheat, CWAD wheat, barley, oats, and rye were 98.9, 91.6, 97.9, 100.0, and 91.6%, respectively. Because the images were obtained in the form of rectangular pixels which were then converted to square pixels, this may have resulted in slight distortion of the originally captured optical information.

Paliwal et al. (2001) evaluated nine different neural network architectures for classifying five different kinds of cereal grains namely, CWRS wheat, CWAD wheat, barley, oats, and rye by using the frequently used morphological features as inputs. Images of 7500 kernels (1500 kernels of each grain type) were taken for testing. Eight morphological features namely, area, perimeter, length of major axis, length of minor axis, elongation, roundness, Feret diameter, and compactness were extracted and used as input features. The networks were trained using 70% of the kernels of each grain type and 20% of the kernels were

used for validation of each grain type and the remaining 10% of the kernels were used for testing. The best results were obtained by using a 4-layer back-propagation network and the classification accuracy were in excess of 97% for CWRS wheat, CWAD wheat, and oats. The classification accuracy for barley and rye were about 88%.

2.2.2 Colour Features

Colour is an important visual feature for grain inspection and grading. Different grains types can usually be classified by their colour, and certain degrading factors like grass-green, bin-burnt, mildewed, and fungal damage are also easily identified as discolouration. Because colour features extracted from images are usually variable and unreliable due to the illumination variations that exist in common light sources, not much research has been reported. Limited work has been done on calibrating illumination systems for colour grain image analysis.

The use of colour image analysis for identifying different wheat classes and varieties was reported by Neuman et al. (1989a, b). The mean reflectance value of red (R), green (G), and blue (B) pixels of individual wheat kernels were used for identification of kernels as to one of six wheat classes grown in Western Canada. In general, the red, white, and amber coloured wheat types were well separated, while some confusion existed between certain red kernel types. On average, correct classification rates for individual varieties varied from 34 to 90%.

Cardarelli et al. (1998) used a machine vision system for internal inspection and classification of rough rice. A modified dark field illumination technique was

used to direct light through the rice kernels without saturating the CCD camera. Under bright field illumination, the good portions of the rough rice kernels appeared translucent, while the damaged portions appeared opaque. Two algorithms were used to differentiate between one of three categories: Undamaged, Spot, and Damaged. One method used the RGB average intensity for each kernel, while the other method used an approximated percent damage algorithm to extract the damaged portions from each kernel image. The results for the RGB average intensity method of classifying Undamaged, Spot, and Damaged categories were 96%, 80%, and 85%, respectively. The results for the approximated percent damage algorithm were l00%, 82%, and 81%, respectively.

A set of morphological and colour features were used by Luo et al. (1999a, b) for classification of cereal grains, and the average classification accuracies obtained were 98.2, 96.9, 99.0, 98.2, and 99% for CWRS wheat, CWAD wheat, barley, rye, and oats, respectively. The result showed that combining morphological and colour features improves the classification accuracies over using morphological or colour features alone.

Majumdar and Jayas (2000b) developed a colour features based algorithm to classify individual kernels of CWRS wheat, CWAD wheat, barley, oats, and rye. Eighteen colour features (mean, variance, and range of red, green, and blue, and hue, saturation, and intensity) were used for the discriminate analysis. Grains from 15 growing regions (300 kernels per growing region) were used as the training data set and grains from another five growing regions were used as the test data set. When the first 10 most significant colour features were used in

the colour model and tested on the independent data set (the test data set where total number of kernels used was 10,500; for CWRS wheat, 300 kernels each were selected for three grades), the classification accuracies of CWRS wheat, CWAD wheat, barley, oats, and rye were 94.1, 92.3, 93.1, 95.2, and 92.5%, respectively. When the model was tested on the training data set (total number of kernels used was 31,500), the classification accuracies were 95.7, 94.4, 94.2, 97.6, and 92.5%, respectively, for CWRS wheat, CWAD wheat, barley, oats, and rye.

2.2.3 Textural Features

Texture is observed in the structure patterns of the surface of objects such as wood, grain, sand, grass and cloth. It may be coarse, fine, smooth, granulated, rippled, regular, irregular or linear. Because texture is an important feature of agricultural products, Al-Janobi and Kranzler (1994) used an image processing technique for grading date fruits into quality classes on the basis of colour and surface texture. They used the co-occurrence matrix approach for classification of manually separated dates according to the USDA grading standards. They used a total of 39 features and tested eight models by applying a nonparametric discriminate analysis procedure to each model and by incorporating subsets of the features. The classification error for all models ranged between 0.8 and 26.4%. The selected feature extraction and classification techniques required extended processing time.

Han and Hayes (1990) developed an interactive image processing technique to estimate percent soil cover using the textural difference between

soil and residue or canopy. They compared the method with the photographic grid method and found that it can measure percent soil cover quickly, accurately, and with less error than humans. The image classification algorithm using textural features was able to classify residue or canopy region even when the average gray level of residue or canopy was overlapping with that of the soil background.

Park and Chen (1994) used textural features (based on co-occurrence matrices) of multi spectral images containing visible and near-infrared wavelengths for discriminating abnormal poultry carcasses from normal poultry carcasses. For the statistical classifiers, the accuracy of separation of normal carcasses was 94.4% and that of abnormal carcasses was l00%, whereas with neural network models the accuracy of separation was 100% for both normal and abnormal carcasses. When neural network classifiers were employed to classify poultry carcasses into three classes (normal, septicaemic, and cadaver), the accuracies of separation were 88.9, 92.0, and 82.6%, respectively.

Petersen (1992) used morphological and textural features for classification of 40 species of weed seeds, with 25 seeds per species. The classification rates based on various shape and textural feature analyses ranged from 26.2 to 77% and from 31.7 to 61.3%, respectively. When a combination of features describing size, shape, and texture was used (25 features: 1 size feature, 10 shape features, and 14 texture features; using a stepwise selection procedure) a maximum classification rate of 97. 7% was achieved.

Shearer et al. (1994) developed a maturity classification algorithm for

analysis of line-scan images of broccoli plants using a one-dimensional co-occurrence texture analysis approach. For 480 observations from three broccoli cultivars, they tested classification by using gray level images of size 512 by 512 pixels. They achieved a maximum accuracy of 90% for individual cultivars and 83.1% for multiple cultivars, at a gray level resolution of 64 (gray level was reduced from 256 to 64). To avoid the co-occurrence direction disturbance, the matrix was calculated for all eight directions.

Huang et al. (1997) used wavelet analysis for textural features extraction from images of beef samples. A wavelet transform of meat elastogram was used for extraction of textural features. Then, wavelet analysis was applied on beef samples for elastogram feature extraction and compared with the work on Haralick's method. For beef tenderness prediction, wavelet features produced significantly higher R^2 values (0.7-0.9) in linear statistical models than Haralick's features (0.1-0.8).

Majumdar and Jayas (2000c,d) used the textural features of individual kernels of CWRS wheat, CWAD wheat, barley, oats, and rye to develop algorithms for grain classification. For bulk samples, the textural features extracted from the red colour band at maximum gray level value 32 gave the highest classification accuracies of 92.0 % using non-parametric estimation. For individual kernels, the textural features extracted from the green colour band at maximum gray level value 8 gave the highest classification accuracies of 92.9% using non-parametric estimation.

Visen (2002) extracted 51 morphological, 123 colour, and 56 textural features from images of grain kernels. Grain identification was tried using images of

individual and bulk kernels. Classification of individual kernels was done using morphological, colour, textural, and all the features combined together, whereas, for bulk samples, classification was tried using colour, textural, and both the features combined together. The top 20 features from each of morphological, colour, and textural sets were selected and classifications were carried out using the combined 60 and the combined 30 features. Three types of classifiers, namely back propagation neural network (BPNN), non-parametric, and specialist probabilistic neural network (SPNN), were used for classification purposes. An overall classification accuracy of 96.9, 94.3, 95.0, and 95.5% were obtained for individual kernel images when the top 20 morphological, colour, and textural features were used for grain classification using BPNN, non-parametric, SPNN, and modified SPNN classifiers, respectively.

2.4 Grain Kernels Positioning and Separating Systems

In general, the above studies dealing with applications of MVS for grain identification had been limited to the closely controlled conditions of a laboratory. Most of the experiments were performed on grain kernels that were manually placed on some type of plate or tray and then moved into the field of view (FOV) of the imaging equipment. When a large number of grain kernels in a bulk kernel sample are to be analyzed, this procedure is tedious and labour intensive. For example, a representative 1 kg wheat sample has about 30,000 kernels.

Different automated or semi-automatic grain kernel positioning systems were developed for mechanically picking up the grain kernels and separating the grain kernels for presentation to a camera for imaging. For semi-automated grain

kernel positioning system, a circular rotating table was designed and built to move grain kernels into the camera's field of view. An algorithm was also developed for controlling the rotation of the table and measuring the physical properties of each individual seed. This system allowed unattended measurement of approximately 50 seeds at a time and manually placing singulated kernel into the camera's field of view (Churchill et al. 1991). A vacuum apparatus, vibratory bowl, and variable speed conveyors were more than 90% efficient in singulating grain kernels (Casady and Paulsen 1988).

Jayas et al. (1999) developed a kernel positioning system that can automatically pick up and separate the kernels of various grain types. This system consisted of a vacuum drum, a vacuum and pressure unit, a rotary air valve, a positioning unit, a controlling unit, and a seed hopper. It worked basically on the principle that the kernels were attracted and held onto a surface of a perforated plate due to a vacuum. The plate was moved and the kernels were released when the vacuum was broken. When the kernels of wheat, barley, canola, and lentils were tested for the system's ability to separate, the occurrences of single kernels picked up for all tests were above 90%, the occurrences of double kernels and three or more kernels were around 5% and below 3%. It was also stated that this system's ability to pick up and separate kernels was not influenced by moisture content. In the mixtures of grains (e.g., barley in wheat at 1, 3, and 5% levels by mass), there was no significant difference in the number of imageable wheat kernels. The system, however, had a bias to pick more kernels of the major grain component present in the mixtures of wheat and canola.

This grain kernel positioning system could not pick and separate kernels for presenting to a camera without errors. Some touching kernels were still present and it consisted of several moving parts thus making it unsuitable for industrial applications. Another device with two moving belts was developed by Spewak (1995) and tested by Crowe et al. (1997). This device also resulted in an incomplete separation of touching kernels. Because physical systems can not separate 100% of touching kernels and there are several applications where identification of 100% kernels is needed, separation using software is desired. For example, to accurately quantify foreign material in grain, all objects must be separated and correctly classified. On the other hand, if the idea was only to identify a sample for its types, e.g. during railcar unloading, then, 100% separation is not necessary. In this case, if all separated kernels can be correctly identified with a reasonable accuracy and others could be placed in an unknown class than by analyzing large number of objects, one can make a decision. For example, if 90% kernels of a wheat sample were separated out of which 80% were kernels positively identified as wheat and 20% were as other objects. Then, there is a high probability that the sample is a wheat sample. Therefore, this information can be used to confirm the contents of the railcar and automatic decision can be made to unload the grain and transfer it to the right bin.

2.5 Separating of Touching Objects

When a machine vision system obtains the image of the grain flow, the grain kernels in the image should be treated as individuals. A common difficulty occurs when objects touch, and features of grain kernels cannot be separately

measured. This situation may arise even when examining images from grain sample presentation systems, because grain-kernels tend to touch each other. An efficient and accurate algorithm should be developed to solve this problem of touching kernels.

An important area of image processing is the segmentation to distinguish objects from background. Image segmentation can be categorized by three popular approaches: image threshold methods, edge-based methods, or region-based methods.

The threshold method is the process of separating an image into different regions based on a predetermined gray level. Because the image histogram defines the gray level distribution of pixels, the image histogram can be used to locate the threshold value. However, as this method ignores image spatial information, inappropriate touching regions still exist.

The edge-based methods use discontinuities between gray level regions to detect edges within an image. The edge detection can recognize objects present within an image. Its weakness is in connecting together broken contour lines making it prone to failure in the separation of touching objects.

Region-based method partitions an image into different regions by grouping neighboring pixels of similar gray levels. Adjacent regions can be merged based upon some criteria involving homogeneity or sharpness of region boundaries.

Because these three methods may cause the separated objects in an image to touch improperly during segmentation, a connectivity preserving segmentation method was proposed. The main idea was to represent different forms of spine curves for initial boundary shapes of image objects, then iteratively modify them

by applying various mathematical morphology methods to prevent adjacent image regions from merging (Gonzalez and Woods1992).

After segmentation, the output image may cause disjoined regions to be merged together, even in images where most humans can see very clear separated regions. The reasons are noise and gray level gradual transition between the isthmus and closing regions. These touching regions need to add separating lines to split. Two common approaches have been used for separating such touching regions and are known as the mathematical morphology method and the watershed method (Beucher and Meyer 1993).

2.5.1 Mathematical Morphology

The word 'morphology' stems from the Greek words "morphe" and "logos", meaning 'the study of forms'. The term is encountered in a number of scientific disciplines including biology and geography. In the context of image processing it is the name of a specific methodology designed for the analysis of the geometrical structure in an image. Mathematical morphology was invented in the early 1960s by Georges Matheron and Jean Serra who worked on the automatic analysis of images occurring in mineralogy and petrography (Serra 1982).

Mathematical morphology represents the geometrical structure of an image based on small patterns, called "structuring elements", of varying size and shape. Set theory is the mathematical basis for morphology. Sets in mathematical morphology represent the shape of objects in an image. When a binary image is considered as Euclidian space Z^2 (2-D integers space), sets describe object pixels either as the black or white pixels. A gray scale image can be represented

as sets whose components are in Z^3 (3-D integers space). Therefore, two components of each set element correspond to the coordinates of a pixel, and the third refers to gray level. Sets are also used for describing time series of 2-D binary images as well as 2-D colour images.

The results processed by morphological operations and algorithms dictate the choice of the structuring element. For example, erosion by a small disc can clean the isolated noise points and smooth the contours while erosion by a larger disc can remove the entire foreground.

A general discussion on the choice of the structuring element can be found in Serra (1982). He also described a set of mixed structuring elements and named them Golay's alphabet. These structuring elements were especially designed to give useful results when used in hit-or-miss transform, sequential thinning, and sequential thickening.

The usefulness of mathematical-morphology-based image transforms and algorithms in machine vision related applications in agriculture was demonstrated by McDonald and Chen (1990a). Corn kernel size distribution, plant leaf identification, and texture analysis of marbling in beef longissimus dorsi muscle using simple morphological operations and algorithms were shown. The authors commented that many machine vision related applications could be addressed using a small set of basic operators. In another study, McDonald and Chen (1990b) developed algorithms to separate muscle tissues connected to beef carcasses.

A mathematical morphology-based-algorithm was developed and tested for disconnecting the conjoint kernel regions in an image of touching grains

(Shatadal et al. 1995 a, b). This algorithm found the marker for each grain in the image. It constructed the image of disconnected kernels by growing the markers within the boundaries of the kernels in the original image with a logic which prevented the merging in the neighboring regions. Random touching patterns of the kernels were used to test the algorithm. The algorithm was successful in disconnecting 95% wheat, 95% barley, 89% rye, and 79% oats conjoint kernel regions, but it was time-consuming and not suitable for real time operation. Moreover, when this method was used for touching long elliptical kernels (e.g. oats), the error rate was high.

2.5.2 Watershed

The watershed method relies on the fact that encoding the binary image will usually cause touching features to separate before they disappear (Lantejoul 1980). Accomplishing this separation with the watershed method is an iterative process. The image is repetitively encoded, and at each step separate features that disappeared from the previous step are designated ultimate eroded points (UEPs) and saved as an image, along with the iteration number. This is necessary because the features will, in general, be of different size and would not all disappear in the same number of iterations, until the image is erased. Then, beginning with the final image of UEPs, the image is dilated using dilation, but with the added logical constraint that no new pixel may be turned "ON", if it causes a connection to form between previously separate features or it was not "ON" in the original image. At each stage of dilation, the image of UEPs that corresponds to the equivalent level of erosion is added to the image using a

logical "OR". This process causes the features to grow back to their original boundaries, except lines of separation appear between the touching features.

The watershed method just described has two practical drawbacks: the iterative process is slow, requiring each pixel in the image to be processed many times, and the amount of storage required for all of intermediate images is quite large. The same result can be obtained more efficiently using EDM (Euclidean distance map). The brightness values of each pixel within features in an EDM correspond to a physical elevation. The features then appear as mountain peaks. The ultimate eroded points are the peaks of the mountains, and where features touch the flanks of the mountains intersect. The saddles, or watersheds, of these mountains are the lines selected as boundaries by the segmentation method. The placement of these lines according to the relative height of the mountains (size of the features) gives the best estimate of the separation lines between features (Serra 1982). Unfortunately, the watershed transformation often leads to over segmentation of the image.

The standard binary watershed algorithm has over segmentation problems if the boundary is irregular or complex (Beucher and Meyer 1993). When applied to grain kernel images, the defined "problem" arose. Because a kernel has an irregularly shaped boundary, the complement of its cross-sectional plot has a minimum at the center of the kernel and a local minimum on the irregular kernel extension. Multiple basins and boundary lines were also found when the objects were not oval. Tian et al. (1997) developed and tested a machine vision system to detect and locate tomato seedlings and weed plants in a commercial agricultural environment. An environmentally adaptive watershed algorithm was

developed to improve machine recognition of plants under these conditions. The system was able to identify the majority of non-occluded target plant cotyledons, and to locate plant centers even when the plant was partially occluded. Of all the individual target crop plants 65% to 78% were correctly identified and less than 5% of the weeds were incorrectly identified as crop plants.

2.5.3 Ellipse Fitting

One of the major problems of computer vision is the localization of an object of interest. Much of the structural information in an image is encoded within the edges, which gives the information about the shape of an object in the form of an image. The shapes are important information for representing the object. Ellipses commonly occur in many images, often being formed as the projection of approximately circular objects onto the image plane. Ellipses provide a useful representation of parts of the image, because they are more convenient to represent the curve, and their detection is reasonably simple and reliable. Thus, they are often used by computer vision systems for model matching (Forsyth et al. 1991).

Regarding the importance of ellipses, many different methods have been proposed for ellipse detection and fitting. These approaches exploit various methods, like: Hough transform (Yuan et al. 1989), RANSAC algorithm (Rosin 1993,), Kalman filtering (Porrill 1990, Rosin and West 1995), or least squares method (Bookstein 1979, Sampson 1982). In general, these approaches can be divided into two main groups: clustering methods and optimization methods. The approaches of the clustering methods group (Hough transform, RANSAC

algorithm) are robust against outliers and they can detect multiple primitives at once. Unfortunately, these methods are slow; they require extensive memory and their accuracy is low. Moreover, for the Hough transform, there are problems with the detection of ellipses due to blurred and spurious peaks in the accumulators (Grimson and Huttenlocher 1990). Therefore, they are not suitable for real time machine vision systems.

The approaches of the optimization methods group (the least squares method and its variations) are based on optimization of an objective function that characterizes the goodness of a particular ellipse with respect to the given set of data points. The main advantages of optimization methods are their speed and accuracy. On the other hand, these methods can fit only one primitive at a time. Also, the sensitivity to outliers of the optimization methods is higher than for the clustering methods. But the least squares method and its variations are still the most common algorithms for ellipse fitting, as they are efficient and accurate (Fitzgibbon et al. 1996).

The least squares method is used to find the set of parameters that minimize the distance measure between the data points and the ellipse. Thus, the ellipse can be represented algebraically by an equation $F(x,y) = 0$, where x and y are the coordinates of the pixel.

The general second order polynomial for an ellipse is (Bookstein 1979):

$$F(a,x)= C_0+ C_X X + C_Y Y + C_{XY} XY + C_{XX} X^2 + C_{YY} Y^2 \qquad (2.10)$$

Where $a=(C_0, C_X, C_y, C_{XX}, C_{XY}, C_{YY})$, $x=(1, X, Y, XY, X^2, Y^2)^T$

This equation can also be expressed as:

$$\mathbf{x}^T\mathbf{A}\mathbf{x} + \mathbf{b}^T\mathbf{x} + \mathbf{c} = 0 \qquad (2.11)$$

where A is a 2 by 2 real symmetric matrix, **x** is the coordinate vector and $\mathbf{x}=(x, y)^T$. If new coordinate vector **x'** was introduced with **x'** = **Qx+t**, then rotating and shifting the ellipse, the equation 2.11 becomes:

$$\mathbf{x'}^T(\mathbf{Q}^T\mathbf{A}\mathbf{Q})\mathbf{x'} + (2\mathbf{t}^T\mathbf{A} + \mathbf{b}^T)\mathbf{Q}\mathbf{x'} + \mathbf{t}^T\mathbf{A}\mathbf{t} + \mathbf{b}^T\mathbf{t} + \mathbf{c} = 0 \qquad (2.12)$$

Let $\mathbf{A'} = \mathbf{Q}^T\mathbf{A}\mathbf{Q}$, and similarly **b'** and **c'**, this equation can be written:

$$\mathbf{X'}^T\mathbf{A'}\mathbf{x'} + \mathbf{b'}^T\mathbf{x'} + \mathbf{c'} = 0 \qquad (2.13)$$

If Q and t are properly chosen, such that $A = diag(\lambda_1 + \lambda_2)$, **b' = 0**; then equation 2.13 is transferred to:

$$\lambda_1 x^2 + \lambda_2 y^2 + c' = 0 \qquad (2.14)$$

Thus, the center **z** and the axes (*a* and b are short and long axis) of the ellipse in the non-transformed system are given by:

$$\mathbf{z} = \mathbf{t} \qquad (2.15)$$

$$a = \sqrt{-c'/\lambda_1} \qquad (2.16)$$

$$b = \sqrt{-c'/\lambda_2} \qquad (2.17)$$

Because $\mathbf{Q}^T\mathbf{Q} = \mathbf{I}$, the matrix ***A*** and ***A'*** have the same eigenvalues λ_1, λ_2, and λ_1 and λ_2 are invariant to rotation and shifts. Also,

$$\det A = a_{11}a_{22} - a_{21}a_{12} = \lambda_1\lambda_2 \qquad (2.18)$$

$$traceA = a_{11} + a_{22} = \lambda_1 + \lambda_2 \qquad (2.19)$$

To avoid the trivial solution about *A* and c, and recognizing that any multiple of a solution *A* represents the same ellipse, *A* should be constrained. To constrain, Bookstein (1979) suggested an invariant constraint:

$$\lambda_{11}^{\ 2} + \lambda_{22}^{\ 2} = a_{11}^2 + 2a_{12}^2 + a_{22}^2 = 1. \qquad (2.20)$$

When A is positive and c < 0, it is assured that the above equation would represent an ellipse. Expanding the above equation with the Bookstein constraint yields:

$$a_{11}x^2 + 2a_{12}xy + a_{22}y^2 + b_1x + b_2y + c = 0 \qquad (2.21)$$

Let *m* points in the plane, (x_1, y_1), (x_2, y_2), ...,(x_m, y_m) be applied to the above equation, and let

$$\mathbf{u} = (a_{11}, 2a_{12}, a_{22}, b_1, b_2, c)^T,$$

and $$\mathbf{s} = \begin{pmatrix} x_1^2 & x_1y_1 & y_1^2 & x_1 & y_1 & 1 \\ \vdots & \vdots & \vdots & \vdots & \vdots & \vdots \\ x_m^2 & x_my_m & y_m^2 & x_m & y_m & 1 \end{pmatrix}$$

Then the linear system of *m* equations is expressed:

$$\mathbf{su}=0 \qquad (2.17)$$

Ideally, if all *m* points actually lie on an ellipse, then this system has a solution. However, if all *m* points do not lie on an ellipse, there is no solution for this linear system. To avoid this no solution, $||\mathbf{su}|| = \mathbf{r}$ should be considered to find a **u** which minimizes $||\mathbf{r}||$. Furthermore, we need to put constraints on **u.** To minimize $||\mathbf{su}||$ and solve the parameter vector **u**, the constraint $||\mathbf{u}||=1$ can be used. If we define vectors

$$\mathbf{v}= (b_1, b_2, c)^T$$

$$\mathbf{w}= (a_{11}, \sqrt{2}\, a_{12}, a_{22},)^T$$

With the Bookstein constraint $||\mathbf{w}|| = 1$, $\mathbf{su}=0$ can be rewritten to:

$$\mathbf{s}\begin{pmatrix} \mathbf{v} \\ \mathbf{w} \end{pmatrix} \approx 0 \qquad (2.18)$$

The Bookstein constraint is appropriate to ellipses, hyperbolas and parabolas. For the specialized problem of fitting ellipses, ellipse fitting may use the specialized constraint $a_{11} + a_{22} = \lambda_1 + \lambda_2 = 1$ (Rosin 1993). The ellipse fitting solution obtained by the Bookstein algorithm and the constrained least square method are shown in Figure 2.1.

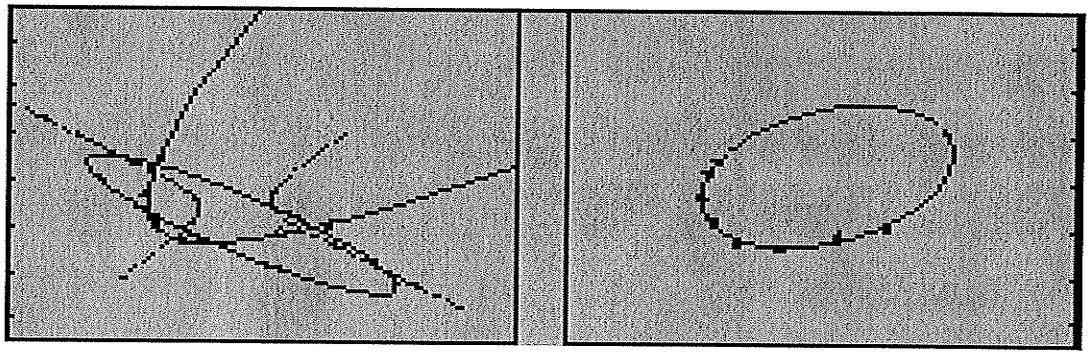

Figure 2.1: The ellipse fitting solution obtained by the Bookstein algorithm (left) and the constrained least square method (right) (Fitzgibbon et al. 1996).

Ellipse fitting by least-squares methods with constraint are computationally efficient and perform well (Rosin 1993), if the data belong to a precisely elliptical arc with little occlusion. But, it has the major disadvantages that under less ideal conditions (not strictly elliptical data, moderate occlusion or noise), they often yield unbounded fits to hyperbolae. When ellipses are specifically desired to fit precisely, such fits must be rejected as useless. Porrill (1990) and Ellis et al. (1992) initialize a Kalman filter that iteratively minimizes some error metrics in order to find the right ellipse. This approach alleviates this problem, but they also are computationally demanding.

Kim et al. (2000) used the ellipse-fitting method for human face detection. After detecting the template region that includes features like eyes and mouth,

elliptical face regions were detected around template regions by a least square ellipse fitting algorithm. The success detection rate was 77% for 108 images. Eleftheriadis and Jacquin (1995) proposed a face model using an assisted coding method to obtain better face quality. The face region was detected using edge thresholding and least square ellipse fitting. The tracking accuracy for eyes-nose-mouth regions was 95% on average.

When grain kernels were approximated as ellipsoid of revolution, it was assumed that each grain kernel could be identified by the dimensions of its approximating ellipsoid. Or equivalently (in two dimensions), the identification could be done by determining the ellipse, which "covers" the silhouette of the grain kernel and by comparing the dimensions of the ellipse with typical dimensions for a variety of grain types. Shashidhar et al. (1997) and Visen et al. (2001) developed an ellipse fitting algorithm for the touching grain kernels separation. Because this algorithm was using an Eigen-solution based method without constraint to find the fitted ellipses, many hyperboles and non-precisely fitted ellipses were created during ellipse fitting. Therefore, finding the representative fitted ellipses became time consuming and was affected by the noise.

3. MATERIALS AND METHODS

3.1 Vision Hardware

The vision hardware used in this research included the following components:

1. A colour camera (Model DXC 300A, Sony). It was fitted with a zoom lens of 10-120 mm focal length (VCL-1012BY), and a close-up lens set (72 mm, Tiffen, Hauppauge, NY);
2. A camera control unit (Model CCU-M3, Sony); the option of the manual iris control was used to achieve repeatability in the experiments, and the automatic gain control of the camera was disabled;
3. A camera support stand (m3, Bencher Inc., Chicago, IL) for vertical movement of camera;
4. A colour frame grabbing board (Matrox Meteor-II multi-channel, Matrox Electronic Systems Ltd., Montreal, PQ), to digitally capture and display images;
5. A personal computer (PIII 450 MHz) with Windows NT 4.0 workstation operating system;
6. An image acquisition chamber.

The National Television System Committee (NTSC) colour signal from the camera was converted by the camera control unit into red (R), green (G), and blue (B) analog video signals, and a synchronous signal. Then, the RGB video signals from control unit were converted to 24 bit 640 x 480 digital images by the frame grabber board. The program to control the frame grabber was the Matrox imaging library (Matrox Electronic Systems Ltd., Montreal, PQ). The images were

displayed on the monitor and then saved in a tagged image file format (tiff) for further analysis. The camera mounted on the support stand and the image acquisition chamber are shown in Figure 3.1.

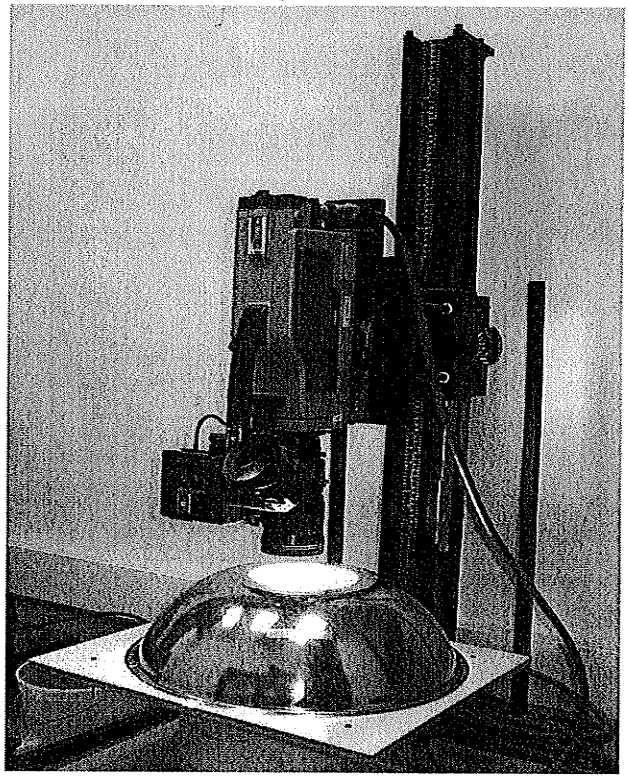

Figure 3.1 Machine Vision System

3.2 Sample Illumination

Illumination is critical to machine vision systems, because it can either accentuate or obscure object features and no amount of image processing can ever correct for details that were never captured (Paulsen and McClure 1986). An ideal illumination source should provide uniform light distribution over the field of view (FOV). Luo et al. (1997) evaluated incandescent, halogen, and flourescent lamps for their sensitivity to lamp voltage variations, stability with

time, and uniformity over FOV. They suggested that flourescent lighting is best suited for the system, because of:

- The availability for enhanced colour rendition and visual clarity.
- Long lamp life. Flourescent lamp life is 20,000 h, compared with only 2,000 h for an incandescen lamp.
- Cooler operating ambient temperature.
- Less generation of infrared wavelengths that tend to bias video camera sensors.
- Insensitivity to lamp voltage variations.

Uniform diffuse lighting was used in all experiments. A flourescent tube with a 305 mm diameter, 32-W circular lamp (FC12T9/CW, GE Lighting, USA) with a rated voltage of 120 V was placed around and just below the surface level of the sample placement platform of the light chamber. A semi spherical steel bowl of 0.39 m diameter, painted white and smoked with magnesium oxide on its inner side, was used as a diffuser (Figure 3.1). A 0.125 m diameter opening was at the top of the bowl, through which the camera could view the FOV. A voltage regulator (CVS, Sola Canada Inc., Toronto, ON) supplied stable AC power (± 0.5 V) to the light source. A variac was used to adjust the voltage (120 ± 1v) of the lamp. A light controller (FX0648-2/120, Mercron, Richardson, TX) fitted with a photodiode light sensor was used with the flourescent lamp. The sensor can automatically detect the illumination level in the light chamber, thus the light controller adjusted the AC frequency of the lamp to maintain a stable level of illumination.

3.3 Illumination standardization

Luo et al. (1999a) developed a method for illumination standardization. The illumination level was standardized by using a Kodak white card with 90% reflectance (E152-7795, Eastman Kodak Co., Rochester, NY) as a white reference. When the lamp voltage was set to the rated 120 V, the image of the white card was acquired over a small central area of 50 x 50 pixels, and the mean gray level values of the R, G, and B bands were computed and used as the illumination level indicators. The iris control of the camera control unit was manually adjusted to perform white balance until all three values (R, G, and B) were 250 $\pm$1.

3.4 Spatial Calibration

All the morphological features in image analysis were calculated in pixels. To convert these pixel dimensions into real-world measurement units, the spatial resolution of pixels was determined. The image of a Canadian 10 cent coin was taken, and the coin's diameter was calculated. The calculated pixels were compared to the coin's measurement diameter of 17.96 mm with a micrometer (No. 961, Moore and Wright, Sheffield, England), and the spatial calibration was determined. When the camera setting was fixed to take the images, the calibration was done frequently to make sure the spatial resolution was not changed. Before starting each imaging session, spatial calibration was done by imaging a Canadian 10 cent coin. This ensured that all the sessions had same spatial resolution and the coin image could be later used as a reference image of

spatial calibration. Based on the fixed camera setting, the spatial resolution of the images was around 6.38 x 10^{-2} mm/pixel.

3.5 Grain Samples

The grain samples for this study were obtained from the Industry Services Division of the Canadian Grain Commission (Winnipeg, MB). For the 1998 growing year, clean grain samples of CWRS wheat (Grade 1, 2, and 3), CWAD wheat (Grade 1, 2, and 3), barley (Special Select Malt Barley), and oats (Grade 1) were used to test the separation algorithm and related image analysis. Samples were collected from 30 growing regions of western Canada (Figure 3.2). These growing regions were chosen using the climatic subdivisions of the Canadian Prairies (Putnam and Putnam 1970).

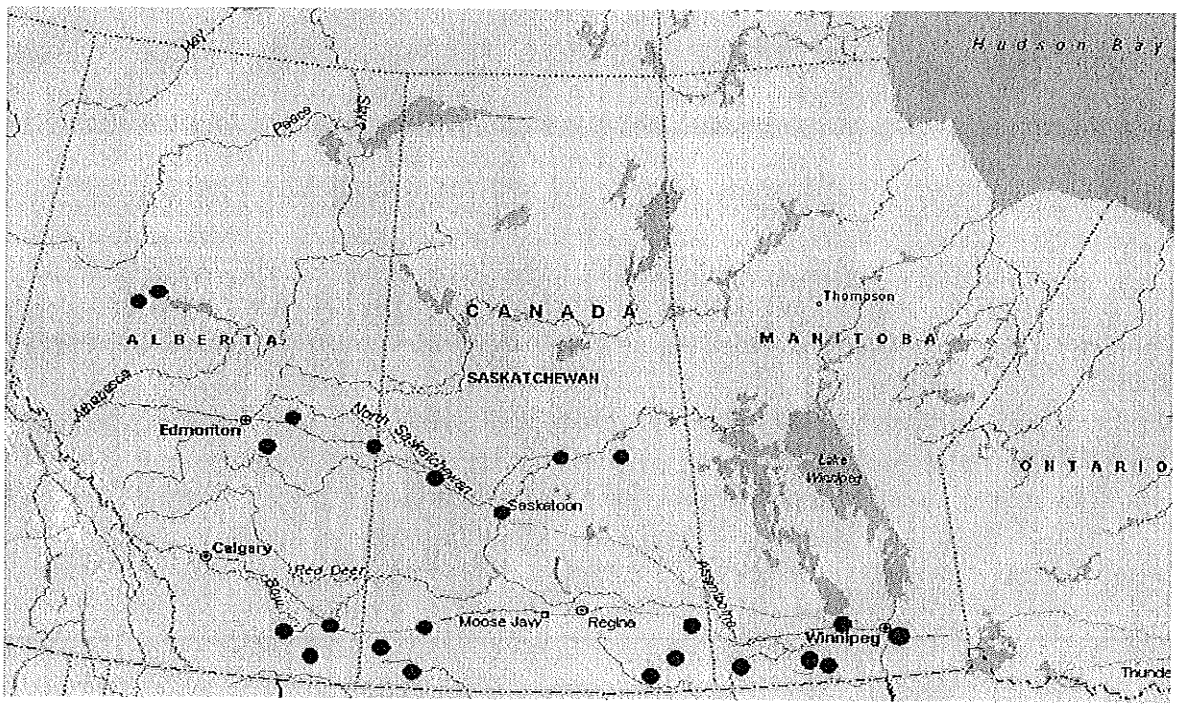

Figure 3.2 A map showing different locations from where the grain samples were collected

3.6 Image Acquisition

For its stabilization, the image acquisition system was switched on 30 min prior to acquiring images. The gray level calibration (white balance) of the (FOV) was done using a Kodak white card. The spatial calibration was done with an object of known dimension (a Canadian 10 cent coin).

For the touching instances, one grain kernel was randomly dropped as the center, and other kernels were manually placed to touch the center kernel to simulate possible different touching instances. Touching instances were created to result in a point or a line contact or in between possibilities (Figure. 3.3). Care was taken not to let kernels overlap. After the image of the touching kernels was acquired, the kernels were then manually separated without disturbing the orientations of the kernels (Figure. 3.4). The reorientation of some kernels could have occurred unintentionally. Because the morphological features extracting algorithm used in this study are independent of kernel orientation, the relocating kernel orientation will not affect the extracted features values. With the morphological feature extracted algorithm, the values of extracted morphological features from the same grain kernel with different orientations was changed within 0.8%. Detailed information about this algorithm is in section 3.7. Then, an image of manually separated kernels was also acquired with the same hardware and software settings.

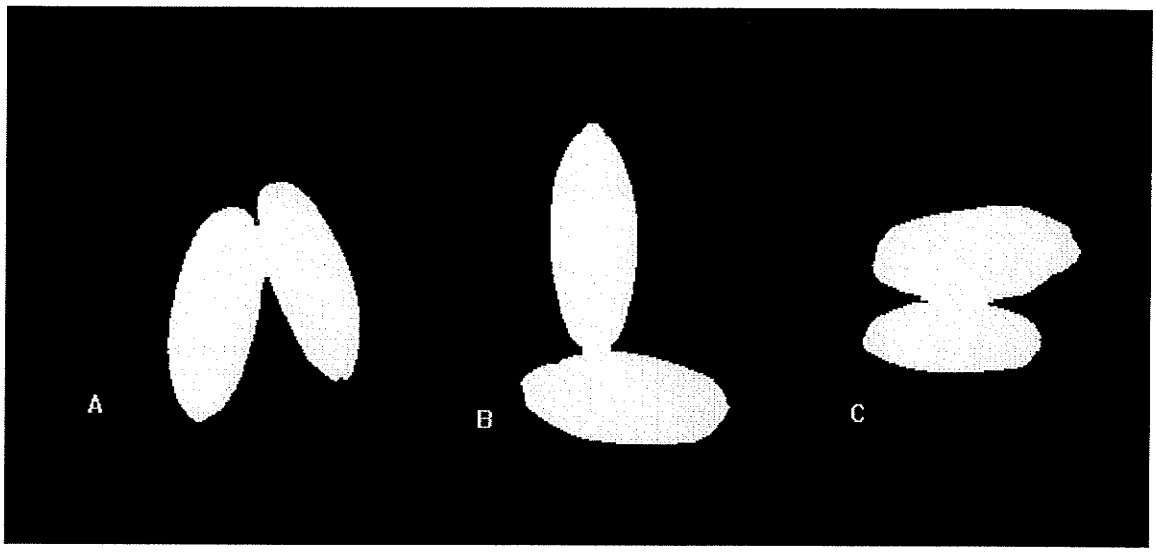

Figure 3.3 Examples of an in between or short line contact (A), a point contact (B), and a long line contact (C).

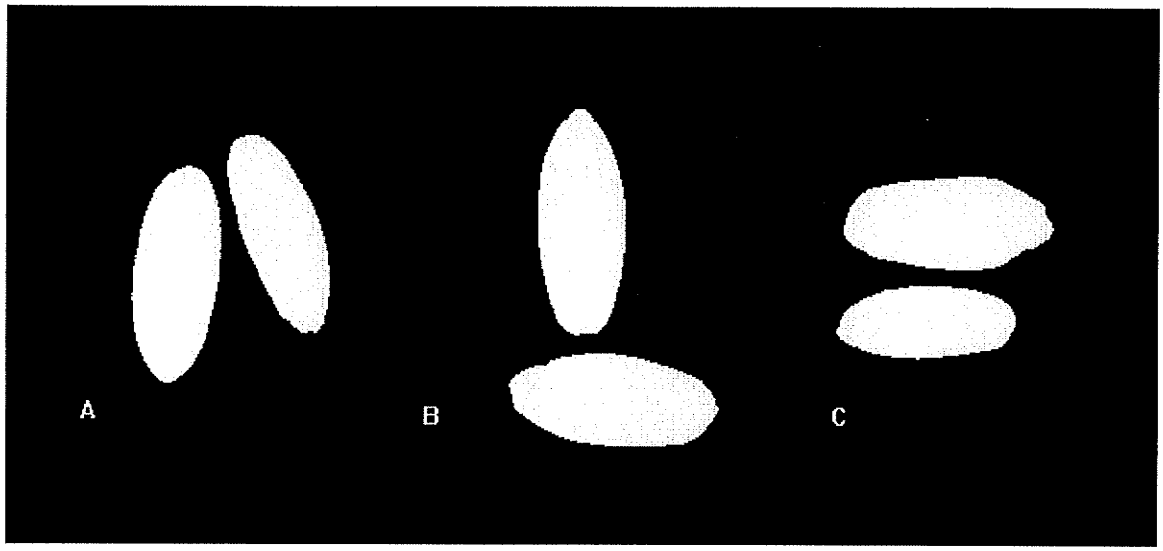

Figure 3.4 Examples of manually separated images from Figure 3.3 (A), (B), (C).

3.7 Image Analysis

The original images of the touching grain kernels were first thresholded to binary images. Then, these binary images with joint kernel regions were processed by the ellipse fitting algorithm to separate the touching kernel regions,

and the disconnected kernel regions were referred to as software separated kernels. The term "physically separated" refers to manually separated kernels. All of the images of software separated kernels and physically separated kernels were labeled and the morphological features of all of the kernels were extracted using the same algorithm. The morphological features used for analysis were: area, perimeter, maximum radius, minimum radius, mean radius, major axis, minor axis, shape moment, Fourier transcript, major length, and minor length.

The morphological features used for assessing the effectiveness of the separation algorithm are described below (Majumdar and Jayas 2000a):

Area: The pixel area of the interior of an object is defined as area. The total number of pixels inside the grain kernel were calculated, including the kernel boundary.

Perimeter: The pixel distance around the circumference of an object is defined as the perimeter. The Euclidean distance between all the successive pairs of pixels around the kernel boundary was added to calculate the perimeter based on the 8-neighbor connectivity method. The distance represented by each pixel was 1 if all neighbors were horizontal or vertical, 1.414 if all neighbors were diagonal, and 1.207 if there was one diagonal and one non-diagonal pixel.

Major axis length: It is the distance of the longest line that can be drawn through the center of a kernel. The distance between each possible pair of boundary pixels, which could be drawn through the center, was computed and the maximum distance was taken as the length of the major axis.

Minor axis length: The minor axis length is the distance between the pixels of the longest line that can be drawn perpendicular to the major axis.

Maximum radius: It is the maximum distance between a boundary pixel and the centroid of the grain kernel.

Minimum radius: It is the minimum distance between a boundary pixel and the centroid of the grain kernel.

Mean radius: It is the mean value of the distances between the boundary pixels and the centroid of the grain kernel.

Major length: It is the length of the rectangle bounding the kernel.

Minor length: It is the width of the rectangle bounding the kernel.

Spatial moments: The spatial moments are statistical shape measures related to an object's characterization: moments of binary objects describe their shape. The general moments (m_{pq}) of different orders were determined as:

$$m_{pq} = \sum_{i} \sum_{j} i^{p} j^{q} X(i,j) \qquad (3.1)$$

where $p, q = 0, 1, 2, \ldots$ is the order of the moment and $X(i, j)$ is the gray level of the object at coordinate (i, j).

In binary images, the gray level of the object, $X(i, j)$ is 1 for all pixels. The first-order spatial moments (m_{10} and m_{01}) of an object in a binary image were the x and y sums of the object's pixels. The second order moments m_{20} and m_{02} represent the moment of inertia. For identification of objects, the moments have to be independent of position and orientation of the object in the image and size of the objects. The central moments μ_{pq} that are invariant to translation (position of the object in a given image) and normalized central moments η_{pq} (Gonzalez

and Woods 1992) that are invariant to translation and size of the object are given by:

$$m_{pq} = \sum_i \sum_j (i - x_c)^p (j - y_c)^q X(i,j)$$

$$\eta_{pq} = \frac{\mu_{pq}}{\mu_{00}^{\gamma}} \tag{3.2}$$

where

$$\gamma = \frac{(p+q)}{2} + 1 \tag{3.3}$$

The first four moments that are invariant to translation, rotation, and scaling of the object were as follows:

$$\phi_1 = \eta_{20} + \eta_{02} \tag{3.4}$$

$$\phi_2 = (\eta_{20} - \eta_{02})^2 + 4(\eta_{11})^2 \tag{3.5}$$

$$\phi_3 = (\eta_{30} - 3\,\eta_{12})^2 + (\eta_{21} - \eta_{03})^2 \tag{3.6}$$

$$\phi_4 = (\eta_{30} + \eta_{12})^2 + (\eta_{21} + \eta_{03})^2 \tag{3.7}$$

Fourier Descriptors: Fourier descriptors are shape recognition features based on the Fourier series expansion of periodic functions. They were used to represent the boundary of an object as a periodic function with a period of 2. The obtained periodic function was then expanded in a Fourier series and its coefficients were calculated.

Consider an object with an *N*-point boundary (x_0, y_0), (x_1, y_1), (x_2, y_2),....(x_{N-1}, y_{N-1}). These xy coordinates can be expressed in the form $x(k) = x_k$ and $y(k) = y_k$. Then, the boundary can be represented as the sequence of coordinates $f(k)$ =

[x(k), y(k)], for *k = 0,1,2...., N-1*. Each coordinate pair can be treated as a complex number so that *f(k) = x(k) + j y(k)* for *k = 0,1,2,....N-1*, i.e., the discrete Fourier transform of *f(k)* is:

$$f(k) = \frac{1}{N}\sum_{k=0}^{N-1} F(u)e^{j2\pi uk/N} \qquad (3.8)$$

for *u = 0, 1, 2,...., N-1*. The complex coefficients *F(u)* are called the Fourier descriptors of the boundary.

$$F(u) = \frac{1}{N}\sum_{k=0}^{N-1} f(k)e^{-j2\pi uk/N} \qquad (3.9)$$

for *k = 0, 1, 2,...., N-1*. Because these features are extracted by taking the Fourier transform of the coordinates along the boundary of the kernel, they were called *boundary Fourier descriptors*. The magnitude of *F(u)* is the square root of the sum of squares of its real and imaginary values.

3.8 Morphological Image Operations

Morphological image operations are based on set-theoretic operations. The two basic morphological set transformations are erosion and dilation. These transformations involve the interaction between an image A (the object of interest) and a structuring set B. Typically, the structuring element B is a circular disc in the plane, but it can be any shape. In a binary image, structuring element sets are the sets in the 2D plane. Let A and x be subsets of Z^2, the *translation* of a set A by a vector x is denoted A_x, and is defined as:

$$A_x = \{c : c = a + x, a \in A\} \qquad (3.10)$$

where x is a vector from a fixed and specified origin to a given point. The translation of an image may cause shifting of all foreground pixels of the image

by a given length and along a specified direction. The reflection of a set A, denoted $\hat{A}$, is defined as:

$$\hat{A} = \{x : x = -a, a \in A\} \tag{3.11}$$

Reflection reverses all the related pixels in the image. The complement of *A* is denoted A^c, and the difference of two sets *A* and *B* is denoted *A* - *B*.

Dilation and erosion are two basic morphological transforms. All other transforms are based on them.

- **Dilation**

Dilation of the object *A* by the structuring element *B* is given by (Serra 1982):

$$A \oplus B = \{x : \hat{B}_x \cap A \neq \emptyset\} \tag{3.12}$$

The process consists of obtaining the reflection of *B* about its origin and then shifting this reflection by x. Therefore, the dilation of *A* by *B* is set of all x displacements such that *A* and $\hat{B}$ overlap by specified elements.

- **Erosion**

Erosion of the object A by a structuring element B, is denoted as $A \ominus B$, and defined as (Serra 1982):

$$A \ominus B = \{x | (B)_x \subseteq A\} \tag{3.13}$$

The erosion of *A* by *B* is the set of all points x such that *B*, translated by x, is contained in *A*.

Dilation and erosion are duals of each other with respect to set complementation and reflection. That is:

$$(A \Theta B)^c = A^c \oplus \hat{B} \qquad (3.14)$$

Erosion and dilation can be used in a variety of ways, in parallel and series, to give other transformations including thickening, thinning, skeletonisation and many others.

- **Opening and closing**

Two very important transformations are opening and closing. Opening generally smoothes a contour in an image, breaking narrow isthmuses and eliminating thin protrusions. Closing tends to narrow smooth sections of contours, fusing narrow breaks and long thin gulfs, eliminating small holes, and filling gaps in contours.

The opening of *A* by *B*, denoted by $A \circ B$, is given by the erosion of A by *B*, followed by the dilation by *B*, that is

$$A \circ B = (A \Theta B) \oplus B \qquad (3.15)$$

Opening is like "rounding from the inside". The opening of *A* by *B* is obtained by taking the union of all translations of *B* that fit inside *A*. Parts of *A* that are smaller than *B* are removed. Thus

$$A \circ B = \bigcup \{(B)_x | (B)_x \subset A\} \qquad (3.16)$$

Closing is the opposite operation of opening. It is produced by the dilation of *A* by *B*, followed by the erosion by *B*:

$$A \bullet B = (A \oplus B) \Theta B \qquad (3.17)$$

This is like "smoothing from the outside". Holes are filled in and narrow valleys are "closed".

Samples of graphical illustrations of opening, closing, dilation, and erosion are shown in Figure 3.5 (a), (b), (c), and (d). (for details see Haralick et al. (1987) and Serra (1982))

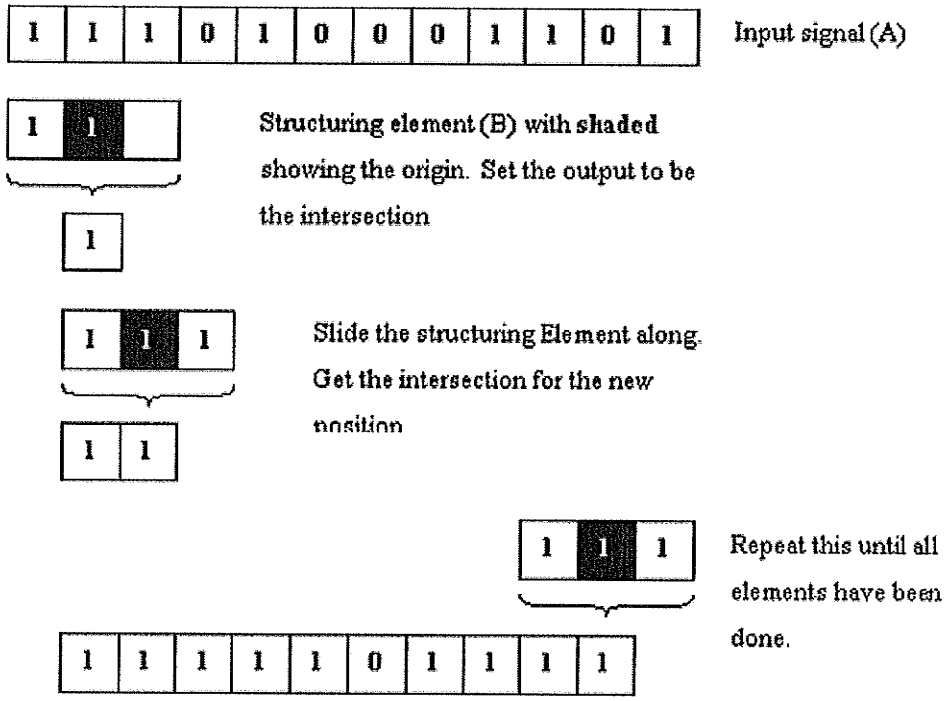

Figure 3.5 (a). Example of dilation (Sources: Serra (1982))

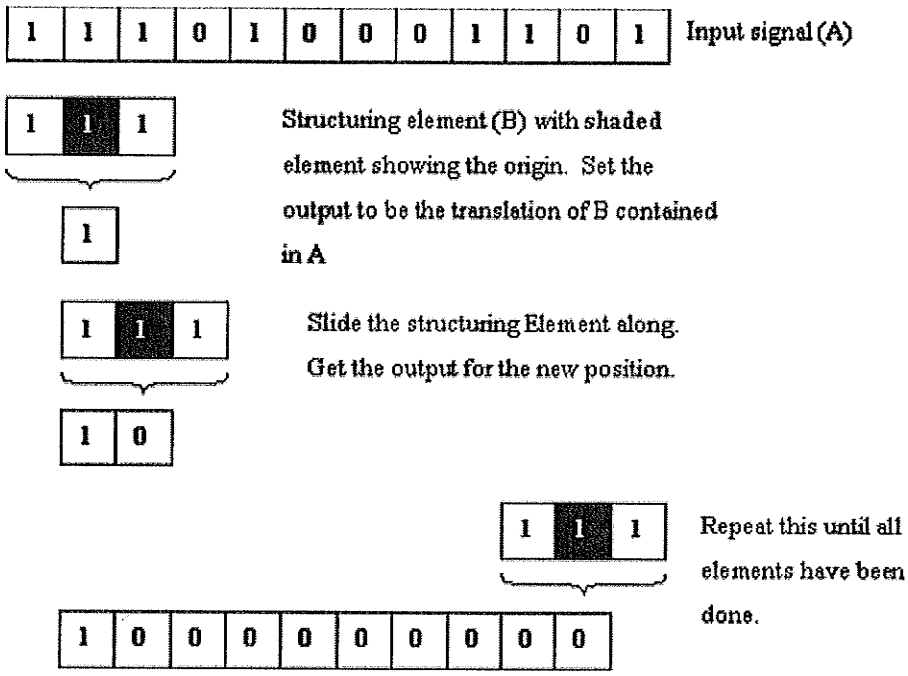

Figure 3.5 (b). Example of erosion. (Sources: Serra (1982))

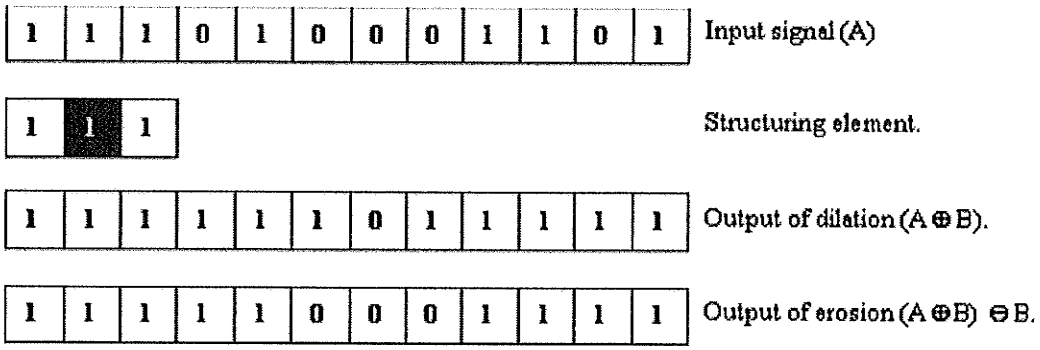

Figure 3.5 (C): Example of closing. (Sources: Serra (1982))

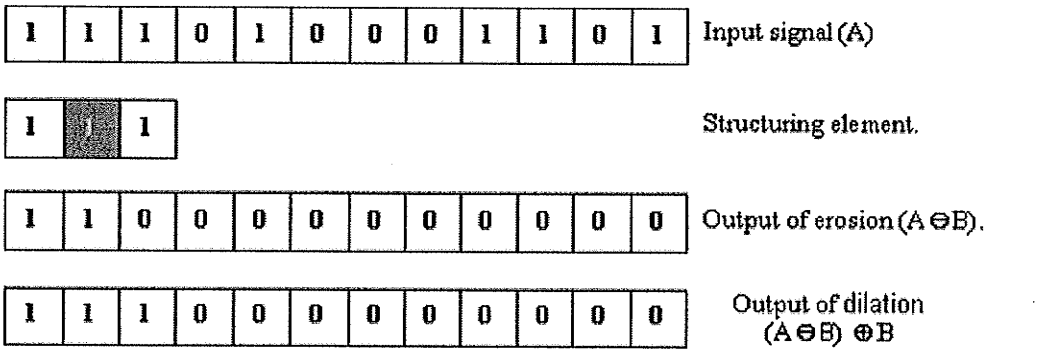

Figure 3.5 (d). Example of opening. (Sources: Serra (1982))

- **Hit-or-miss transform**

Hit or miss transform is the basic tool for shape detection. It selects out sets that have certain geometric properties such as corner points, isolated points or border points, and then performs template matching, thinning, thickening and centering. This transformation is accomplished by using intersections of erosions.

Let B_1 and B_2 be two structuring elements of a mixed structuring element B, where B_1 is the set formed from elements of B associated with an object, and B_2 is the set of elements of B associated with the corresponding background. The making up of B also satisfies the $B_1 \cap B_2 = \varnothing$. Hit-or-miss transform of a set A by B= (B_1, B_2) is defined by:

$$A \otimes B = (A \ominus B_1) \cap (A^c \ominus B_2) \qquad (3.18)$$

The hit-or-miss transform can be used to locate spatial patterns.

3.9 Ellipse Fitting Algorithm Development

Before the development of the ellipse fitting algorithm, the watershed and combined mathematical morphology model were used to compare with the ellipse fitting algorithm to test the separation result. When watershed was applied to separate the touching grain kernels instances, it did not work for disconnecting certain touching instances, such as two kernels touching side by side and creating a long touching isthmus. In this condition, watershed method could not find the center of each touching object and considered as a non touching case for separation, the separation was not done. Shataldal et al. (1995a) developed a combined mathematical morphology model which used the logic of watershed

and added heuristics for separation. This model used eight steps to separating the touching instances. These steps were:

1. Progressive erosion,
2. Sequential thickening,
3. Pruning dendrites,
4. Dilation of small components,
5. Adding dendrites,
6. Finding the constrain disc,
7. Eliminating the corners, and
8. Removing the notches.

Though, in their model, heuristics (such as adding the dilated dendrite) was used to reduce the chances of bisecting a kernel, some touching instances could not be separated. This was mainly caused by the condition that a larger isthmus area biased the location of the center disc towards it. Also, this algorithm was very time consuming. Figure 3.6 shows the unsuccessful separation by the mathematical morphology model (Shataldal et al. 1995a).

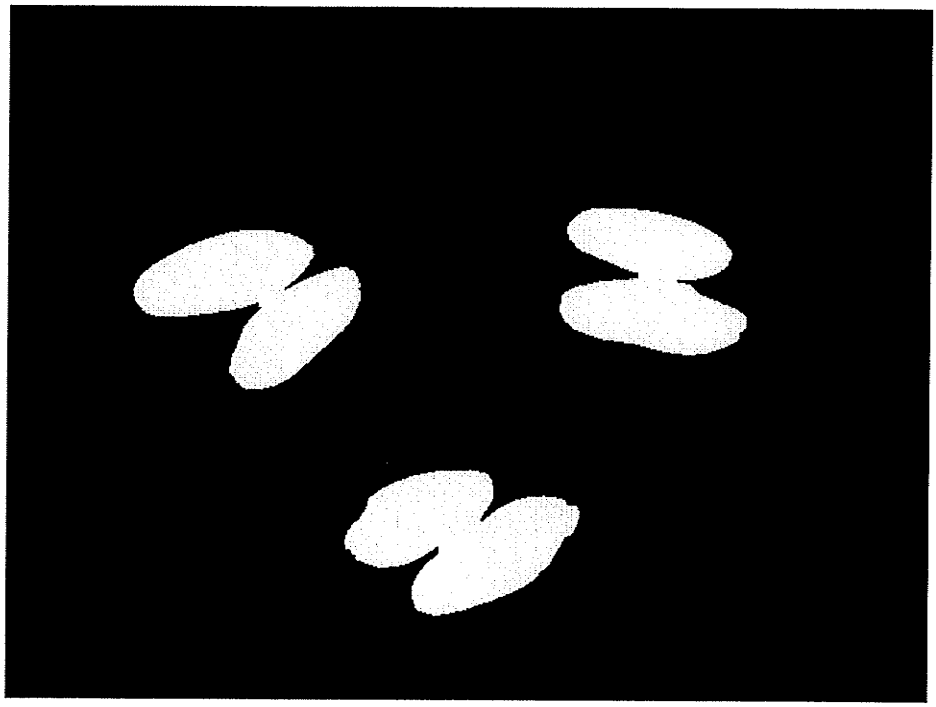

Figure 3.6 (a) Original touching kernel image

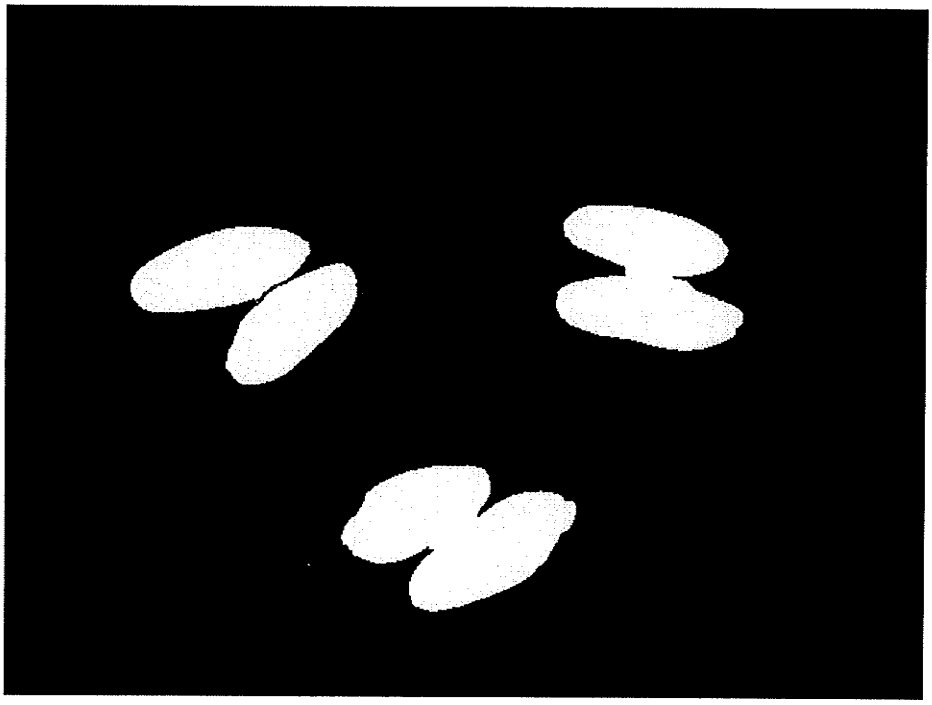

Figure 3.6 (b) Unsuccessful separation with mathematical morphology model.

The fitted ellipse algorithm used the fitted ellipses to simulate the grain kernels in the image, if the representative ellipses were correctly selected and could "cover" the silhouette of the grain kernel, the isthmus area of touching instances could be identified and separated. Therefore, finding the right fitted ellipse was the most important step for this algorithm. Fitzgibbon et al. (1996) noted, compared to other methods, the least square method is an efficient and accurate method for ellipse fitting. However, if the least square method is not constrained, many hyperboles and non-precisely fitted ellipses are created during ellipse fitting. To find the right least square method for grain kernels' ellipse fitting, general least square method, least square method with Bookstein constraint (Bookstein 1979), and direct least square method (Fitzgibbon et al. 1996) were compared to develop the most suitable fitted ellipse algorithm. For preliminary testing, 400 grain kernels (100 for each grain type) were used for testing. The successful ellipses fitting rates with general least square method, least square method with Bookstein constraint, and direct least square method were 74%, 90% and 94%, respectively. Based on above result, the direct least square method was selected as the ellipse fitting method for separation of grain kernel images.

When the direct least square method was applied to each touching instance, the fitting ellipses were created in different sizes and shapes. Some fitted ellipses were too big, or some were too small. Therefore, several filters had to be set to pick the right fitted ellipses. Because the fitted ellipses should be similar to the grain kernel, when a grain kernel was considered as ellipsoid, the ratio of a/b (a is the short axis of the ellipse, b is the long axis) should be limited.

Two thousand grain kernels were taken for determining this ratio and the ratio was found between 0.3 and 0.9. So the $0.3<a/b<0.9$ was applied as the first criteria. However, only one criterion is not enough for ellipse selection. The second criterion was the measurement of the overlap between touching objects and fitted ellipse. Three measurements (0.90, 0.95, and 0.99) were tested. The measurement of 0.95 was proven to be the suitable selection, as fitted ellipses did not require to be too precise for future grouping. After all fitted ellipses were created, the fitted ellipses were grouped to find the representative ellipse for each kernel of the touching instance. If too many fitted ellipses are generated, it is time consuming for grouping. However, if not enough fitted ellipses were generated, the grouping could not be done. Four numbers (50, 100, 150, and 200) of generated fitted ellipses for each touching instance were tested to find which number is the suitable one. One thousand touching instances (250 for each grain type) were used for testing.

Table 3.1 Separation accuracy for different numbers of fitted ellipses

The number of fitted ellipses generated for each touching instance	50	100	150	200
Separation accuracy	79%	97.2%	96.4%	98%

Based on the result of table 3.1, a number of 100 generated fitted ellipses for each touching instance was selected, because additional ellipses did not further improve the separation accuracy.

After the fitted ellipses were generated, grouping would be the next step to find the representative ellipses. For each fitted ellipse, l_x, l_y, a, b, and θ are five main parameters, where (l_x, l_y) = center of the ellipse, a = short axis, b = long axis, and θ= orientation of the long axis from the x-axis. These five parameters were dimensions of Euclidean space to determine the difference and similarity of fitted ellipses, to an ellipse identified as a point of this Euclidean space R^5. A distance measure based on the above features space was defined as the Euclidean distance d. Based on threshold of Euclidean distance, all fitted ellipses were grouped to clusters. With each cluster, a representative ellipse was created. Eight hundred touching instance (200 each grain type) were used to find the suitable threshold for clustering. For each touching instance, the representative ellipses for a grain kernel were manually picked and Euclidean distance between these representative ellipses was calculated. The value of Euclidean distance was arranged from 0.52 to 0.87 and around 72% of these calculated Euclidean distances were around 0.58 to 0.65. Therefore, the value of 0.6 was selected as a Euclidean distance threshold for clustering. When it was tested for the grouping, around 91% correct representative ellipses could be selected.

3.10 Neural Network Development

Paliwal et al. (2001) evaluated the most commonly used neural network architectures for cereal grain classification using the frequently used morphological features as inputs. An evaluation of the classification accuracy of 9 different neural network architectures was done to classify five different kinds of cereal grains namely, CWRS wheat, CWAD wheat, barley, oats, and rye. To

evaluate the classification accuracy of the different neural network architectures, images of 7500 kernels (1500 kernels of each grain type) were taken. For each grain kernel, eight morphological features (area, perimeter, major axis, minor axis, two spatial moments, two Fourier descriptors) were extracted as input features for the neural networks. The networks were trained using 70% of the kernels and 20% of kernels for each grain types were used for validation. The remaining 10% kernels were used as test data set. The best results were obtained using a 4-layer back-propagation neural network (BPNN) with each layer connected to immediately previous layer. The classification accuracies were in excess of 97% for CWRS wheat, CWAD wheat, barley and oats. The classification accuracy for rye was about 88%. A general-regression neural network architecture was found to be the least suitable for grain classification.

Based on the above study, a typical four-layer BPNN was selected as the classifier for grain types. A four-layer BPNN consisting of two hidden layers and one output layer was developed for classification of both software separated and physically separated kernel images. The neural network architecture was developed using a commercial software called NeuroShell 2 Version 4 (Ward Systems Group, Frederick, MD). Thirteen input nodes represented 13 input morphological features. Paliwal et al. (2001) stated that one-hidden layer can perform most of the classification tasks, however, it is better to use a two-hidden layer network. More than two-hidden layers may also be used, but it does not increase the efficiency. On the other hand, using more than two-hidden layers may result in a lower accuracy because these networks are more prone to fall

into a local minimum. The number of nodes n in the hidden layer was calculated using the formula:

$$n = (I + O)/2 + y^{0.5} \qquad (3.19)$$

where: I is the number of inputs; O is the number of outputs; and y is the number of input patterns in the training set (Ward Systems Group 1998). Because there were two hidden layers in this neural network, the number of nodes of each hidden layer was the half of the number calculated by the formula. The four outputs nodes corresponded to four grain types. The success of BPNN networks is dependent upon the smoothing factor. The calibration procedure of genetic adaptive was used to decide which smoothing factor was best. It used a genetic algorithm to find appropriate individual smoothing factors for each input and an overall smoothing factor.

Training for BPNN using the genetic adaptive option took place in two parts. The first part trained the network with the data in the training set. The second part used a calibration set to test a whole range of smoothing factors, trying to optimize a combination that works best on the test set with the network created in the first part. Training was stopped after 1500 epochs. An epoch is defined as the time during which a network is trained by presenting each pattern in the training set exactly once. In an earlier study, it was found that 1000 epochs were enough for the network to train as the coefficient of multiple determination became constant around 1000 epochs (Paliwal et al. 2001).

4. DEVELOPMENT OF AN ELLISPE FITTING ALGORITHM FOR SEPARATING TOUCHING GRAIN KERNELS

The algorithm development for this thesis research was programmed using Microsoft Visual C++ (version 6.0) programming language. This algorithm starts by reading the original images of touching grain kernels followed by thresholding, ellipse fitting, separating the touching regions, and outputting the processed images. The various steps of this algorithm are described in this chapter.

4.1 Segmentation and boundary extraction

An adaptive thresholding technique based on R, G, B values of image pixels and hue histograms was used to determine the threshold value (Luo et al. 1999a). After the threshold value was determined, the pixels with gray value higher than threshold were given the value of 1 as objects; others had the value of 0 as background (Fig 4.1.). Therefore, the colour image was transferred to a binary image. If a small dark region within an object fell below the threshold, this region was assigned as background and represents a "hole". With "region growing" to find all inter-connected background pixels, the "holes" were identified and removed.

An object boundary is the closed edge that surrounds a region. If a pixel's neighbors have different values (0 or 1), it may represent an edge point. Because the edge detection operator could find the relationship that a pixel had with its neighbors, the boundary extraction was implemented using edge detection

operator. Compared to other edge detection operators, the Sobel edge detection masks look for edges in both the horizontal and vertical direction with high efficiency (Gonzalez and Woods 1992). Therefore, the object edge pixels were tracked by Sobel edge and stored in an ordered points list. This ordered points list could be used as sample points for ellipse fitting. The edge tracking result is shown in Fig 4.2.

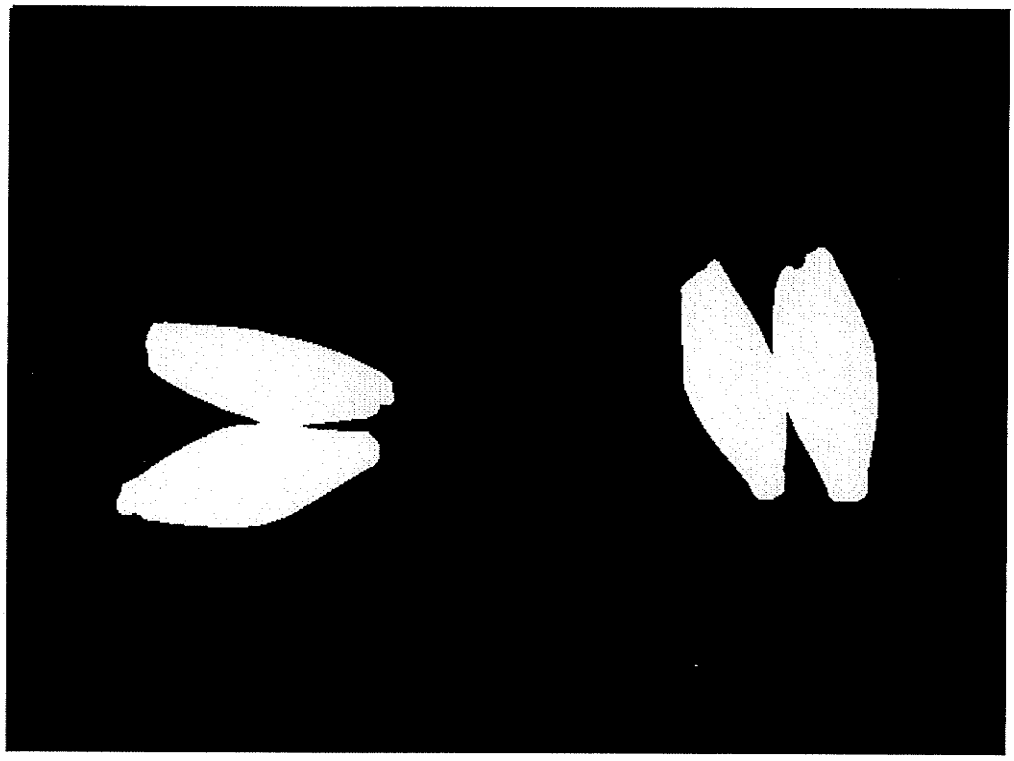

Figure 4. 1 The touching grain kernels (CWAD Wheat)

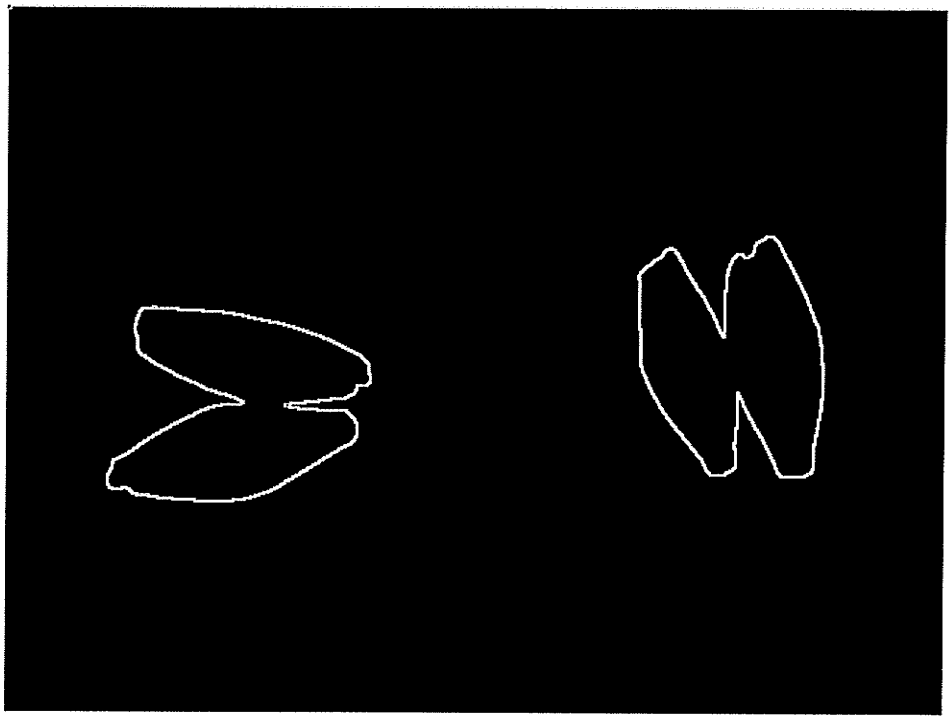

Figure 4. 2. Image after edge tracking for grain kernels shown in Figure 4.1.

4.2 Ellipse fitting

When grain "touching instances" in the image had been thresholded, the touching region cannot be split. The touching instance with multiple grain kernels was then considered as one object in the binary image. Since the grain kernels in the image are similar to an ellipsoidal shape, to separate the touching kernels, an ellipse fitting algorithm was implemented to approximate every kernel.

The direct least squares based ellipse-fitting method was used for the ellipse fitting in this algorithm. This method centers on finding the set of parameters that minimize some distance measure between sample data points and the ellipse.

An ellipse is a conic that can be described by an implicit second order polynomial.

$$F(x, y) = ax^2 + bxy + cy^2 + dx + ey + f = 0 \qquad (4.1)$$

With an ellipse-specific constraint.

$$b^2 - 4ac < 0 \qquad (4.2)$$

where *a, b, c, d, e, f* are coefficients of the ellipse and (*x, y*) are coordinates of sample points lying on it. The polynomial *F*(*x, y*) is called the *algebraic distance* of a point (*x, y*) to the conic *F*(*x, y*)=0. By introducing vectors

$$\boldsymbol{a} = [a, b, c, d, e, f]^T$$

$$\boldsymbol{x} = [x^2, xy, y^2, x, y, 1] \qquad (4.3)$$

The equation (4.1) can be rewritten to the vector as:

$$F_a(x) = \mathrm{x} \bullet \mathrm{a} = 0 \qquad (4.4)$$

The fitting of a general conic to a set of sample points (x_i, y_i), $i = 1...N$ may be approached by minimizing the sum of squared algebraic distances of the data points to the conic which is represented by coefficients **a**:

$$\min\left(\sum_{i=1}^{N} F(x_i, y_i)^2\right) = \min\left(\sum_{i=1}^{N} (\mathrm{x}_i \bullet \mathrm{a})^2\right) \qquad (4.5)$$

Equation 4.5 can be solved directly by the standard least squares approach. However, without constraint, the result of standard least square fitting could be any general conic, such as hyperbolas, and parabolas.

To ensure an ellipse-specificity of the solution, the appropriate constraint of equation 4.2 had to be considered. Under a proper scaling, the inequality constraint of equation 4.2 could be transferred into an equality constraint (Fitzgibbon et al. 1996)

$$4ac - b^2 = 1 \qquad (4.6)$$

This constraint could be expressed as $\mathbf{a}^T\mathbf{C}\mathbf{a} = 1$, where *constraint matrix* **C** is of the size 6 x 6.

$$C = \begin{bmatrix} 0 & 0 & 2 & 0 & 0 & 0 \\ 0 & -1 & 0 & 0 & 0 & 0 \\ 2 & 0 & 0 & 0 & 0 & 0 \\ 0 & 0 & 0 & 0 & 0 & 0 \\ 0 & 0 & 0 & 0 & 0 & 0 \\ 0 & 0 & 0 & 0 & 0 & 0 \end{bmatrix} \tag{4.7}$$

Then, the ellipse-specific fitting problem can be reformulated as

Minimizing $E=\|\mathbf{D}\mathbf{a}\|^2$ subject to $\mathbf{a}^T\mathbf{C}\mathbf{a} = 1$ (4.8)

Where the *design matrix* **D** of the size N x 6

$$D = \begin{bmatrix} x_1^2 & x_1 y_1 & y_1^2 & x_1 & y_1 & 1 \\ \vdots & \vdots & \vdots & \vdots & \vdots & \vdots \\ x_i^2 & x_i y_i & y_i^2 & x_i & y_i & 1 \\ \vdots & \vdots & \vdots & \vdots & \vdots & \vdots \\ x_N^2 & x_N y_N & y_N^2 & x_N & y_N & 1 \end{bmatrix} \tag{4.9}$$

represents the least squares minimization equation 4.5.

The minimization problem (equation 4.8) could be solved by a quadratic constrained least squares minimization. By applying the Lagrange multipliers, the following conditions for the optimal solution **a** could be calculated

$$\mathbf{S}\mathbf{a} = \lambda\mathbf{C}\mathbf{a}$$

$$\mathbf{a}^T\mathbf{C}\mathbf{a} = 1 \tag{4.10}$$

where **S** is the *scatter matrix* of the size 6 x 6

$$\mathbf{S} = \mathbf{D}^T\mathbf{D} \tag{4.11}$$

Equation 4.10 could be solved by applying generalized eigenvectors. Six eigenvalue-eigenvector pairs (λ_j , $\mathbf{a}_j$) were given by the equation 4.10. Because

$$\|Da\|^2 = a^T D^T Da = a^T Sa = \lambda a^T Ca = \lambda \qquad (4.12)$$

The eigenvector $\mathbf{a}_k$ corresponds to the minimal positive eigenvalue λ_k. With a proper scaling, the solution of the minimization problem (equation 4.8) represents the best-fit ellipse for the given set of points.

Because direct ellipse fitting is robust to the noise and offered the best trade off between speed and accuracy (Fitzgibbon et al. 1996), it was applied to generate the fitted ellipse in this algorithm. The example of generated ellipses are shown in Fig 4.3.

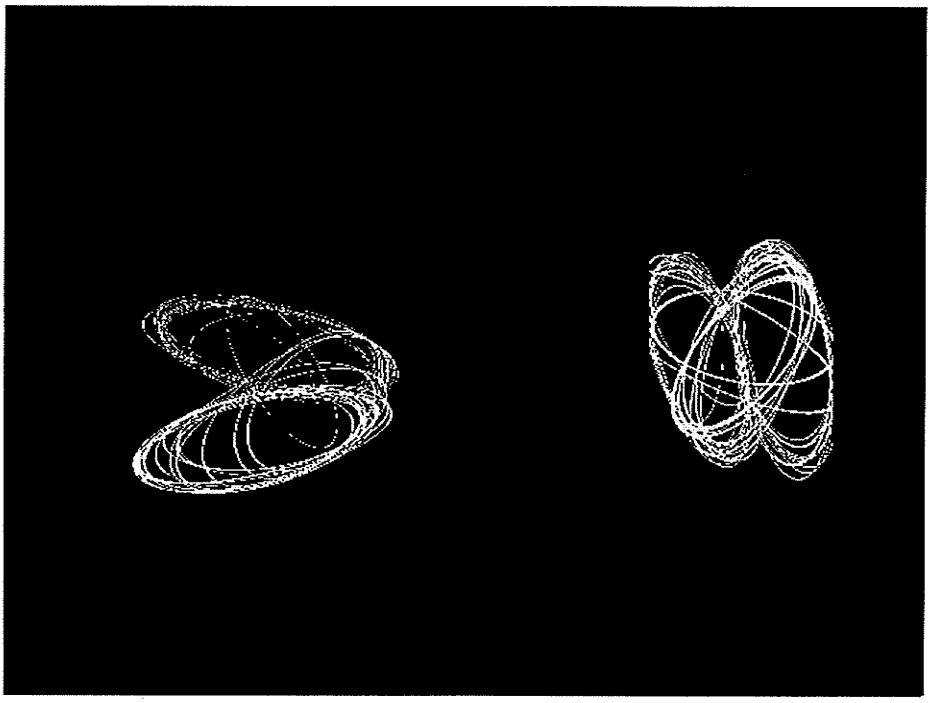

Figure 4. 3. Finding fitted ellipses for the touching instances in Figure 4.1.

4.3 Classifying all generated ellipses to determine the representative fitted ellipse for each kernel

Every trial of the ellipse fitting procedure created an inertial ellipse for the touching kernel groups. For a particular group of touching kernels, 100 fitted ellipses were generated. When a set of similar representative ellipses for every individual kernel in the touching group were generated, some extraneous ellipses were also generated and were excluded. With all filtered generated ellipses, a clustering method was applied to group all fitted ellipses and extract the representative ellipse for each group. This algorithm involved three steps.

4.3.1 Excluding inappropriate fitted ellipses

When all inertial fitted ellipses were created, two selected criteria were applied to eliminate inappropriate fitted ellipses. These criteria were:

- All fitted ellipses must meet $a1 < a/b < a2$, where a is the short axis of the ellipse, b is the long axis of the ellipse. After numerous trials to different types of kernels, the threshold $a1$ was determined as 0.3, and the threshold $a2$ was determined as 0.9.
- The measurement of overlap between the touching object and fitted ellipse were also limited as:

$$\xi = \frac{\omega \cap \varepsilon}{\varepsilon}$$

where ω is the set of touching object pixels, ε is the set of pixels of the fitted ellipse. If the ξ >0.95, the fitted ellipse is a proper by fitted ellipse.

With these two criteria, only those fitted ellipses similar to the original grain kernels were picked.

4.3.2 Features extraction for clustering

Clustering is the organization of a collection of patterns into groups based on similarity (Jain and Dubes 1988). Features extraction is to obtain an appropriate set of features for clustering. In fitted ellipse clustering, if each cluster only contained the ellipses similar to one individual grain kernel, the filtered ellipses could be grouped to clusters to determine the kernel numbers in the touching instance. For each fitted ellipse, l_x, l_y, a, b, and θ are five main parameters, where (l_x, l_y) = center of the ellipse, a = the short axis of the ellipse, b = the long axis of the ellipse, and θ= orientation of the long axis from the x-axis. With these five parameters, the difference and similarity of fitted ellipses could be determined. Because the similarity of ellipses is the fundamental for defining a fitted ellipse cluster, these five parameters were used as clustering features.

When each parameter of an ellipse was considered as a dimension of Euclidean space, that ellipse could be identified as a point of this Euclidean space R^5. To measure the similarity between two fitted ellipses, a distance measure based on the above features space was applied and the distance between two ellipses was defined as the Euclidean distance d.

4.3.3 Clustering

The clustering was based on the minimization of a performance index, which was defined as the sum of Euclidean distances from all patterns in a cluster

domain to the cluster center. With this performance index, the related patterns can be grouped to one cluster. This procedure consisted of the following steps.

1. For two ellipses, x_i and x_j , if $d(x_i, x_j) < \delta$, these two ellipses were considered one cluster, where δ is a threshold determined by many trials. When all ellipses were classified, *K* initial clusters were generated. With each cluster, the cluster center $z_j(k)$ was obtained by: $Z_j(k) = \frac{1}{n}\sum_{i=1}^{n} x_i$ where n is the number of ellipses in each cluster. If one cluster only had a few ellipses that were less than five, this cluster was considered as an inappropriate ellipse cluster and excluded.
2. The ellipses {x} were distributed among the *K* cluster domains, using the relation,

$$x \in S_j(k) \quad \text{if} \quad \|x - z_j(k)\| < \|x - z_i(k)\| \qquad (4.13)$$

for all $i=1,2, \ldots, K$, $i \neq j$, where $S_j(k)$ denotes the set of ellipses, with cluster center as $z_j(k)$.

3. From the result of the above step, the new cluster center $z_j(k+1)$ ($j=1,2, \ldots, K$) was computed. The sum of the squared distances from all patterns in $S_j(k)$ to the new cluster center was minimized. Therefore, the new cluster center is given by:

$$z_j(k+1) = \frac{1}{N_j} \sum_{x \in S_j(k)} x \qquad i=1, 2, \ldots, K, \qquad (4.14)$$

where the N_j is the number of patterns in $S_j(k)$.

4. If $z_j(k+1)=z_j(k)$ for *i=1, 2, ... , K*, the algorithm had converged and the procedure was terminated. Otherwise, the algorithm went back to step 2.

In the end, the sets of clusters were built up and the center pattern of each cluster was the representative ellipse for that cluster. When representative ellipse had been assigned to each cluster, every kernel of the touching grain group was replaced by a fitted ellipse. Moreover, when these representative ellipses were generated, these fitted ellipses were not allowed to touch each other. If they had joint area with other kernels, the pixels of this area would be turned "off" as the background. An example of representative ellipses is shown in Fig 4.4.

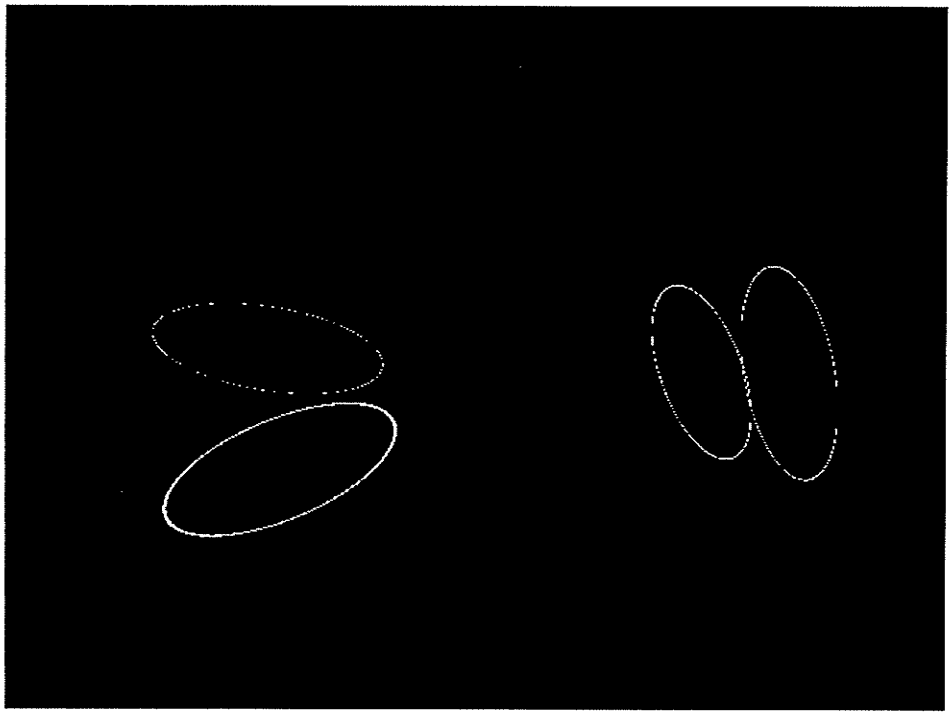

Figure 4. 4. Finding the representative fitted ellipses for touching kernel instances of Figure 4.1.

4.4 Using mathematical morphological method to create the sequential thickening regions

After every representative ellipse for each kernel of a touching case was determined, a mathematical morphological method was used to dilate the fitted ellipses. During the dilation, these dilated ellipses were not allowed to join each other.

This method was used to grow the ellipse and prevent the neighboring expanding components from joining together. This operation applied a mixed structuring element, L=(I_1, I_2). This structuring element is (Serra 1982):

$$\begin{matrix} I_2 & I_2 & I_2 \\ * & I_2 & * \\ I_1 & I_1 & I_1 \end{matrix}$$

That is, only those pixels are included in the hit-or-miss transform of an image with mixed structuring element, L, where simultaneously the I_1 locations hit the foreground of the image and I_2 locations miss the foreground. For a pixel, if, with eight of its neighbors, at least three neighbors as defined by I_1 locations are "on" and at least three other neighbors as defined by I_2 locations are "off", this pixel was turned "on". For sequential thickening, the above configuration of the structuring element, L, and seven other rotation of this grid were used. This logic imposed during growing the fitted ellipses prevented their merger. Sequential thickening was repeated one hundred times for each fitted ellipse to make sure the dilating regions were big enough to cover the silhouette of the original kernels. The example of dilation is shown in Fig. 4.5.

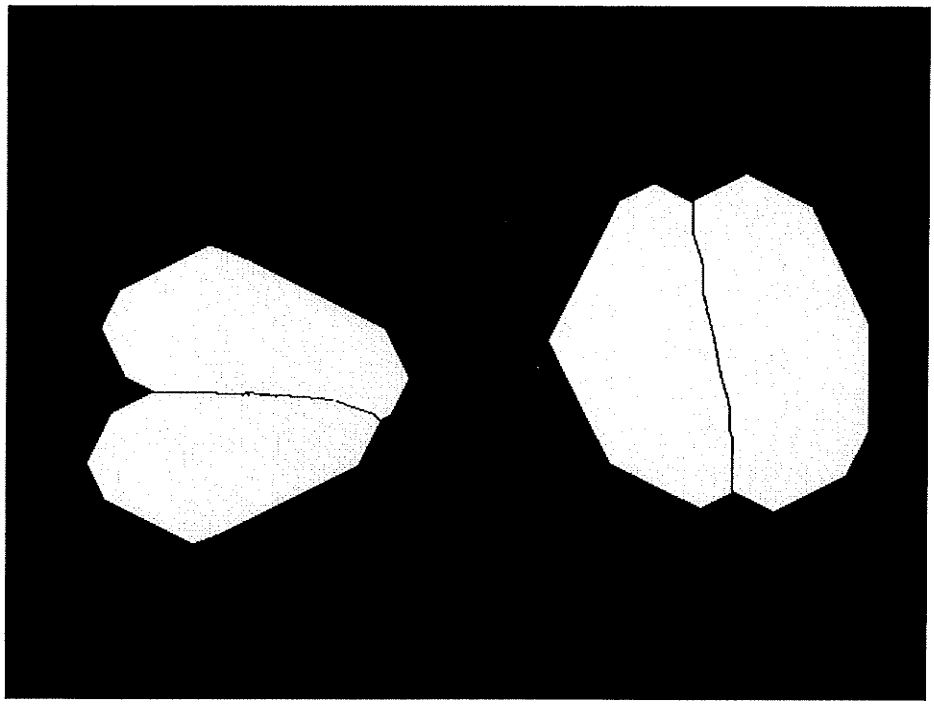

Figure 4. 5. Fitted ellipse dilation

4.5 Using logic "AND" with the detached image and original image to separate the touching grain kernel regions

After dilation, the dilated ellipses can cover the silhouette of the grain kernel of the touching groups. Because all these dilated ellipses are separated, using the logic "AND" with dilated ellipses and the original touching group, the touching isthmus between the kernels were identified, and the clusters of touching kernel regions in the image were separated. The separation result is shown in Figs 4.6 and 4.7.

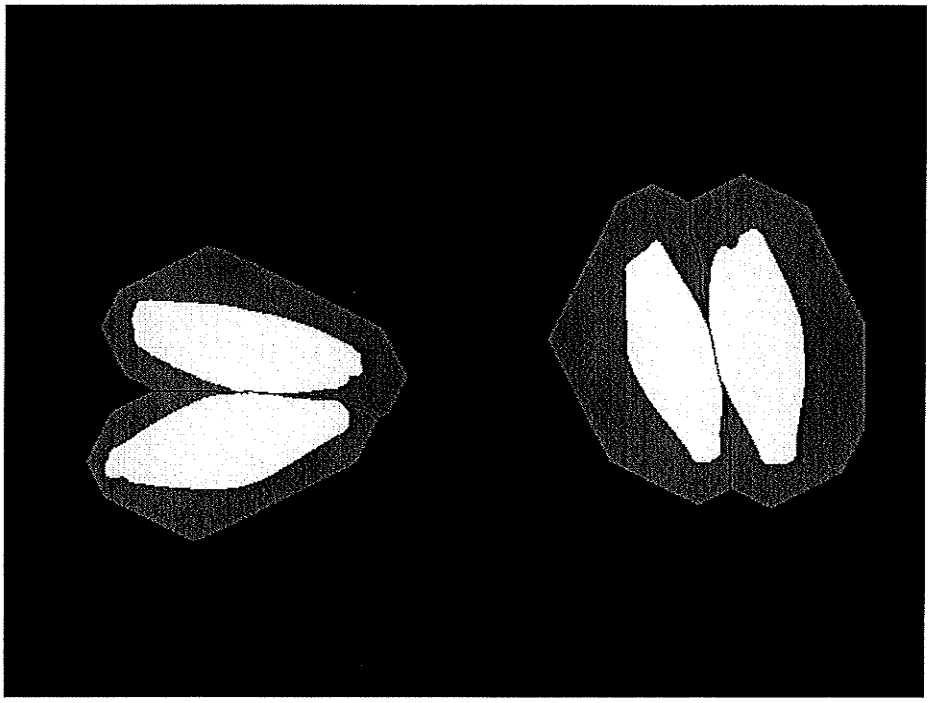

Figure 4. 6. Image morphological logic with grain kernels.

Figure 4.7. Software separated grain kernels shown as touching in Figure 4.1.

4.6. Assessing the capability of the separation algorithm

To assess the classification capability after software separation, a back-propagation neural network (BPNN) was employed in grain type classification based on morphological features. A three-layer neural network was developed with 13 input nodes for 13 morphological features, 16 hidden layer nodes, and one output node for each of the four grain types (CWRS wheat, CWAD wheat, barley and oats). The network used logistic scaling and activation functions at input and processing levels, respectively. Eight thousand physically separated kernels (2000 kernels of each grain type) were used for training and testing the neural network, and 8000 software-separated kernels (2000 for each grain type) were used for assessing the effect of software separation on classification accuracy. The experiments for the neural network training and testing were repeated three times. Each time, the 2000 physically separated kernels of each grain type were divided into two parts, 1000 physically separated kernels of each grain type were randomly selected for training the neural network, another 1000 remaining physically separated kernels were used for testing. This trained neural network was then applied to production data sets of software separated kernels. The production data sets were 4000 software separated kernels (1000 kernels randomly selected for each grain type).

5. RESULTS AND DISCUSSIONS

5.1 Effectiveness of the Separation Algorithm

The separation algorithm was applied to the images of touching kernels of CWRS wheat, CWAD wheat, barley and oats. For each grain type, 1000 touching cases were tested and the effectiveness of the separation algorithm in separating the touching kernels was determined. A representative collection of software-separated images is given in Appendix A. In general, the unsuccessful separated touching grain kernels can be visually identified. However, some small distortions of grain regions after software separation could be introduced and may affect the value of extracted morphological features. After the grain kernels were separated, each separated kernel was processed to extract features for identification. If the morphological features were distorted during separation, the identification of the grain kernel would not be accurate. Therefore, the difference in morphological features between software separated and physically separated kernels were compared to test the effectiveness of the separation algorithm.

5.2 The results of software separation

For software separation, any case of touching kernels, which were not separated or were distorted by improper placement of the separation lines, were considered unsuccessfully separated cases or kernels. For separation algorithm evaluation, one separation error is considered as an unsuccessful separation for the touching case with 2 or 3 touching kernels. The success rate in separating all

grain touching cases by visual inspection was 97.3% for CWRS wheat, 92.4% for barley, 96.1% for CWAD, and 94.8% for oats. Some of the separation results are illustrated in Figs. 5.1 to 5.4.

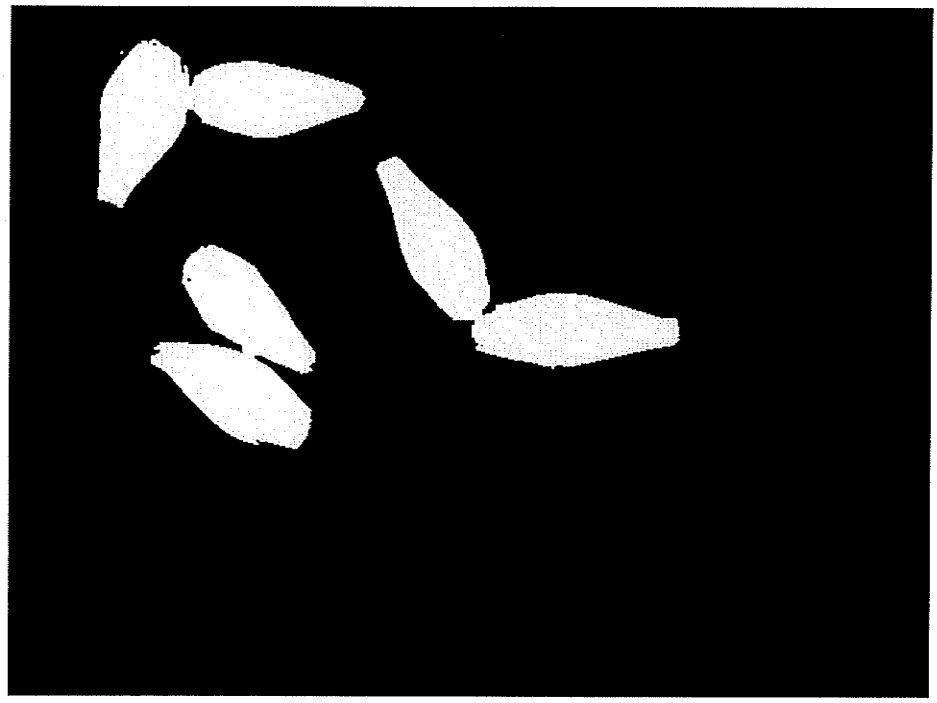

Figure 5. 1. (a) Touching barley kernels

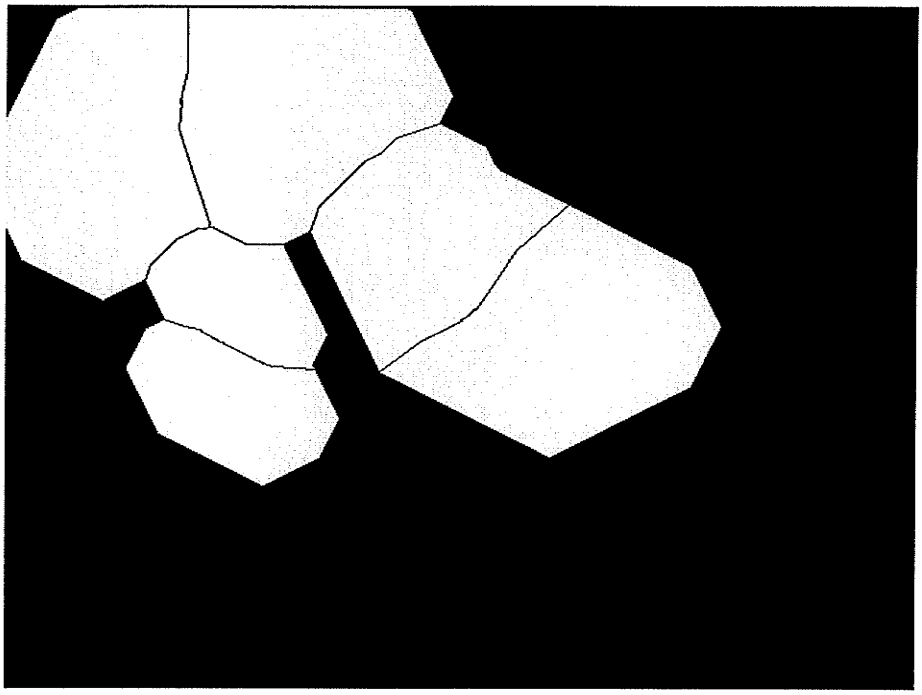

Figure 5.1. (b) Fitted ellipse dilation of barley kernels

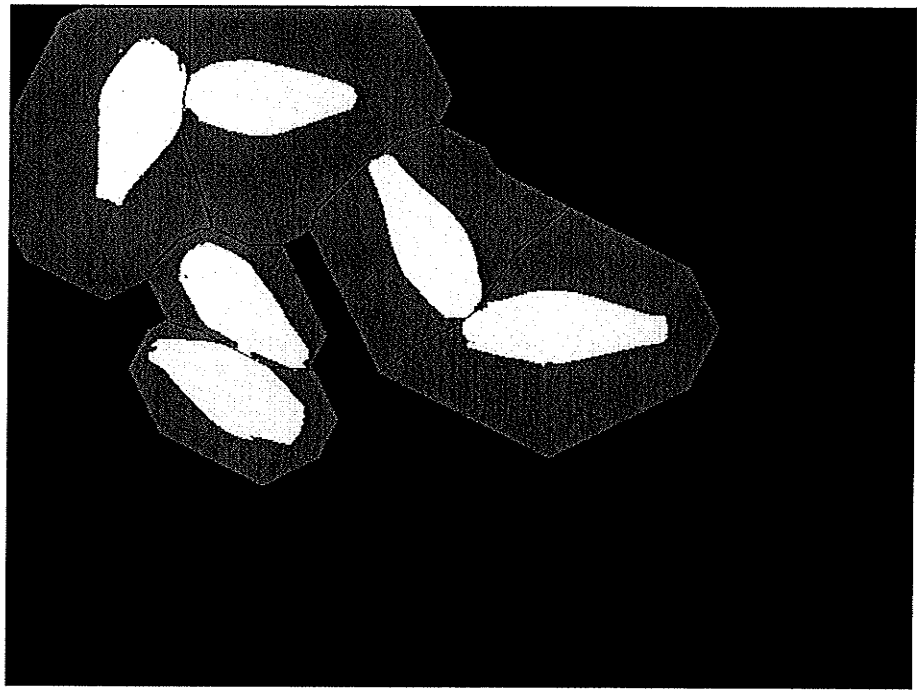

Figure 5. 1. (c). Image mathematical logic for barley kernels

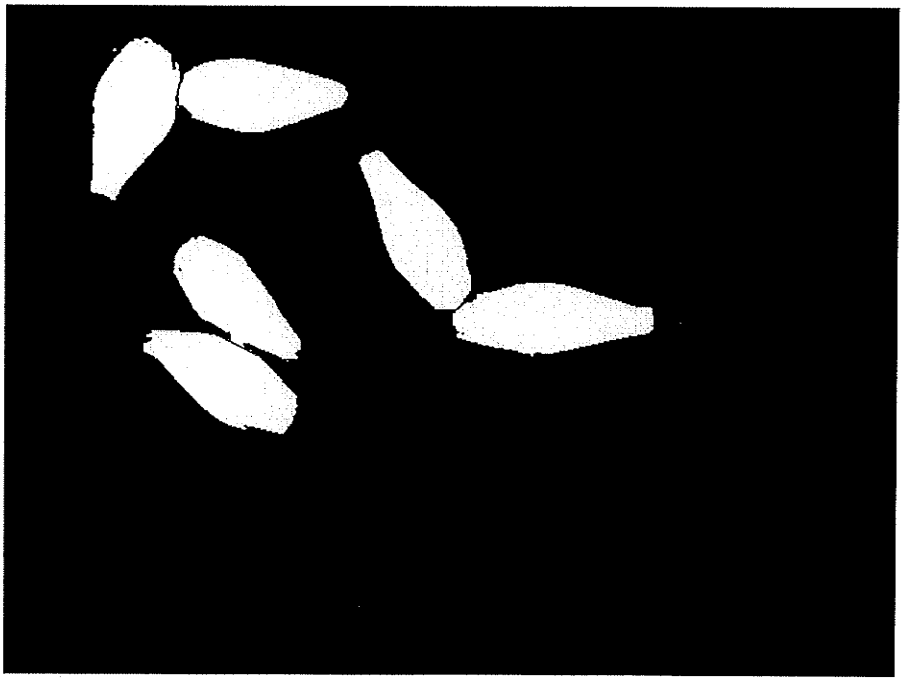

Figure 5. 1. (d) Software separated barley kernels

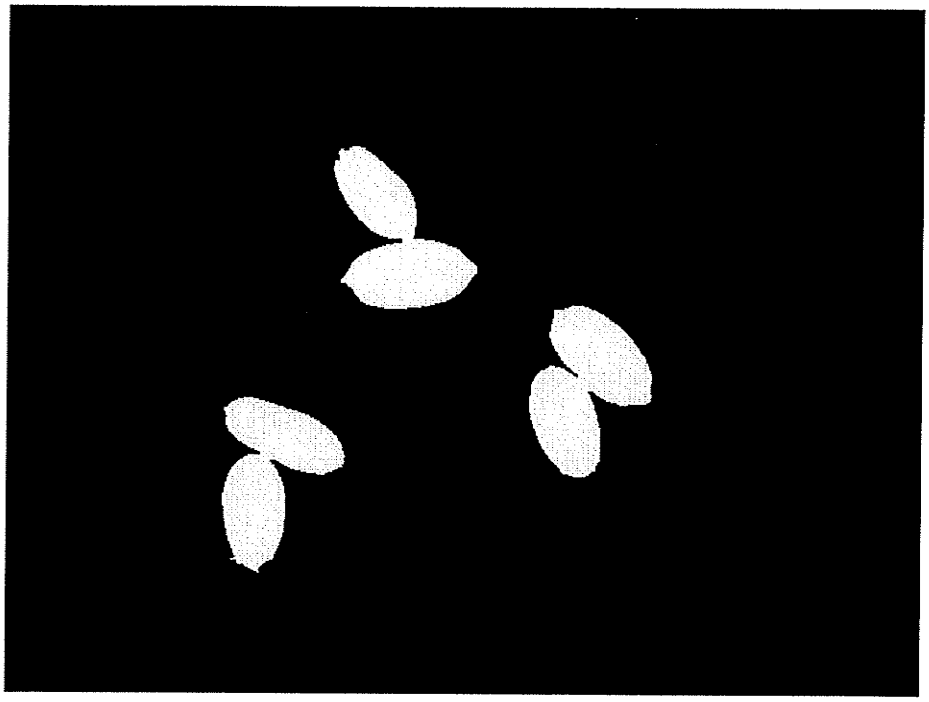

Figure 5.2. (a) Touching CWRS wheat kernels

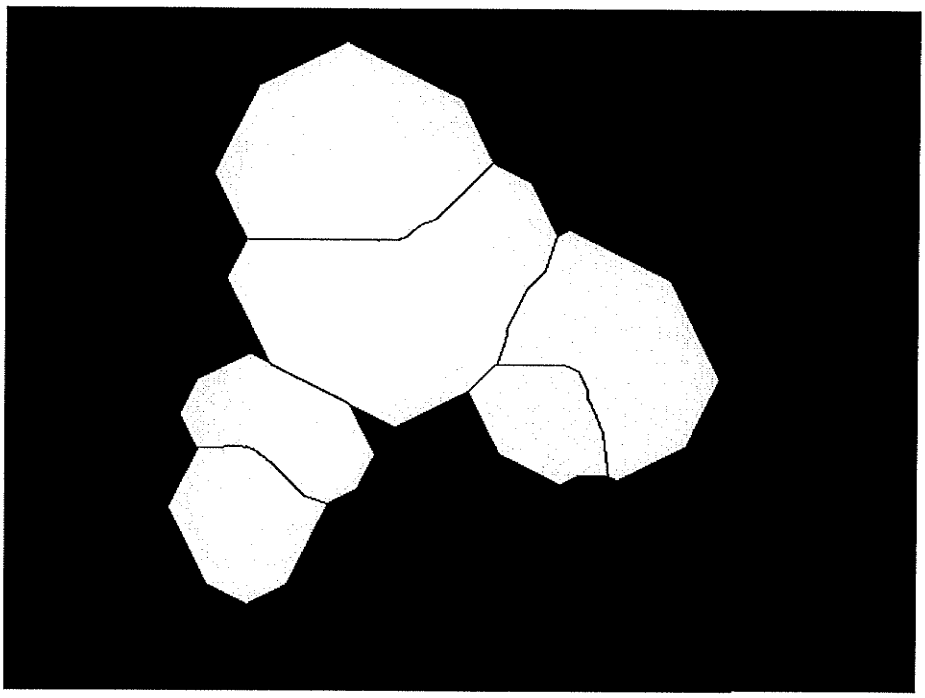

Figure 5.2 (b) Fitted ellipse dilation of CWRS wheat kernels

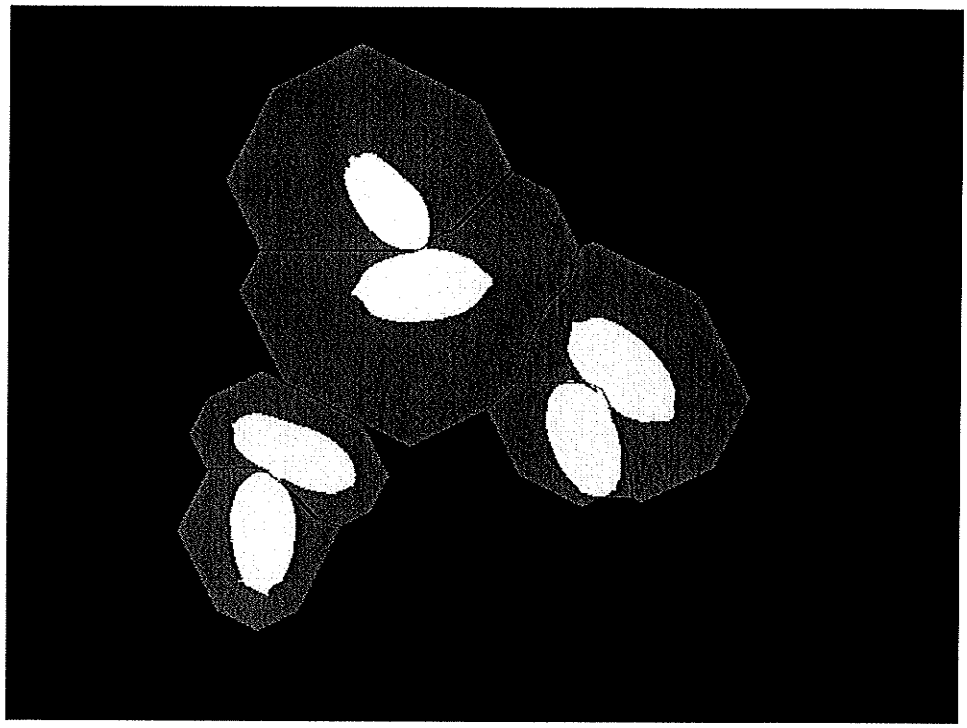

Figure 5.2. (c) Image mathematical logic for CWRS wheat kernels

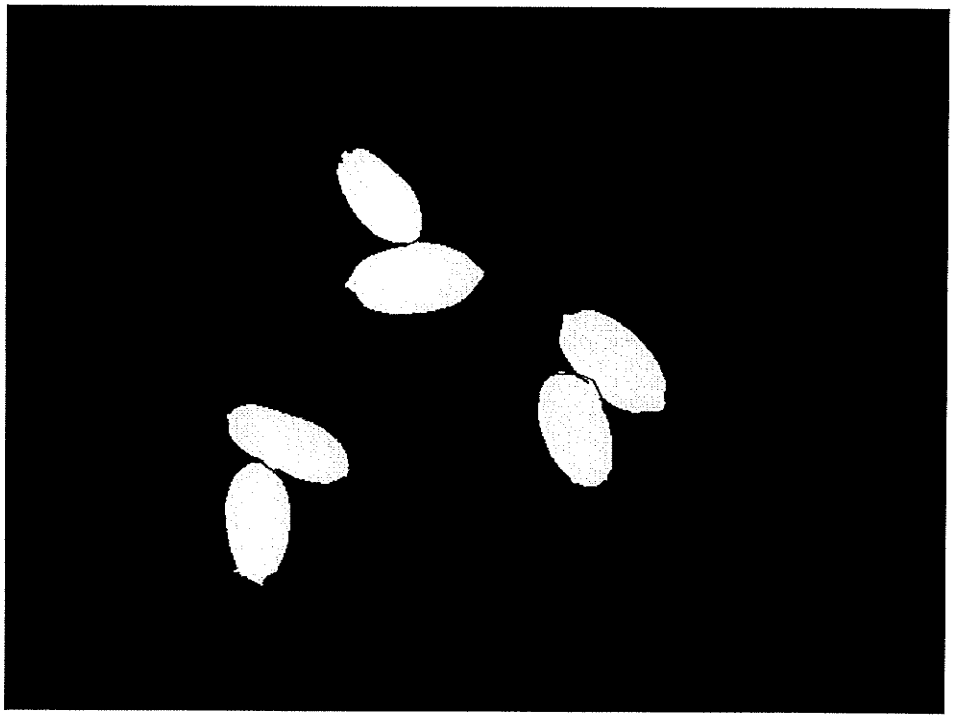

Figure 5.2. (d) Software separated CWRS wheat kernels

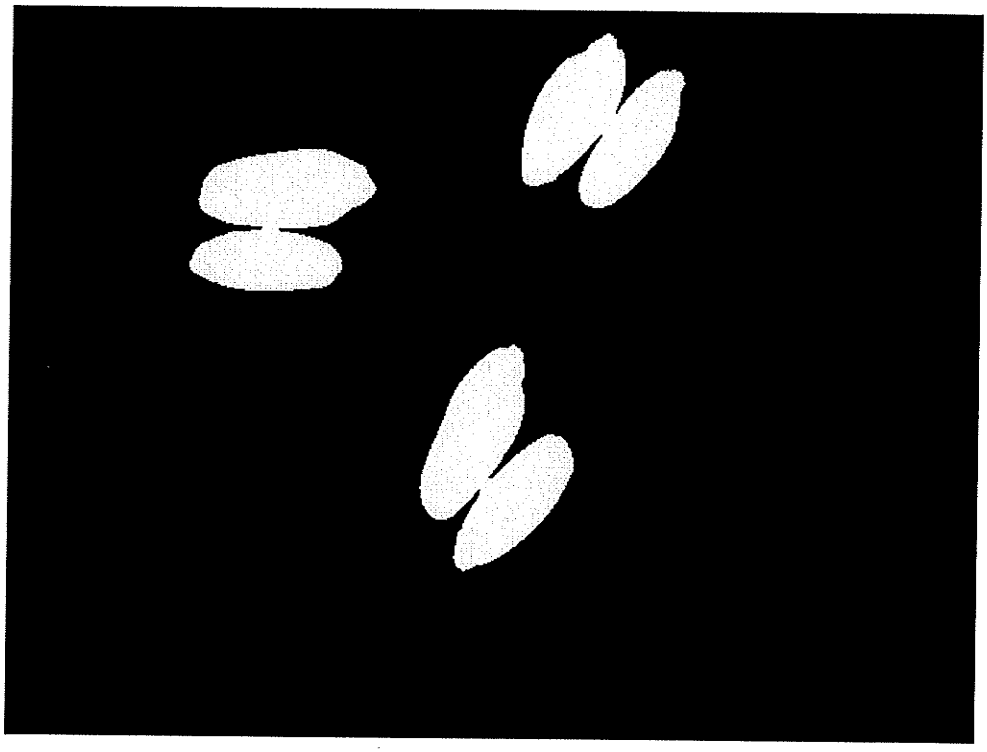

Figure 5. 3. (a) Touching CWAD wheat kernels

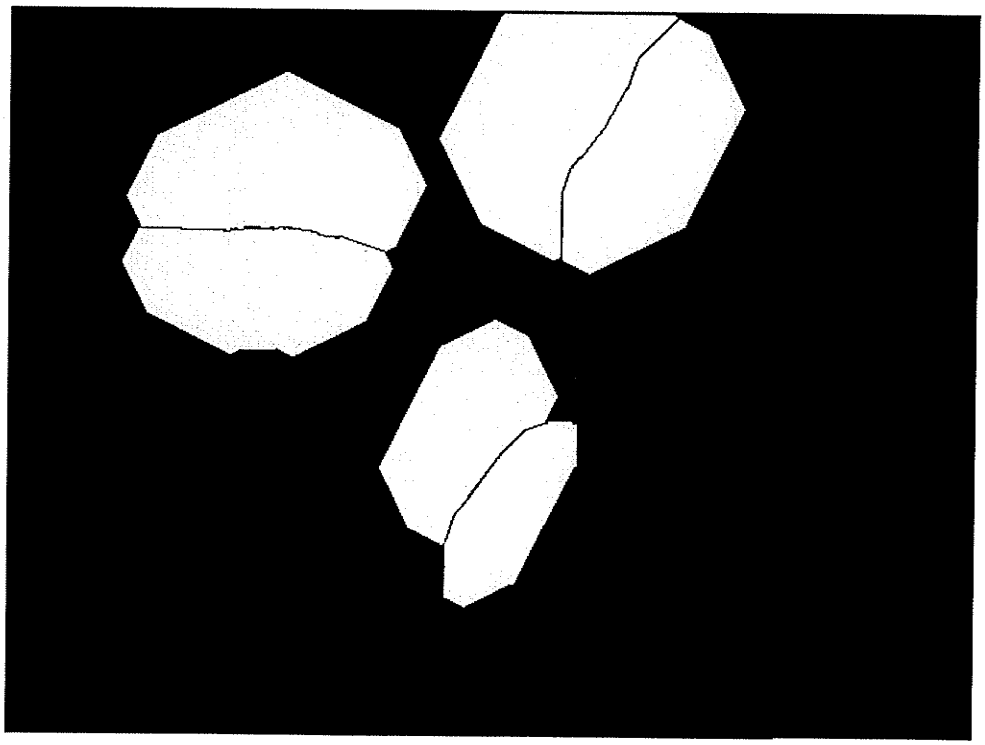

Figure 5.3. (b) Fitted ellipse dilation of CWAD wheat kernels

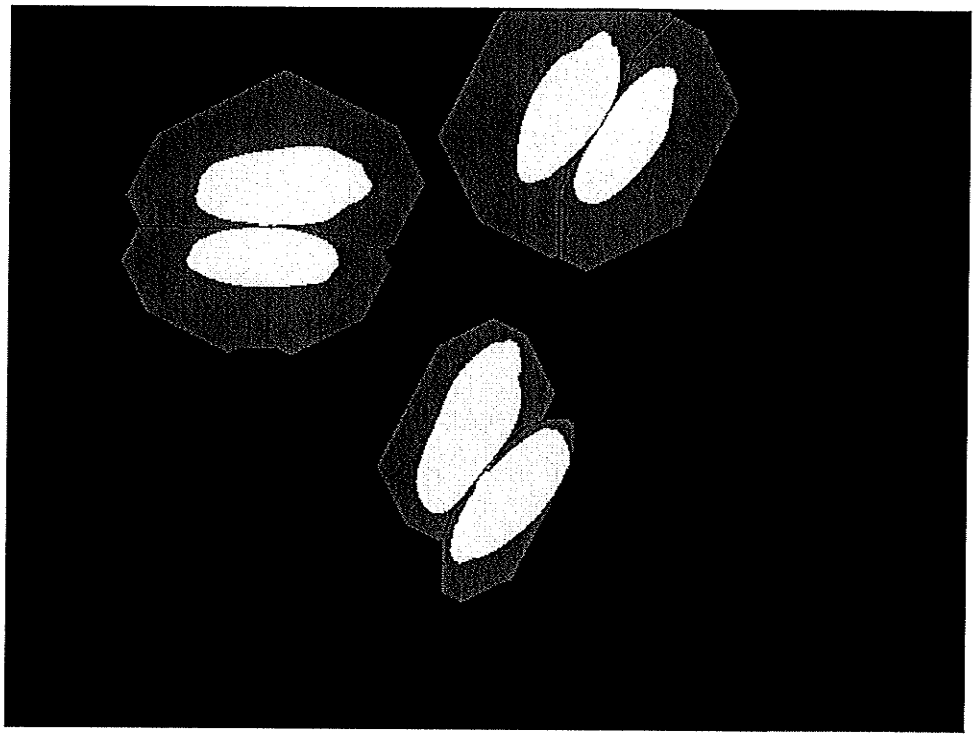

Figure 5.3. (c) Image mathematical logic for CWAD wheat kernels

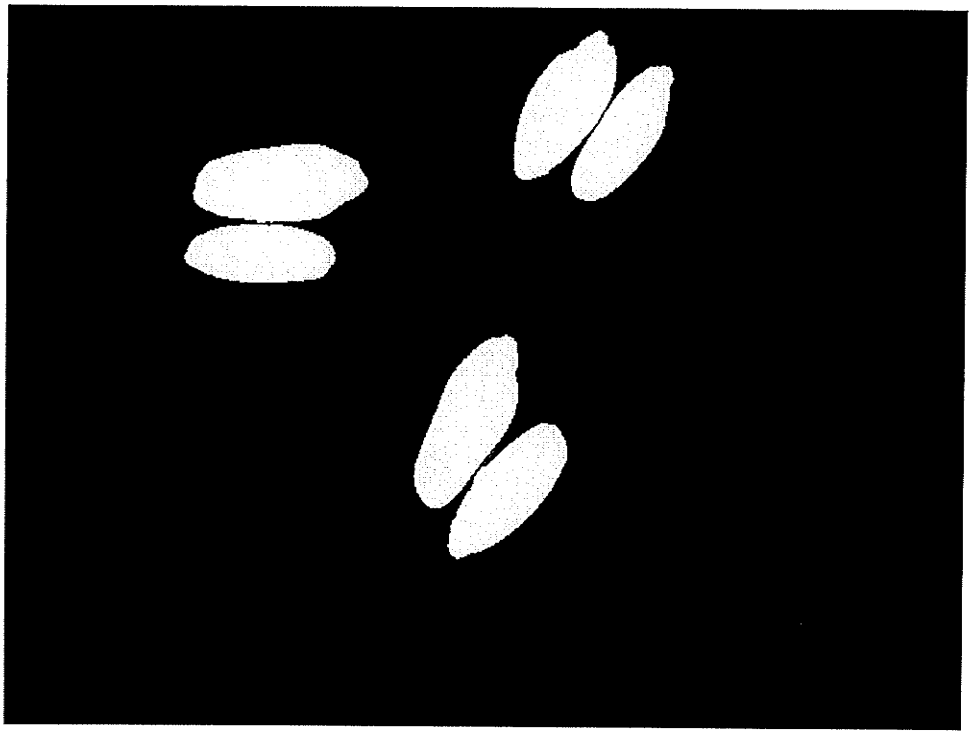

Figure 5.3. (d) Software separated CWAD wheat kernels

Figure 5.4. (a) Touching oat kernels

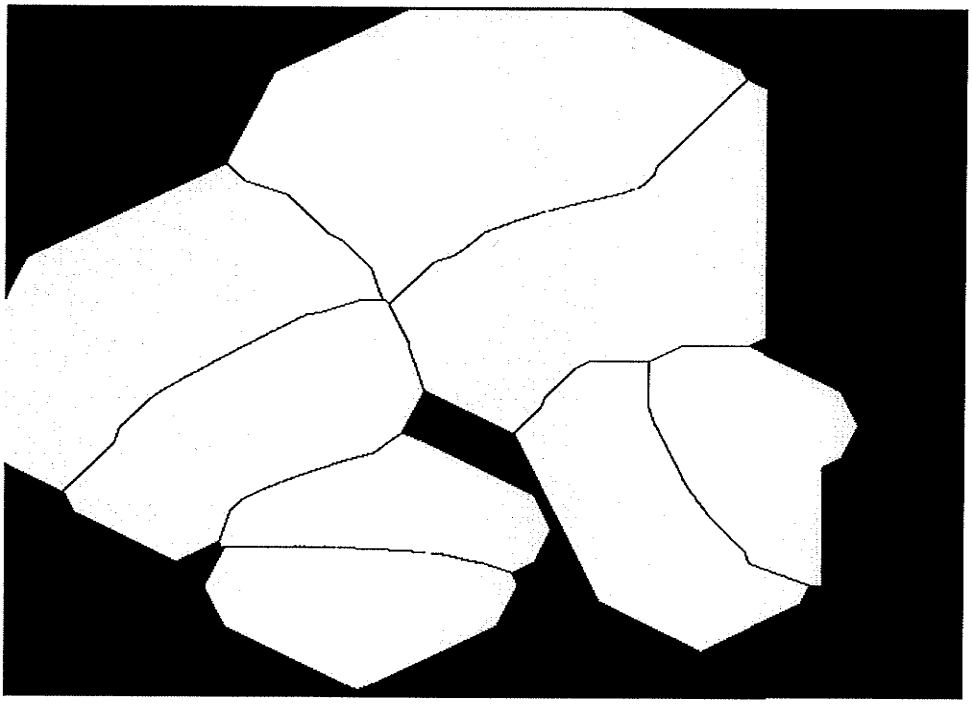

Figure 5.4. (b) Fitted ellipse dilation of oat kernels

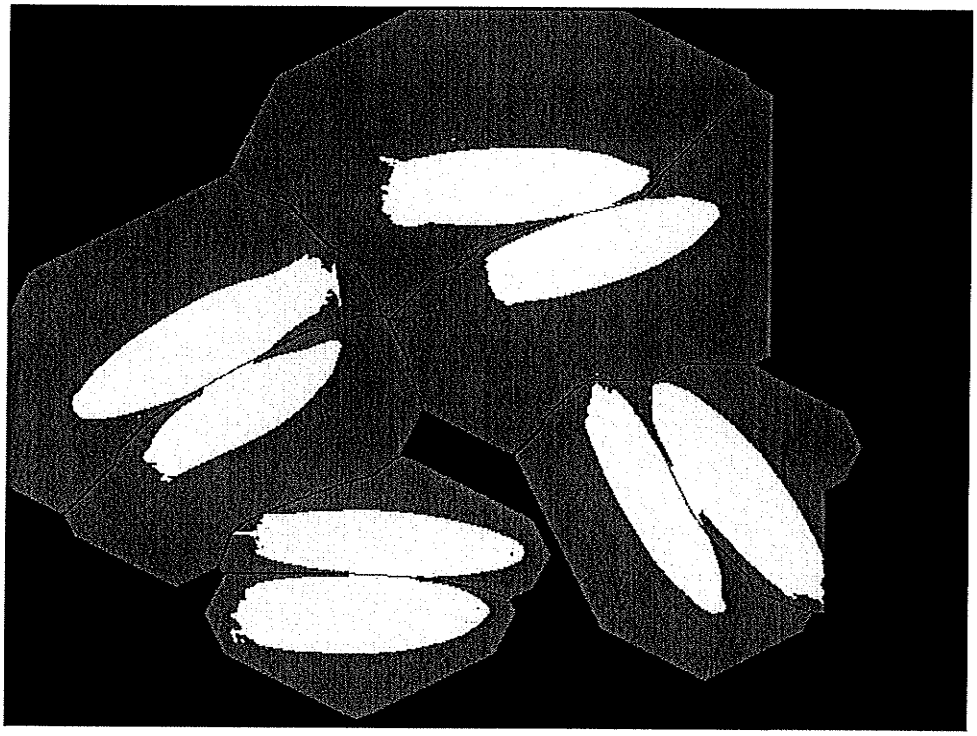

Figure 5.4. (c) Image mathematical logic for oat kernels

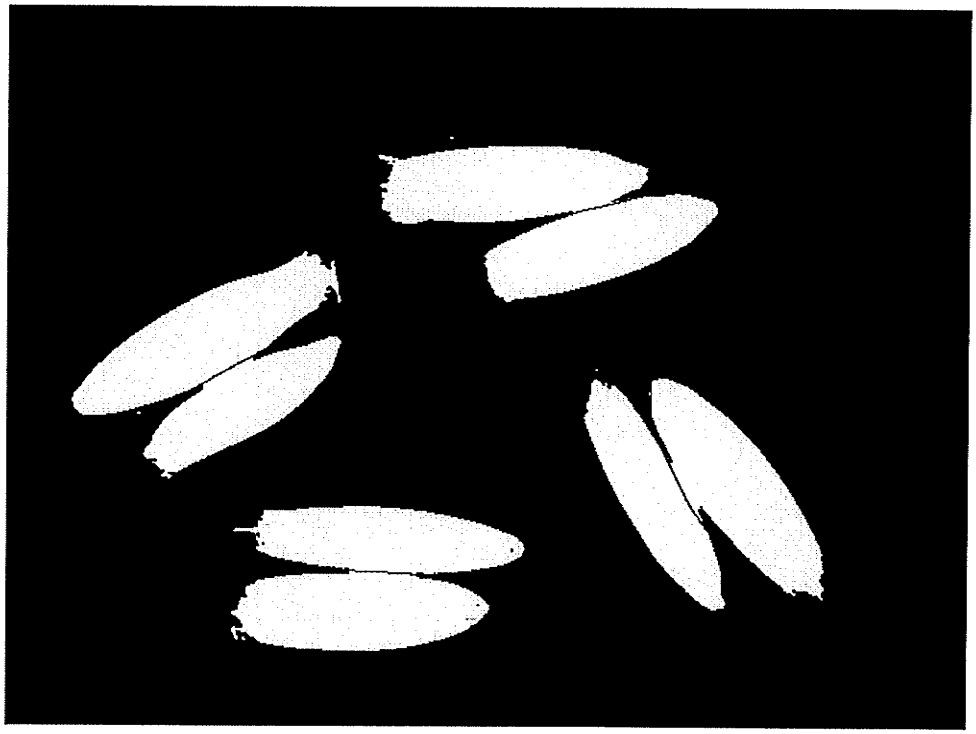

Figure 5.4. (d) Software separated oat kernels

When the mathematical morphological separating algorithm (Shatadal et al. 1995a, b) was applied to the touching cases of long ellipsoid kernels with a longer isthmus area, like oats, it often failed because of over erosion. With the ellipse fitting algorithm, this problem was solved by using a fitted ellipse to isolate the isthmus area. Therefore, the ellipse fitting algorithm performed better in separating the touching oat kernels with 94.8% accuracy, compared to 79% separation accuracy with the mathematical morphological based separation algorithm of Shataldal et al. (1995a).

The ellipse fitting algorithm also had some limitations. During the separation process, if the representative ellipses were improperly selected by the clustering, the separation line could not be placed correctly. Figure 5.5 shows the separation line was placed within a kernel region rather than at the isthmus. This happened because one representative ellipse was too small during dilation. The bigger fitted ellipse dilated too much to set the separation line at the kernel region instead of the isthmus. The separation success rate for barley kernels was lower because some barley kernels were not approximated as ellipsoids. For those kernels with irregular shape, some improperly fitted ellipses were filtered during overlap measurement. However, some smaller improperly fitted ellipses may have passed the overlap filter and clustered to the representative ellipse. This would cause the separation line to move toward the smaller fitted ellipse during dilation and place the separation line within the kernel region.

Another limitation for this ellipse fitting algorithm was that, sometimes the separation line could not be placed exactly at the isthmus, and might be a little out of range and distort the part of the touching boundary (Fig. 5.6). This limitation would change the value of the Fourier transcript, because it representes the boundary features of the kernel. This distortion of the value of the Fourier transcript only became effective when kernels had irregular shapes.

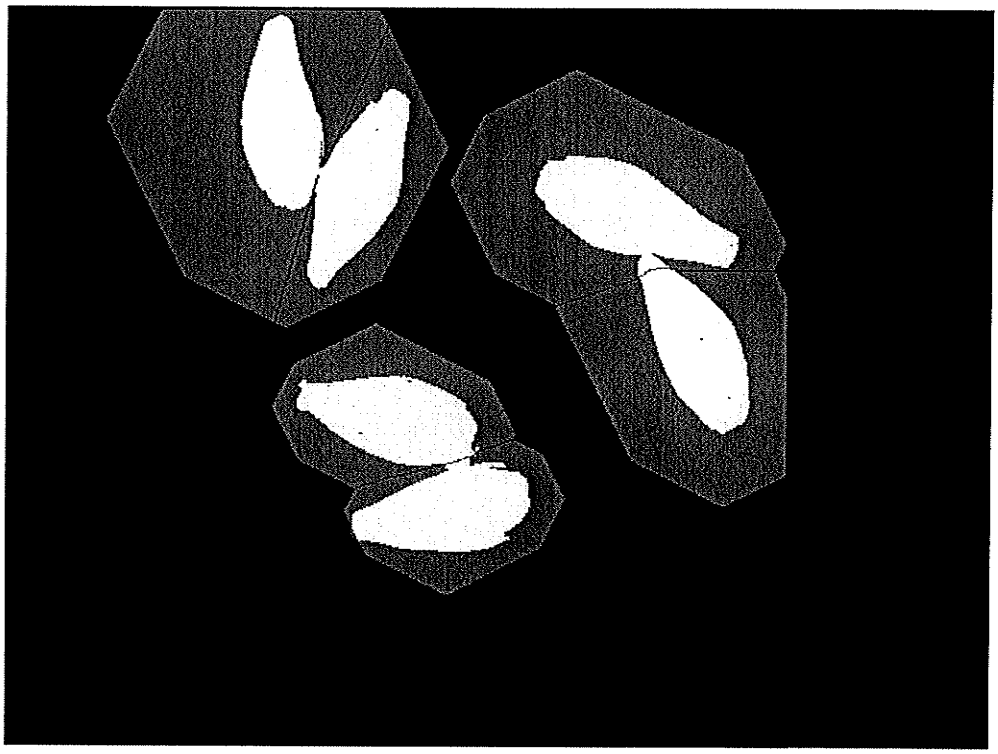

Figure 5.5. (a) Improper placement of the separation lines

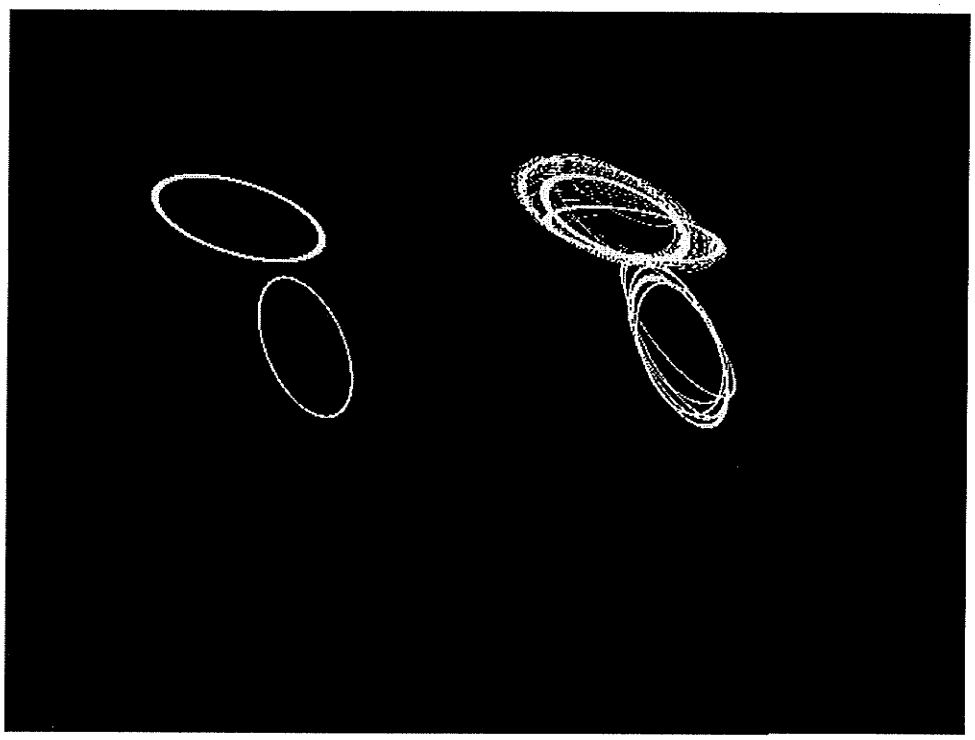

Figure 5.5. (b). Fitted ellipses (right). Improper representative ellipse selection (left)

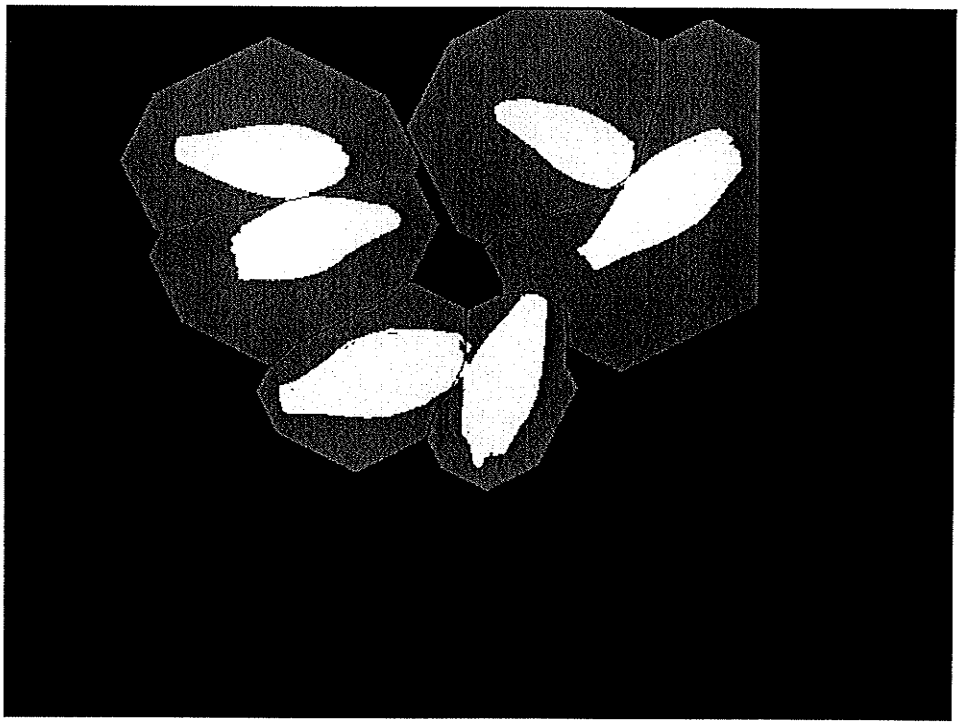

Figure 5.6. Separation line distorting the touching part of the kernel boundary

5.3 Morphological Features Selections

The physical dimensional measures that characterize the appearance of an object are called morphological features in the image. Majumdar and Jayas (2000a) developed an algorithm based on morphological features to classify individual kernels of CWRS wheat, CWAD wheat, barley, oats, and rye. Forty three morphological features were extracted for the discriminate analysis. When the morphology model with the 10 most significant morphological features was tested, the classification accuracies of CWRS wheat, CWAD wheat, barley, oats, and rye were 98.9, 93.7, 96.8, 99.9, and 81.6%, respectively. In their morphological features model, several of the morphological features are derived from a select number of basic features. Assessment of changes to the basic features can give a good idea whether software separation affects morphological features. Therefore, 13 morphological features were picked to assess the separation algorithm: Area, Perimeter, Maximum Radius, Minimum Radius, Mean Radius, Major Axis, Minor Axis, Spatial Moment 1, Spatial moment 2, Fourier Transcript 1, Fourier Transcript 2, Major Length, Minor Length.

5.4 Effectiveness of morphological features of software separated kernels

If the separation algorithm worked well, after software separation, those morphological features did not change considerably from their true values. The true value of a morphological feature is a value extracted from the image when the kernels were physically separated.

The difference in the features between the physically separated and software separated kernels were used to test the effectiveness of the ellipse fitting algorithm. To decide if the difference between two kinds of features was significant, the large sample Z test of hypotheses was employed.

Hypothesis Z tests the difference between two population means μ_1 and μ_2 where data are available in the form of the means and standard deviations of two samples.

In this case ($n_1 \geq 30$ and $n_2 \geq 30$), the difference of the two population means, $\bar{x}_1 - \bar{x}_2$, is approximately normally distributed, with mean μ_1 - μ_2, and standard deviation

$$\sigma_{\bar{x}_1 - \bar{x}_2} = \sqrt{\frac{\sigma_1^2}{n_1} + \frac{\sigma_2^2}{n_2}} \cong \sqrt{\frac{s_1^2}{n_1} + \frac{s_2^2}{n_2}} \qquad (5.10)$$

Where σ_1 and σ_2 are the standard deviations of the two populations, and s_1 and s_2 are the standard deviations from the two groups of samples, one selected from each population. When the values of σ_1 and σ_2 are not known, s_1 and s_2 could be used for calculation.

Testing hypotheses involves

$$H_0: \mu_1 - \mu_2 = \Delta \qquad (5.11)$$

Under the above circumstances, the appropriate standardized test statistic was

$$z = \frac{\bar{x}_1 - \bar{x}_2 - (\mu_1 - \mu_2)}{\sigma_{\bar{x}_1 - \bar{x}_2}} = \frac{\bar{x}_1 - \bar{x}_2 - \Delta}{\sigma_{\bar{x}_1 - \bar{x}_2}} \qquad (5.12)$$

Where Δ was a specific numerical value. When $\Delta = 0$, Z testing was for a difference of any magnitude between the two means. The rules for arriving at a decision were summarized in Table 5.1.

Table 5.1 Z test hypotheses rules

Hypotheses:	reject H_0 at a level of significance α if:
H_0: $\mu_1 - \mu_2 = \Delta$	$z > z_\alpha$
H_A: $\mu_1 - \mu_2 > \Delta$	(single-tailed rejection region)
H_0: $\mu_1 - \mu_2 = \Delta$	$z < -z_\alpha$
H_A: $\mu_1 - \mu_2 < \Delta$	(single-tailed rejection region)
H_0: $\mu_1 - \mu_2 = \Delta$	$z > z_{\alpha/2}$ or $z < -z_{\alpha/2}$
H_A: $\mu_1 - \mu_2 \neq \Delta$	(two-tailed rejection region)

To demonstrate the effectiveness of the separation algorithm, random successfully separated samples (973 touching instances of CWRS wheat, 924 touching instances of barley, 961 touching instances of CWAD barley, 948 touching instances of oats) were tested. For each kernel, one set of morphological features after physical separation was recorded as an initial set of features, and another set of morphological features of the same kernel was extracted after software separation. To confirm that the differences of morphological features between physical separation and software separation were not statistically significant, the hypotheses that needed to be tested are described in the following steps:

1. The null hypothesis: $H_0 : \mu_1 = \mu_2$

   The alternative hypothesis $H_a : \mu_1 \neq \mu_2$ (Two tailed test)

   Where μ_1 : the mean value of morphological features of physically separated kernels. μ_2 : the mean value of morphological features of software separated kernels.

2. Test statistic for Z value:

$$z = \frac{\bar{x}_1 - \bar{x}_2}{\sigma_{\bar{x}_1 - \bar{x}_2}} = \frac{\bar{x}_1 - \bar{x}_2}{\sqrt{\frac{\sigma_1^2}{n_1} + \frac{\sigma_2^2}{n_2}}}. \qquad (5.13)$$

   where σ_1 and σ_2 are the standard deviations of the two populations, n_1, n_2 are the size of two populations. In the present case, the n_1 and n_2 are the same.

3. Rejected region.

$$\text{reject} \quad H_0 : \quad |z| > z_{\alpha/2}$$
$$\text{not reject} \quad H_0 : \quad |z| \leq z_{\alpha/2}$$

   If H_0 is accepted, there is no difference between morphological features of physically separated and software separated kernels. For α=0.05, the rejection region is larger than $Z_{0.025}$ = 1.96 or $Z_{-0.025}$ = -1.96.

Except for Fourier Transcript 1 of barley and CWAD, the hypothesis test showed that there is no difference for all other morphological features for all grain types between physical separation and software separation with 95% confidence.

(Table 5.2). Therefore, software separation did not change the values of the morphological features of CWRS wheat, CWAD wheat, barley, and oats.

Table 5.2 Difference between morphological features of physically separated and software separated kernels (Pixels)

Grain Type	Condition	Area	Perimeter	Maxium Radius	Minmium Radius	Mean Radius	Major Axis	Minor Axis
Barley	Separate	4646.758	313.184	65.564	23.854	41.353	122.723	50.688
	Touch	4592.162	301.011	64.591	22.825	40.313	119.557	50.311
	Variance	1.175%	3.887%	1.484%	4.316%	2.514%	2.580%	0.744%
	Z-test	-0.858	-0.148	-0.383	-0.833	-0.790	-0.271	-2.134
Oat	Separate	5254.973	392.344	84.250	19.573	48.907	162.226	41.121
	Touch	5150.931	379.990	82.170	18.881	47.652	158.627	40.194
	Variance	0.020	0.031	0.025	0.035	0.026	0.022	0.023
	Z-test	0.230	-0.493	-0.302	-1.294	-0.489	-0.484	-0.515
CWAD	Separate	4349.891	288.345	60.016	21.727	39.422	117.682	45.747
	Touch	4316.949	287.105	60.015	21.333	39.159	117.043	45.735
	Variance	0.008	0.004	0.000	0.018	0.007	0.005	0.000
	Z-test	0.537	0.404	-0.262	-1.286	-0.662	-0.466	0.460
CWRS	Separate	3142.656	236.027	47.458	20.274	32.610	92.142	42.440
	Touch	3076.941	231.073	47.295	19.286	32.073	90.773	42.540
	Variance	0.021	0.021	0.003	0.049	0.016	0.015	-0.002
	Z-test	1.304	1.681	-0.497	0.635	0.675	0.973	1.463

Table 5.2 Difference between morphological features of physically separated and software separated kernels (continued)

Grain Type	Condition	Shape Moment 1	Shape Moment 2	Fourier Transcript 1	Fourier Transcript 2	Major Length	Minor Length
Barley	Separate	0.233	0.028	1.806	20.187	120.269	49.168
	Touch	0.235	0.028	2.128	19.561	117.186	49.056
	Variance	-0.008%	-1.328%	-17.856%	3.099%	2.563%	0.226%
	Z-test	1.013	1.000	2.061	-1.829	1.023	0.782
Oat	Separate	0.335	0.088	1.301	30.413	158.171	40.093
	Touch	0.326	0.085	1.446	29.722	154.049	38.082
	Variance	0.000	0.033	-0.112	0.023	0.026	0.050
	Z-test	-0.062	0.083	1.384	0.022	0.432	1.013
CWAD	Separate	0.235	0.030	0.540	22.441	115.328	44.375
	Touch	0.236	0.030	0.608	22.238	114.202	44.333
	Variance	0.000	-0.007	-0.126	0.009	0.010	0.001
	Z-test	0.278	-0.233	-2.154	-0.064	0.473	-0.829
CWRS	Separate	0.206	0.017	0.483	18.228	90.299	41.167
	Touch	0.208	0.017	0.580	17.754	88.758	41.364
	Variance	0.000	-0.028	-0.201	0.021	0.017	-0.005
	Z-test	-1.410	1.357	-1.228	0.905	-0.588	0.535

5.5. Classification of the software separated kernels with an artificial neural network.

The extracted morphological features data after software separation would be ultimately used for grain type classification. To assess the classification capability of extracted morphological features from software separated kernels, artificial neural networks were used for grain type classification. Artificial neural networks (ANN) have been a very active research area since the 1970s, and were used by many researchers from a number of different disciplines (Haykin 1994). Artificial neural networks, resembling biological nervous system, have the potential for solving problems in which some inputs and corresponding output values are known, but the relationship between the inputs and outputs is not well understood. These conditions are commonly found in agri-food industry inspection and sorting problems (Elizondo et al. 1994). The essence of neural networks lies in the connection weights between neurons (inputs and outputs). These weights must be selected consciously before the neural networks can be put into practical application, and this selection is referred to as learning by the neural network. The ultimate purpose of learning is to minimize the cost function, that the actual response of each output neuron in the network approaches the target (or desired) response for that neuron.

To assess the classification capability after software separation, the morphological features extracted from physically separated kernels were used as training and basic testing data sets; the features from software separated kernels were the production testing data. A 4 layer back-propagation neural network

(BPNN) was developed as a grain type classifier based on morphological features. Training and basic testing was done on 8000 physically separated kernels (i.e. 2000 kernels of each grain type), and the entire process was repeated three times using different training and testing data sets. Each time, 50% randomly selected physically separated kernels were used as training data sets, another 50% physically separated kernels were used as basic testing data. The network was trained for 1500 epochs and was then applied on production data set consisting of 8000 software separated kernels (i.e. 2000 kernels of each grain type). The summarized results of classification analysis are shown in Table 5.3 and Table 5.4, respectively and confusion matrics are given in Appendix B.

Table 5.3. Classification accuracies of physically separated grain kernels using a neural network for three trials %

	1	2	3	Mean
Barley	97.8	96.6	97.1	97.2
CWAD	95.9	95.2	95.4	95.5
CWRS	98.1	98.3	97.8	98.1
Oats	97.4	97.7	97.1	97.4

Table 5.4. Classification accuracies of software separated grain kernels using a neural network for three trials %

	1	2	3	Mean
Barley	96.6	96.9	97.4	97.0
CWAD	94.3	94.8	94.9	94.7
CWRS	98.2	97.5	97.3	97.7
Oats	96.9	97.5	97.2	97.2

Compared to 97.1% physically separated grain kernels being correctly classified, the mean classification accuracy for all the software separated grain types was 96.6%. Because the shape and size of CWAD kernels varied a lot, the classification accuracy for CWAD was the lowest among four software separated grain types. One reason for additional misclassification caused by software separation was the use of physically separated kernels as a training and basic testing set and the software separated kernels as a production test set. Another reason for this additional misclassification was CWAD misclassified as CWRS wheat due to improper separation. Results presented in Tables 5.3 and 5.4 show that morphological features of software separated kernels were not distorted during software separation and can be successfully used in grain type classification.

The ellipse fitting algorithm worked well in separating touching grain kernel regions. Implementation of this separation algorithm in a powerful machine vision system (such as a system with a specialized DSP processor) need to be studied

for practical use. With a personal computer (PIII 450 MHz), an image with three grain touching instances could be processed within 60 s by the ellipse fitting algorithm.

6. CONCLUSIONS AND RECOMMENDATIONS

Touching grain kernels separation is essential for automated grain sample analysis. The ellipse fitting algorithm was developed for separating the touching grain kernels in an image. A back-propagation neural network was also developed for grain type classification based on the morphological features model. The study shows that software separated kernels did not distort their morphological features and can be successfully used for grain classification. The following conclusions can be drawn from this research:

1. The ellipse fitting algorithm successfully separated touching grain instances for CWRS wheat, barley, CWAD wheat, oats with 97.3%, 92.4%, 96.1% 94.8%, respectively.

2. Except for Fourier descriptor 1 of barley and CWAD wheat, software separation with the ellipse fitting algorithm did not change the value of morphological features of CWRS wheat, CWAD wheat, barley and oats within the tolerance limits of the measurement system.

3. The mean classification accuracy for all the software separated grain kernels was 96.6%.

If a commercial processor is designed to use with this algorithm, the processing speed can be accelerated to meet real time processing requirements. Finding the representative fitted ellipse with clustering is essential in this algorithm, therefore more clustering techniques need to be tested for this algorithm.

REFERENCES

Al-Janobi, A. A. and G. Kranzler. 1994. Machine vision inspection of date fruits. *ASAE Paper* No.94-3575. St. Joseph, MI: ASAE.

Barker, D.A., T.A. Vouri, M.R. Hegedus, and D.G. Myers. 1992a. The use of ray parameters for the discrimination of Australian wheat varieties. *Plant Varieties and Seeds* 5:35-45.

Barker, D.A., T.A. Vouri, and D.G. Myers. 1992b. The use of slice and aspect ratio parameters for the discrimination of Australian wheat varieties. *Plant Varieties and Seeds* 5:47-52.

Barker, D.A., T.A. Vouri, and D.G. Myers. 1992c. The use of Fourier descriptors for the discrimination of Australian wheat varieties. *Plant Varieties and Seeds* 5:93-102.

Barker, D.A., T.A. Vouri, M.R. Hegedus, and D.G. Myers. 1992d. The use of Chebychev coefficients for the discrimination of Australian wheat varieties. *Plant Varieties and Seeds* 5:103-111.

Bookstein, F.L. 1979. Fitting conic sections to scattered data. *Computer Graphics and Image Processing* 9:56-71.

Beucher, S. and F. Meyer. 1993. The morphological approach to segmentation: The watershed transformation. *Mathematical Morphology in Image Processing*. E. Dougherty ed.. New York, NY: Marcel Dekker Inc.

Canada Grains Council. 2002. *Statistical Handbook*. Winnipeg, MB: Canada Grains Council

Casady, W.W. and M.R. Paulsen. 1988. An automated kernel positioning device for computer vision analysis of grain. *ASAE Paper No.* 88-7003. St. Joseph, MI: ASAE.

Cardarelli A. J., Y. Tao, J.L. Bernhardt, and F.N. Lee, 1998. High resolution machine vision for non-destructive internal inspection of damaged rice grain. *ASAE Paper No.* 98-6024, St. Joseph, MI: ASAE.

Churchill, D.B., T.M. Cooper, and D.M. Sisland. 1991. Rotating table for measuring seed properties. *Transactions of the ASAE* 34(4):1842-1845.

Crowe, T. G., X. Luo., D.S.Jayas, and N. R. Bulley 1997. Colour line-scan imaging of cereal grain kernels. *Applied Engineering in Agriculture* 13(5): 689-694.

Eleftheriadis, A. and A. Jacquin. 1995. Automatic face location detection and tracking for model-assisted coding of video teleconferencing sequences at low bit-rates. *Signal Processing: Image Communication* 7(4): 231-248.

Elizondo, D. A., R. W. McClendon, and G. Hoogenboom. 1994. Neural network models for predicting flowering and physiological maturity of soybean. *Transactions of the ASAE* 37(3): 981-988.

Ellis, T., A. Abbood, and B. Brillault. 1992. Ellipse detection and matching with uncertainty. *Image and Vision Computing* 10:271-276.

Fitzgibbon, A. W., M. Pilu, and R. B. Fischer. 1996. Direct least squares fitting of ellipses. *Proceedings of the 13th International Conference on Pattern Recognition*, pp 253–257, Vienna.

Forsyth, D. A., J.L. Mundy, A. Zisserman, C. Coelho, A. Heller, and C. Rothwell. 1991. Invariant descriptors for 3-d object recognition and pose. *IEEE Transaction PAMI*, 13: 971–991.

Ghazanfari, A., D. Wulfsohn, and J. Irudayaraj. 1998. Machine vision grading of pistachio nuts using gray-level histogram. *Canadian Agricultural Engineering* 40(1): 61-66.

Gonzalez, R.C. and R.E. Woods. 1992. *Digital Image Processing.* Reading, MA: Addison-Wesley Publishing Co.

Grimson, W. E. L. and D. P. Huttenlocher, 1990. On the sensitivity of the Hough transform for object recognition. *IEEE Transaction PAMI* 12:2555–2574.

Han, Y. J. and J. C. Hayes. 1990. Soil cover determination by image analysis of textural information. *Transactions of the ASAE* 33(2): 681-686.

Haralick, R.M., S.R. Sternberg, and X. Zhuang. 1987. Image analysis using mathematical morphology. *IEEE Transaction PAMI* 9: 523-550.

Huang. Y., R. E. Lacey, A. D. Whittaker, R. K. Miller, L. Moore and J. Ophir. 1997. Wavelet textural features from ultrasonic elastograms for meat quality prediction. *Transactions of the ASAE* 40(6): 1741-1748.

Haykin, S. 1994. Neural Networks: *A Comprehensive Foundation.* New York, NY: Macmillan College Publishing Company, Inc.

Jain, A. K. and Dubes, R. C. 1988. *Algorithms for Clustering Data.* Englewood Cliffs, NJ: Prentice Hall.

Jayas,D.S., C.E. Murray, and N.R. Bulley. 1999. An automated seed presentation device for use in machine vision identification of grain. *Canadian Agricultural Engineering* 41(2):113-118.

Karunakaran, C., N.S. Visen, J. Paliwal, G. Zhang, D.S. Jayas, and N.D.G White. 2001. Machine vision systems for agricultural products. *CSAE Paper* No. 01-305. Masonville, PQ: CSAE.

Keefe, P.D. 1992. A dedicated wheat grading system. *Plant Varieties and Seeds* 5127-5133.

Kim, H., W. Kang, J.Shin, and S.Park. 2000. Face detection using template matching and ellipse fitting. *IEICE Transaction Information & System,* 38(11):2008-2011.

Kohler, J.M. 1991. Study of commercial grades of Canada red spring wheat by digital image processing. Unpublished M.Sc. thesis. Department of Biosystems Engineering. Winnipeg, MB: University of Manitoba.

Lantejoul, C. 1980. Skeletonization in quantitative metallography. P107-P135 in: *Issues of Digital Image Processing*, R. M. Haralick and J. C. Simon. Groningen, The Netherlands: Sijthoff and Noordhoff.

Luo, X., D.S. Jayas, T.G. Crowe, and N.R. Bulley. 1997. Evaluation of light sources for machine vision. *Canadian Agricultural Engineering* 39(4): 309-315.

Luo, X.Y., D.S. Jayas, and S.J. Symons. 1999a. Identification of damaged kernels in wheat using a colour machine vision system. *Journal of Cereal Science* 30(1): 49-59.

Luo, X.Y., D.S. Jayas, and S.J. Symons. 1999b. Comparison of statistical and neural network methods for classifying cereal grains using machine vision. *Transactions of the ASAE* 42(2): 413-419.

Majumdar, S. and D.S. Jayas. 2000a. Classification of cereal grains using machine vision. I. Morphology models. *Transactions of the ASAE* 43(6):1669-1675.

Majumdar, S. and D.S. Jayas. 2000b. Classification of cereal grains using machine vision. II. Colour models. *Transactions of the ASAE* 43(6):1677-1680.

Majumdar, S. and D.S. Jayas. 2000c. Classification of cereal grains using machine vision. III. Texture models. *Transactions of the ASAE* 43(6):1681-1687.

Majumdar, S. and D.S. Jayas. 2000d. Classification of cereal grains using machine vision. IV. Combined morphology, colour, and texture models. *Transactions of the ASAE* 43(6):1689-1694.

McDonald, T.P. and Y.R. Chen. 1990a. Application of morphological image processing in agricultural engineering. *Transactions of the ASAE* 33 (2): 1345-1352.

McDonald, T.P. and Y.R. Chen. 1990b. Separating connected muscle tissue in images of beef carcass. *Transactions of the ASAE* 33(3): 2059-2065.

Miller, B.K. and M.J. Delwiche. 1989. A colour vision system for peach grading. *Transactions of the ASAE* 32(4): 1484-1490.

Neuman, M., H.D. Sapirstein, E. Shwedyk, and W. Bushuk. 1987. Discrimination of wheat class and variety by digital image analysis of whole grain samples. *Journal of Cereal Science* 6:125-132.

Neuman, M., H.D. Sapirstein, E. Shwedyk, and W. Bushuk. 1989a. Wheat grain colour analysis by digital image processing: I. Methodology. *Journal of Cereal Science* 10: 175-I 82.

Neuman, M., H.D. Sapirstein, E. Shwedyk, and W. Bushuk. 1989b. Wheat grain colour analysis by digital image processing: II. Wheat class discrimination. *Journal of Cereal Science* 10: 183-88.

Ng, H. F., W. F. Wilcke, R. V. Morey, and J. P. Lang. 1998. Machine vision evaluation of corn kernel mechanical and mold damage. *Transactions of* the ASAE 41(2): 415-420.

Paliwal, J., N.S. Shashidhar, and D.S. Jayas. 1999. Grain kernel identification using kernel signature. *Transactions of the ASAE* 42(6): 1921-1924.

Paliwal, J., N.S. Visen, and D.S. Jayas. 2001. Evaluation of neural network architectures for cereal grain classification using morphological features. *Journal of Agricultural Engineering Research* 79(4):361-370.

Park, B. and Y. R. Chen. 1994. Multi spectral image textural analysis for poultry carcasses inspection. *ASAE Paper* No.94-6027. St. Joseph, MI: ASAE.

Paulsen, M.R. and W.F. McClure. 1986. Illumination for computer vision systems. *Transactions of the ASAE* 29(5):1398-1404.

Petersen, P. H. 1992. Weed seed identification by shape and texture analysis of microscope images. Ph.D. Dissertation. Copenhagen, Denmark: The Danish Institute of Plant and Soil Science.

Porrill, J. 1990. Fitting ellipses and predicting confidence envelopes using a bias corrected kalman filter. *Image and Vision Computing* 8(1):37-41.

Putnam, D.F. and R.G. Putnam. 1970. *Canada: A Regional Analysis*. Toronto, ON: J.M. Dent and Sons, Inc.

Rosin, P.L. 1993. A note on the least squares fitting of ellipses. *Pattern Recognition Letters* 14: 799-808.

Rosin, P.L. and G.A. West. 1995. Nonparametric segmentation of curves into various representations. *IEEE Transaction. Pattern Analysis and Machine Intelligence* 17(12):1140-1153.

Sarkar, N.R. 1986. Machine vision in the food industry. In *ASAE Food Engineering News,* October, 3-5. St. Joseph, MI: ASAE.

Sampson, P.D. 1982. Fitting conic sections to very scattered data: an iterative refinement of the bookstein algorithm. *Computer Graphics and Image Processing* 18:97-108.

Sapirstein, H.D., M. Neuman, E.H. Wright, E. Shwedyk, and W. Bushuk. 1987. An instrumental system for cereal grain classification using digital image analysis. *Journal of Cereal Science* 6:3-14.

Sapirstein, H.D. and W. Bushuk. 1989. Quantitative determination of foreign material and vitreosity in wheat by digital image analysis. In *ICC'89 Symposium: Wheat End-Use Properties*. H. Salovaara (ed.). Lahiti, Finland.

Sapirstein, H.D. and J.M. Kohler. 1995. Physical uniformity of graded railcar and vessel shipments of Canada Western Red Spring wheat determined by digital image analysis. *Canadian Journal of Plant Science* 75(2):363-369.

Segerlind, L. and B. Weinberg. 1972. Grain kernel identification by profile analysis. *ASAE Paper* No. 72-314. St. Joseph, MI: ASAE.

Serra, J. 1982. *Image Analysis and Mathematic Morphology*. New York, NY: Academic Press.

Shashidhar, N.S., D.S.Jayas, T.G. Crowe, and N.R. Bulley. 1997. Processing of digital images of touching kernels by ellipse fitting. *Canadian Agricultural Engineering* 39:139-142.

Shatadal, P., D.S. Jayas, and N.R. Bulley. 1995a. Digital image analysis for software separation and classification of touching grains: I. Disconnect algorithm. *Transactions of the ASAE* 38(2):635-643.

Shatadal, P., D.S. Jayas, and N.R. Bulley. 1995b. Digital image analysis for software separation and classification of touching grains: II. Classification. *Transactions of the ASAE* 38(2):645-649.

Shearer, S. A., T. F. Burks, P. T. Jones, and W. Qiu. 1994. One-dimensional image texture analysis for maturity assessment of broccoli. *ASAE Paper No.* 94-3017. St. Joseph, MI: ASAE.

Spewak, R. 1995. An automated seed singulation device for presenting grains to an image processing system. Unpublished B.Sc thesis. Department of Biosystems Engineering, Winnipeg, MB: University of Manitoba.

Symons, S.J, and R.G. Fulcher. 1988a. Determination of wheat kernel morphological variation by digital image analysis: I. Variation in eastern Canadian milling quality wheat. *Journal of Cereal Science* 8:211-218.

Symons, S.J. and R.G. Fulcher. 1988b. Determination of wheat kernel morphological variation by digital image analysis: II. Variation in cultivars of soft white winter wheat. *Journal of Cereal Science* 8:219-229.

Tang, S., M.J. Delwiche, and J.F. Thompson. 1990. Development and evaluation of a defect sorter for prunes. *ASAE Paper No.* 90-6039. St. Joseph, MI: ASAE.

Tao, Y., C.T. Morrow, P.H. Heinemann, and H.J. Sommer III. 1995. Fourier-based separation technique for shape grading potatoes using machine vision. *Transactions of the ASAE* 38(3):949-957.

Tian, L., D. C. Slaughter, and R. Norris. 1997. Outdoor field machine vision identification of tomato seedlings for automated weed control. *Transactions of the ASAE* 40(6): 1761-1768.

Tillet, R.D. 1990. Image analysis for agricultural processes. Div. note DN 1585, Silsoe, UK: AFRC Institute of Engineering Research.

Visen, N.S. 2002. Machine Vision Based Grain Handling System. Unpublished Ph.D Thesis, Department of Biosystems Engineering. Winnipeg, MB: University of Manitoba.

Visen, N.S., N.S. Shashidhar, J. Paliwal, and D.S. Jayas. 2001. Identification and segmentation of groups of touching kernels. *Journal of Agricultural Engineering Research* 79(2):159-166.

Ward Systems Group. 1998. NeuroShell 2, Version 4. Frederick, MD.

Yuan, H.K., J. Illingworth, and J.Kittler. 1989. Shape using volumetric primitives. *Image and Vision Computing* 1(7):31-37.

Zayas, I., Y. Pomeranz, and F.S. Lai. 1985. Discrimination between Arthur and Arkan wheats by image analysis. *Cereal Chemistry* 62:478-480.

Zayas, I., F.S. Lai, and Y. Pomeranz. 1986. Discrimination between wheat classes and varieties by image analysis. *Cereal Chemistry* 63:52-56.

Zayas, I., Y. Pomeranz, and F.S. Lai. 1989. Discrimination of wheat and non-wheat components in grain samples by image analysis. *Cereal Chemistry* 66:233-237.

Appendix A
REPRESENTATIVE SOFTWARE SEPARATED GRAIN KERNEL IMAGES

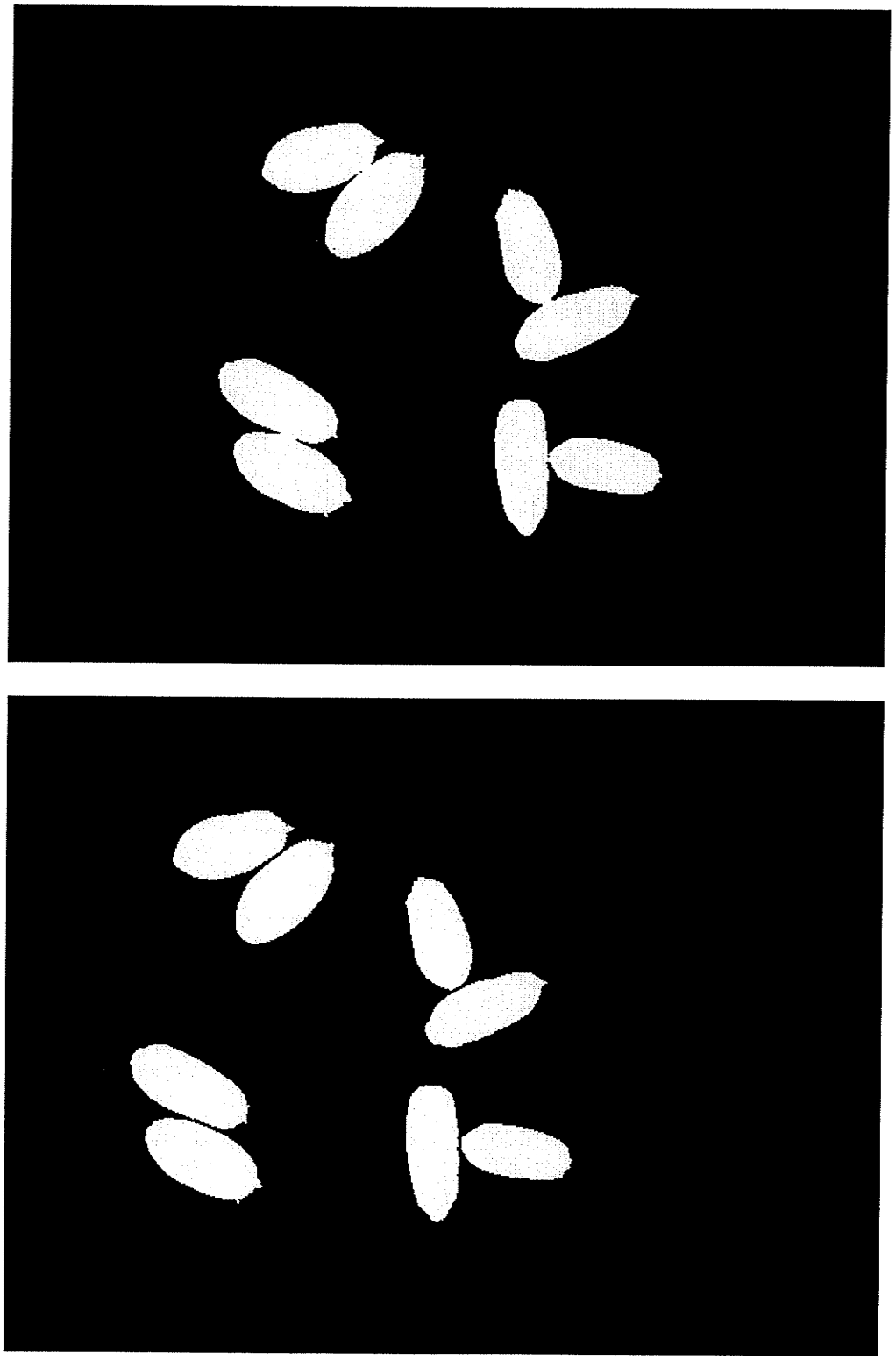

Figure A1 Example of (top) touching and (bottom) separated kernels of CWRS wheat

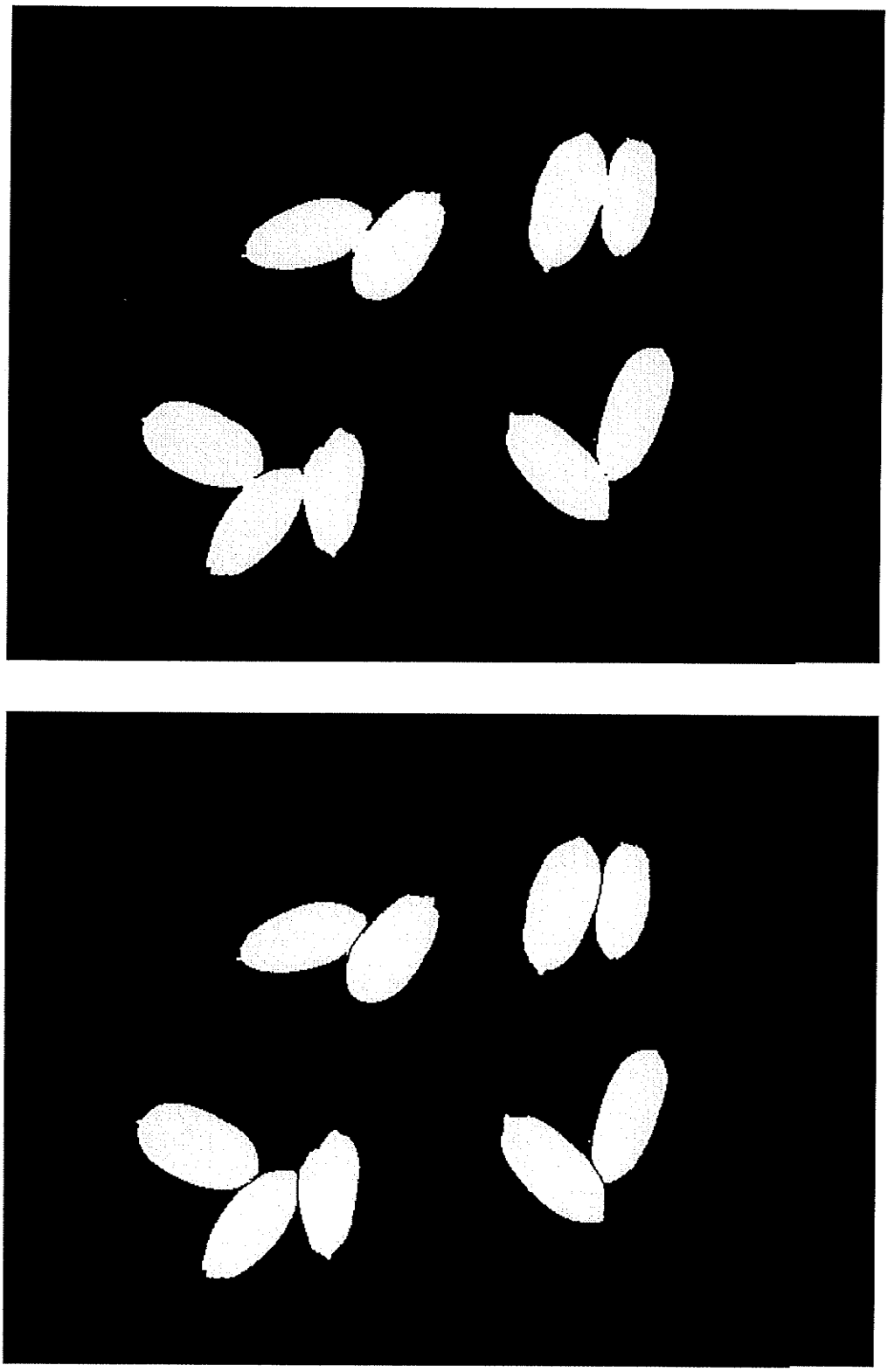

Figure A2. Example of (top) touching and (bottom) separated kernels of CWRS wheat

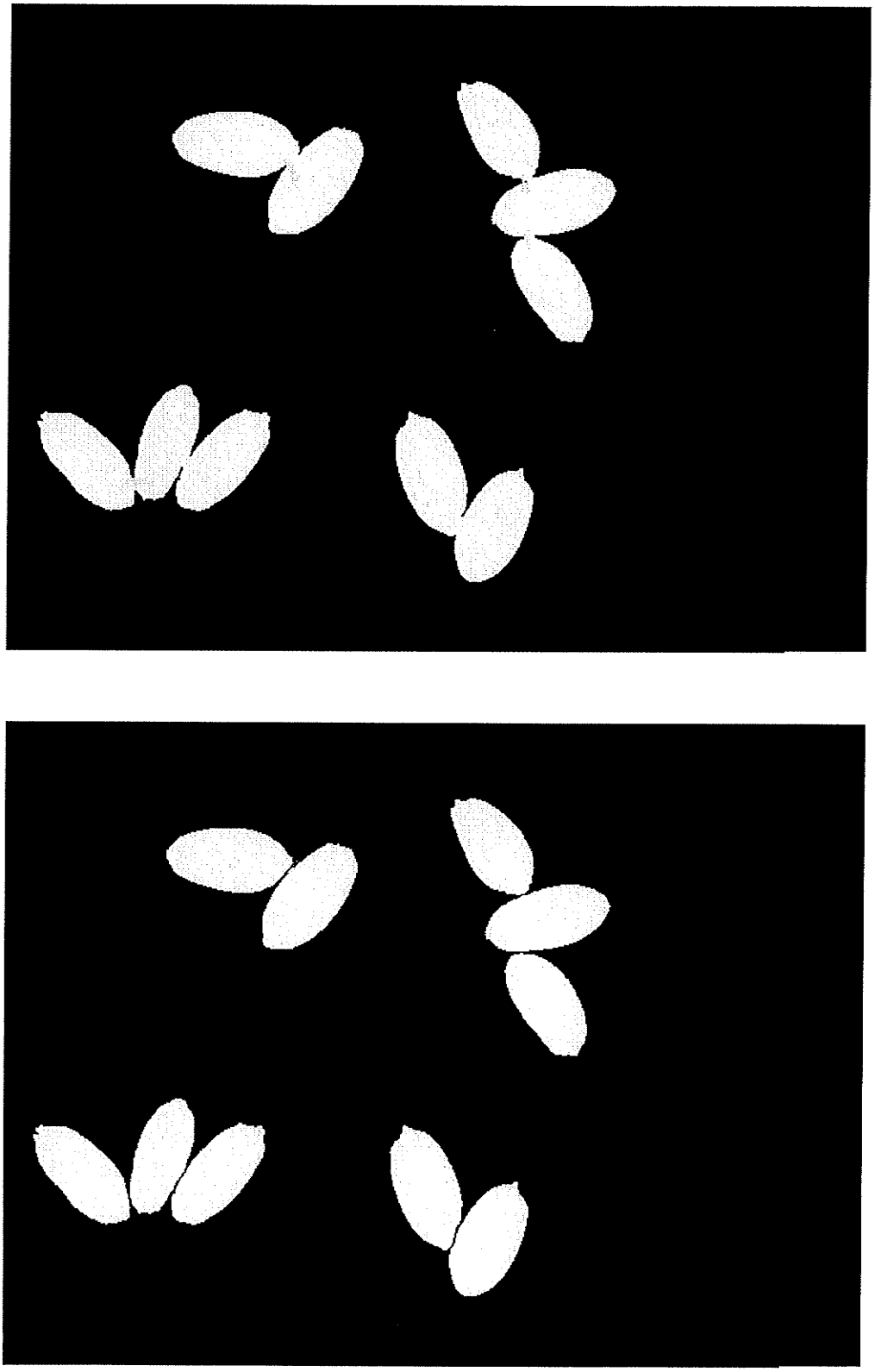

Figure A3 Example of (top) touching and (bottom) separated kernels of CWRS wheat

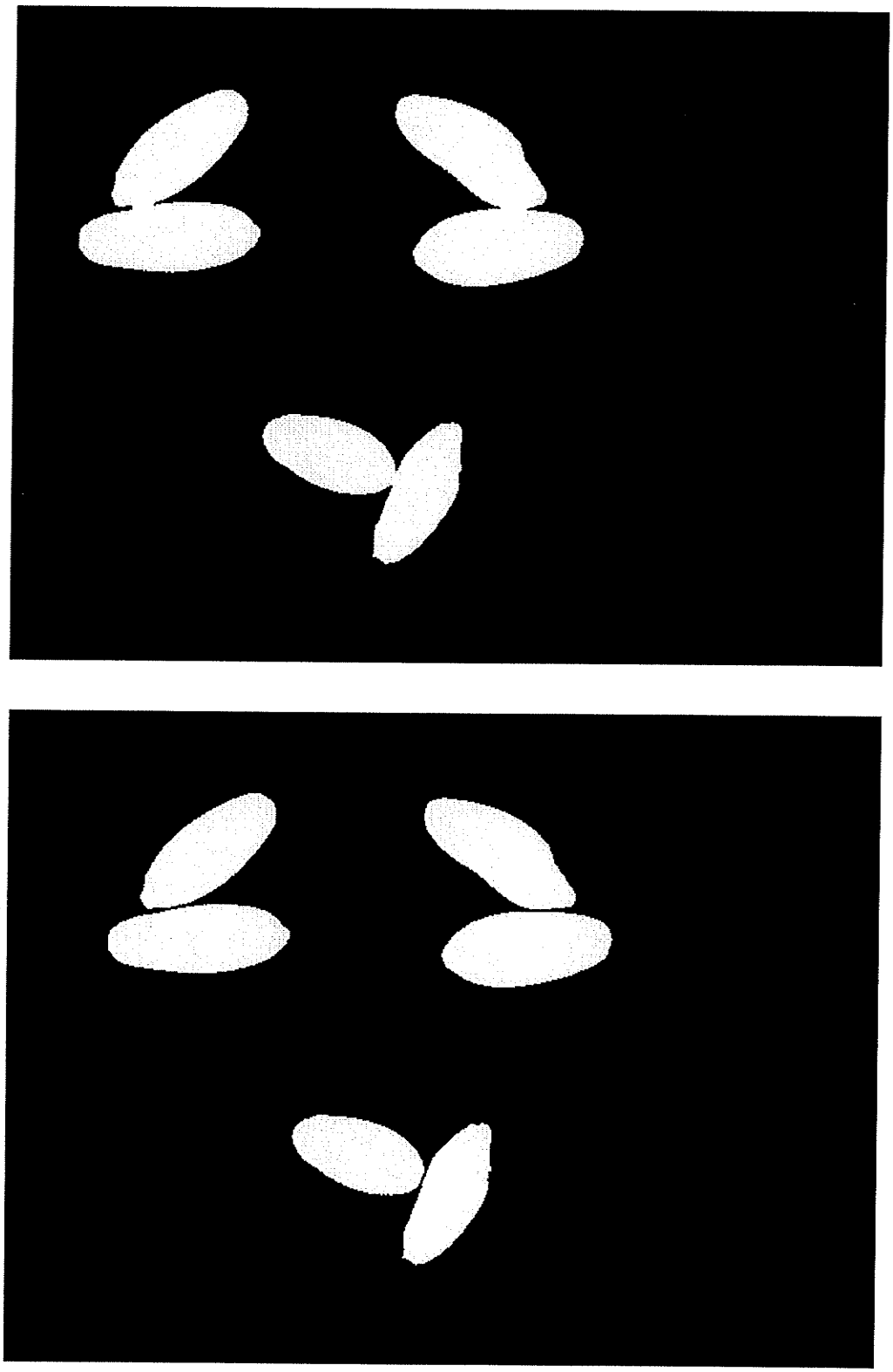

Figure A4 Example of (top) touching and (bottom) separated kernels of CWAD wheat

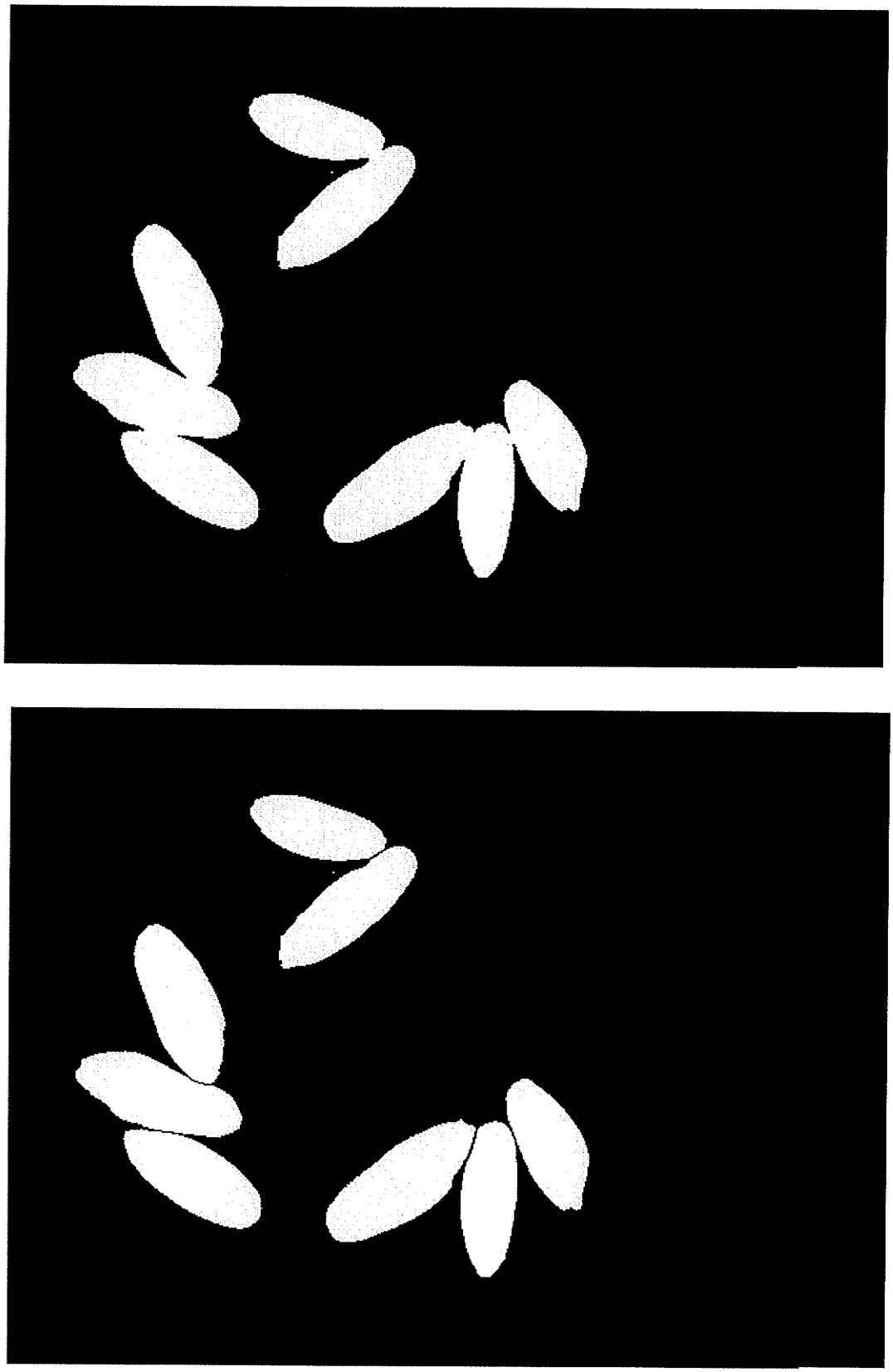

Figure A5 Example of (top) touching and (bottom) separated kernels of CWAD wheat

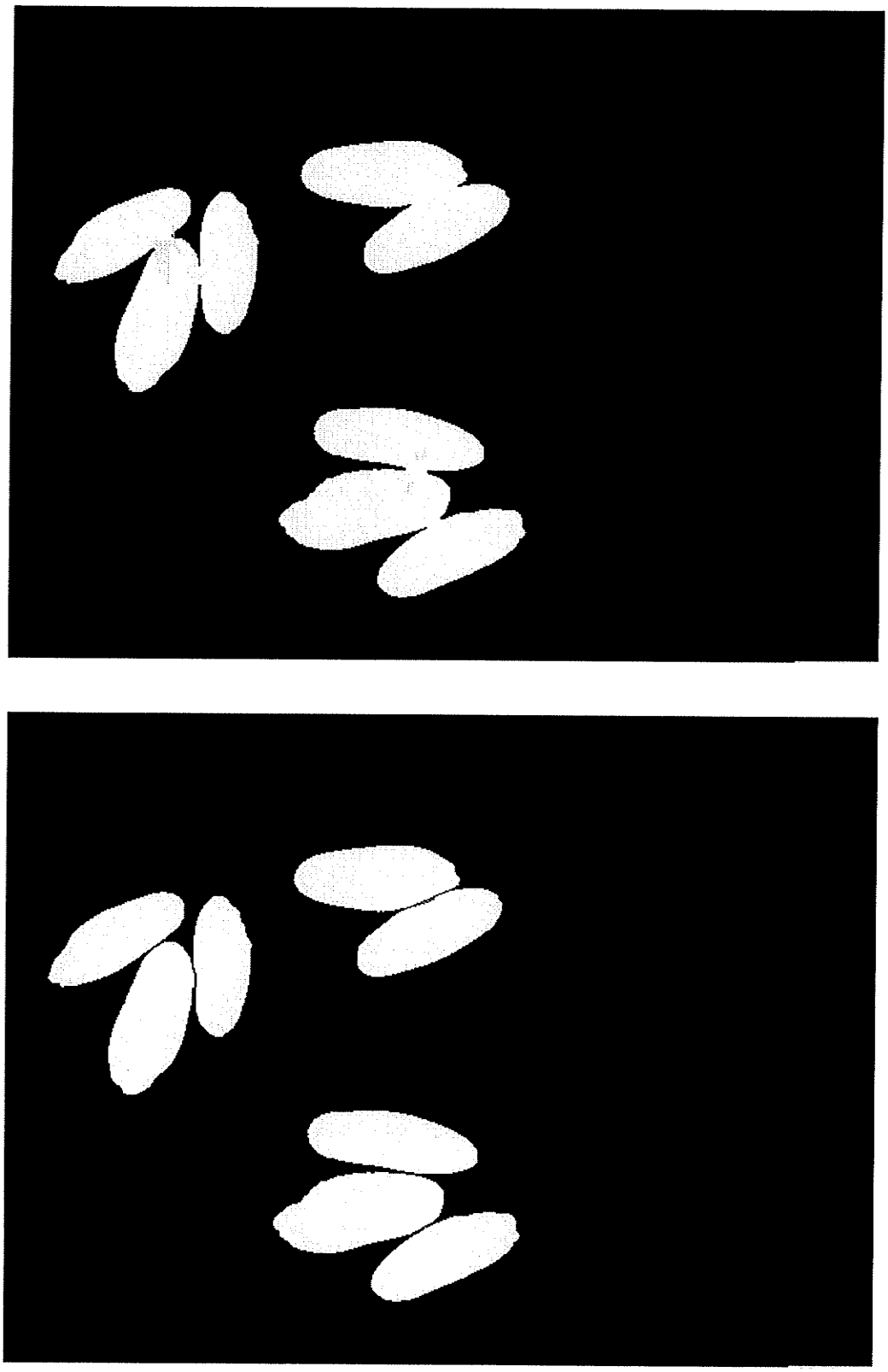

Figure A6 Example of (top) touching and (bottom) separated kernels of CWAD wheat

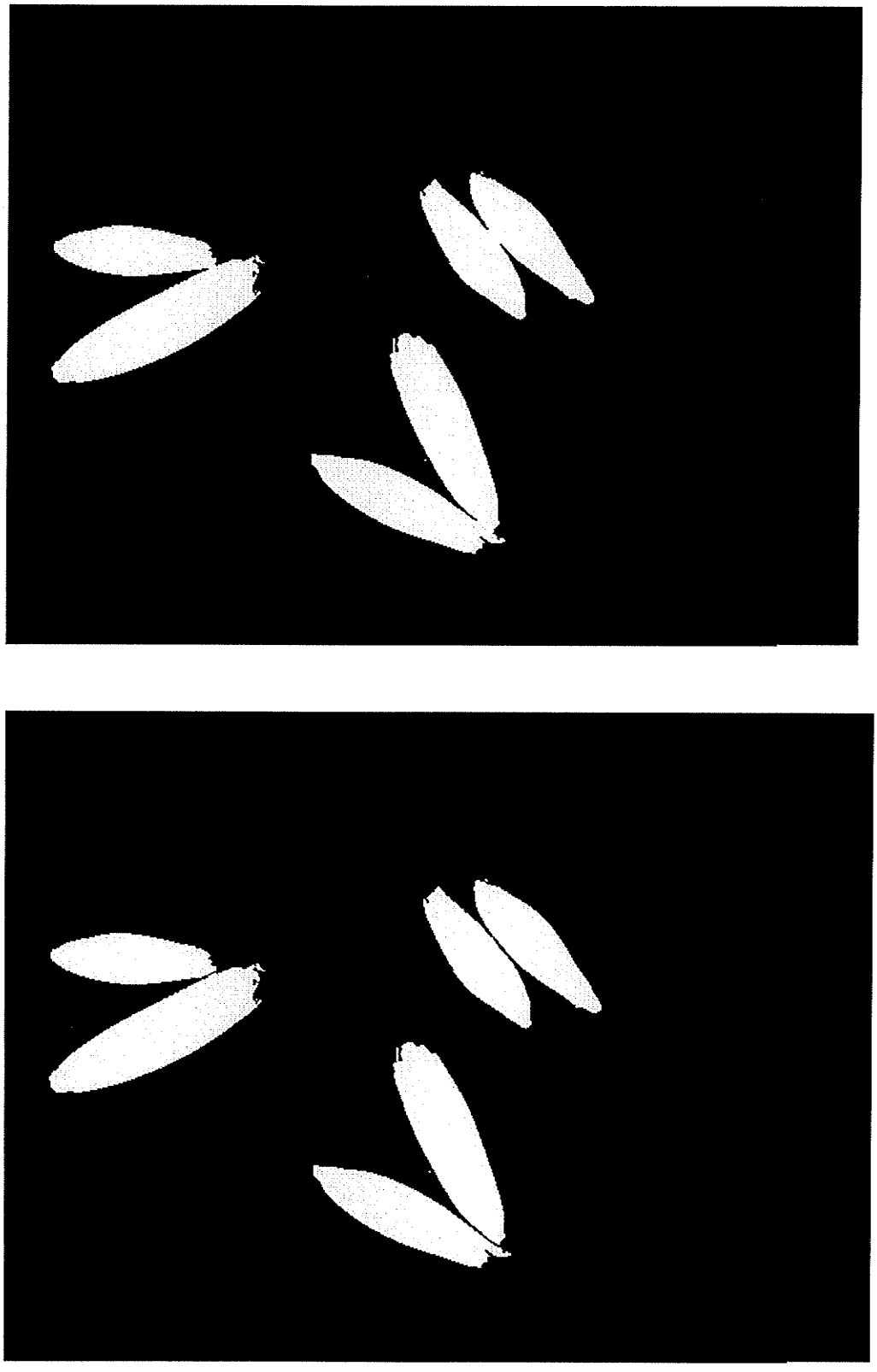

Figure A7. Example of (top) touching and (bottom) separated kernels of oats

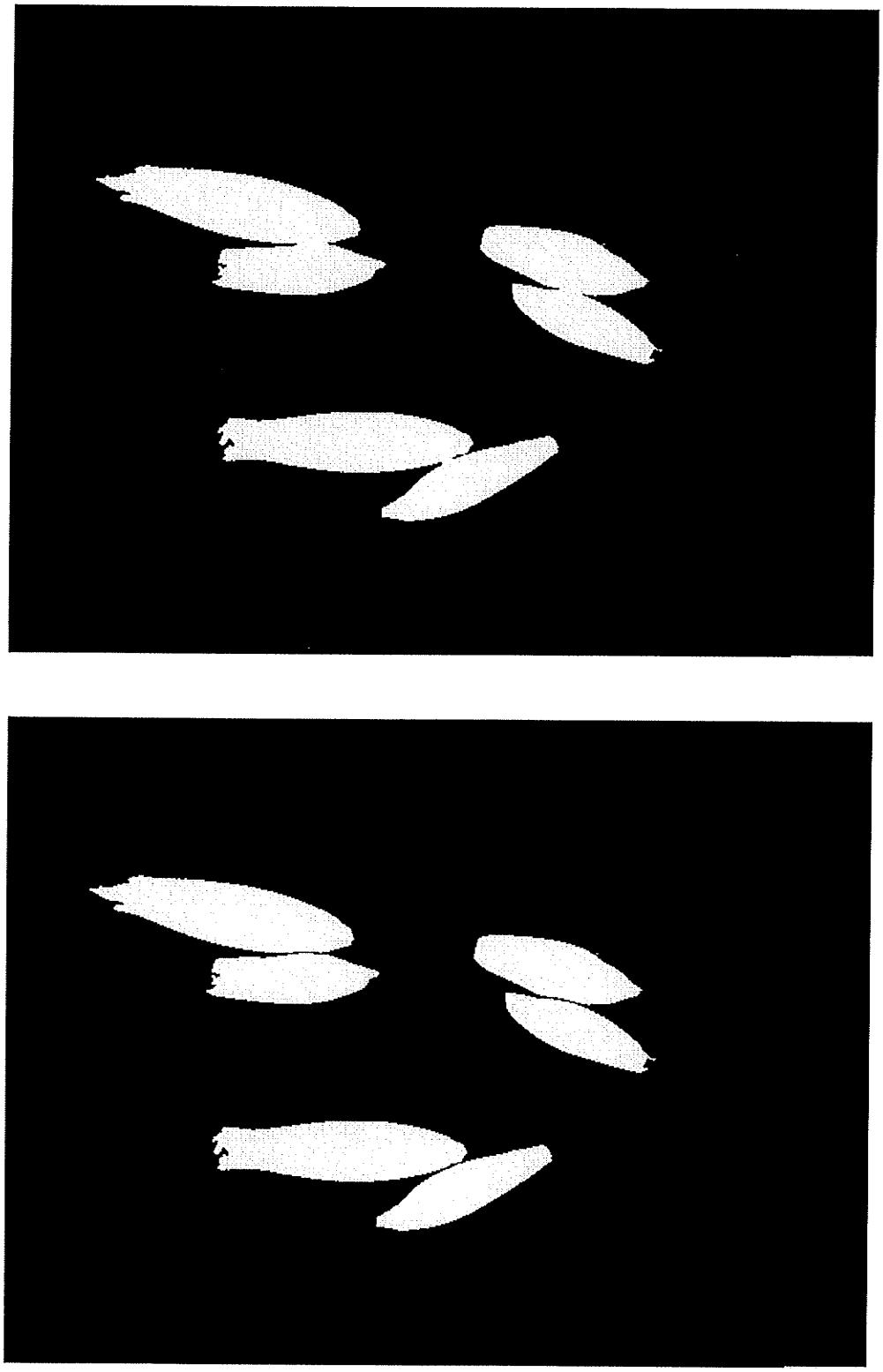

Figure A8. Example of (top) touching and (bottom) separated kernels of oats

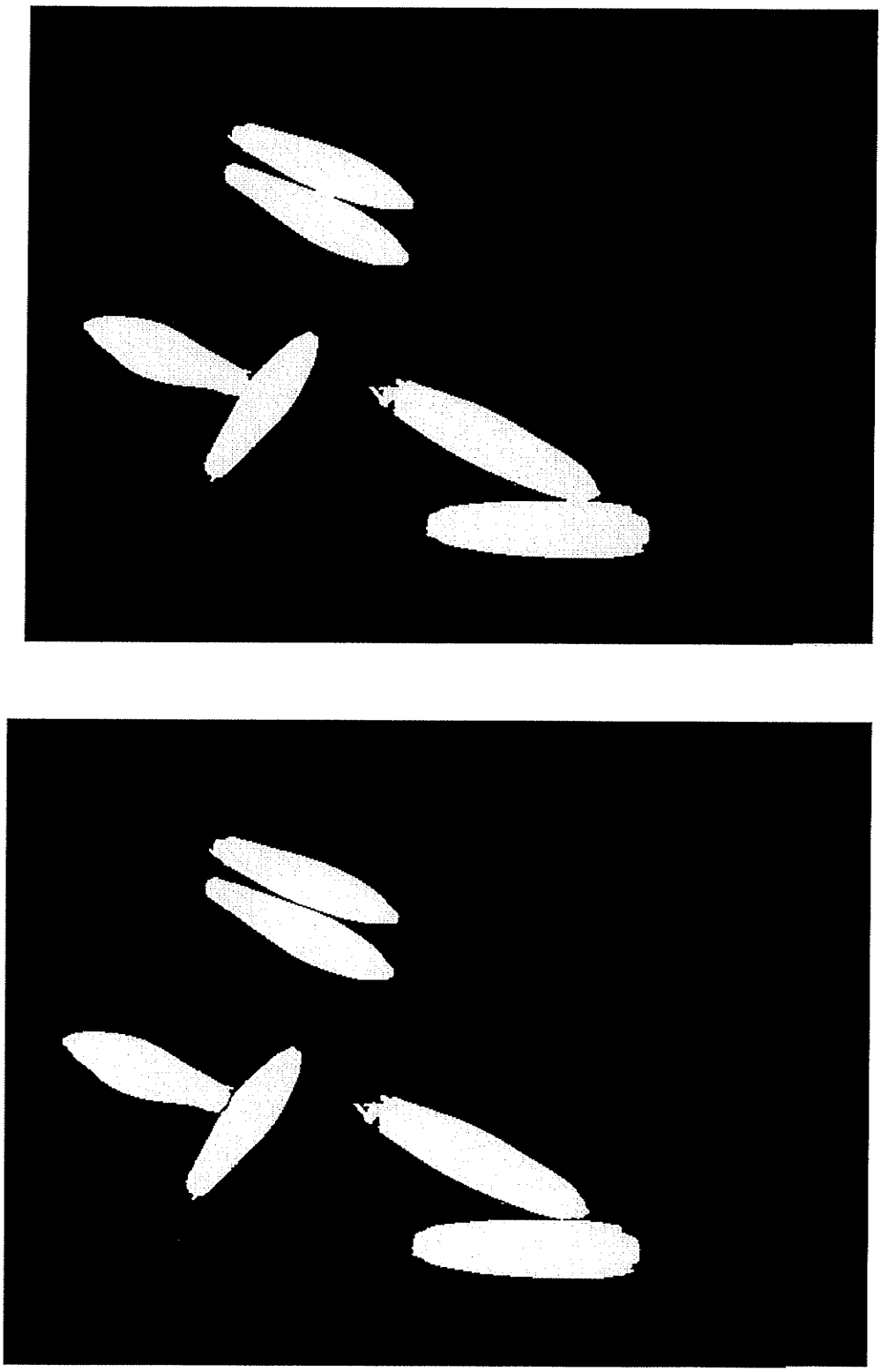

Figure A9. Example of (top) touching and (bottom) separated kernels of oats

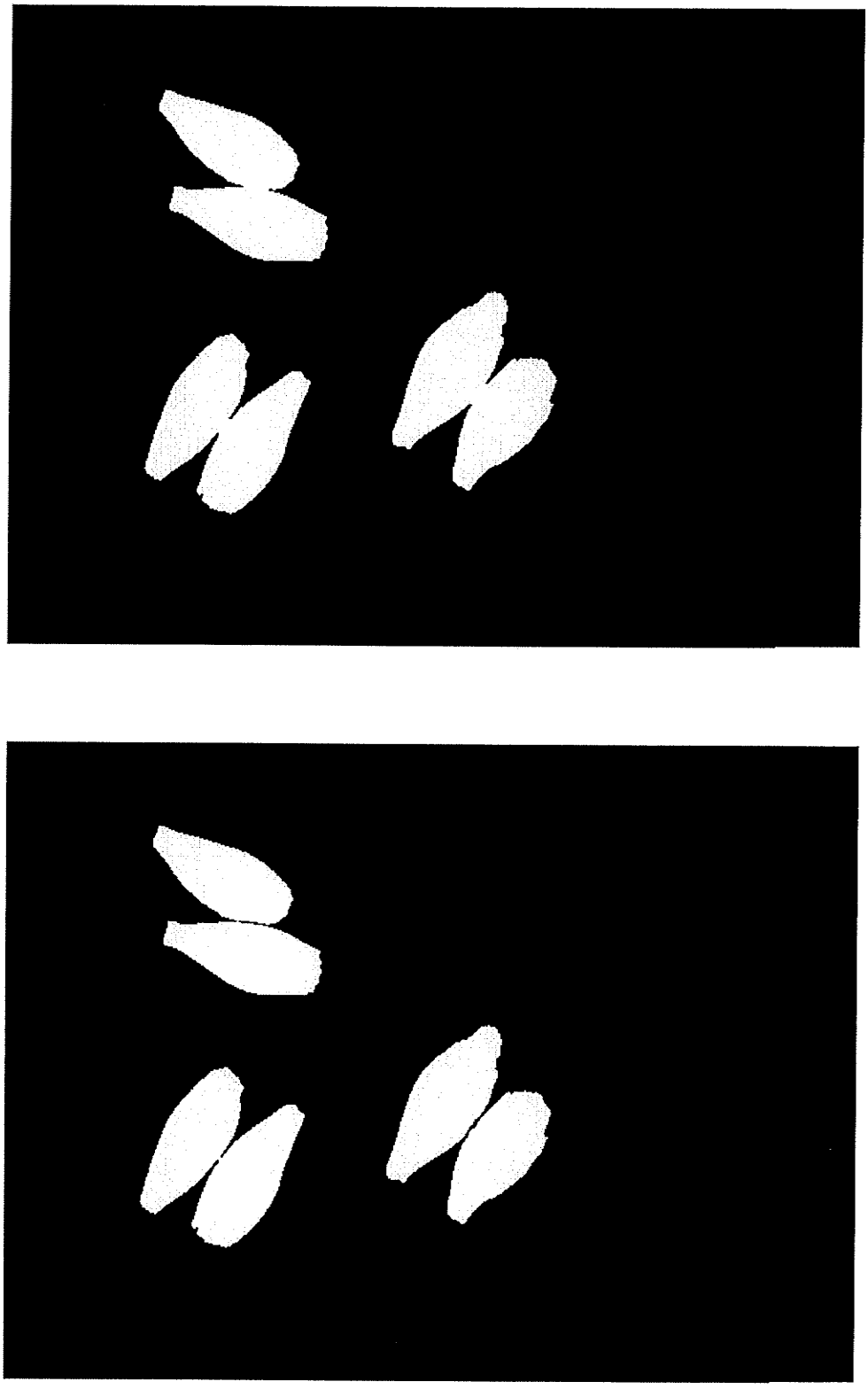

Figure A10. Example of (top) touching and (bottom) separated kernels of barley

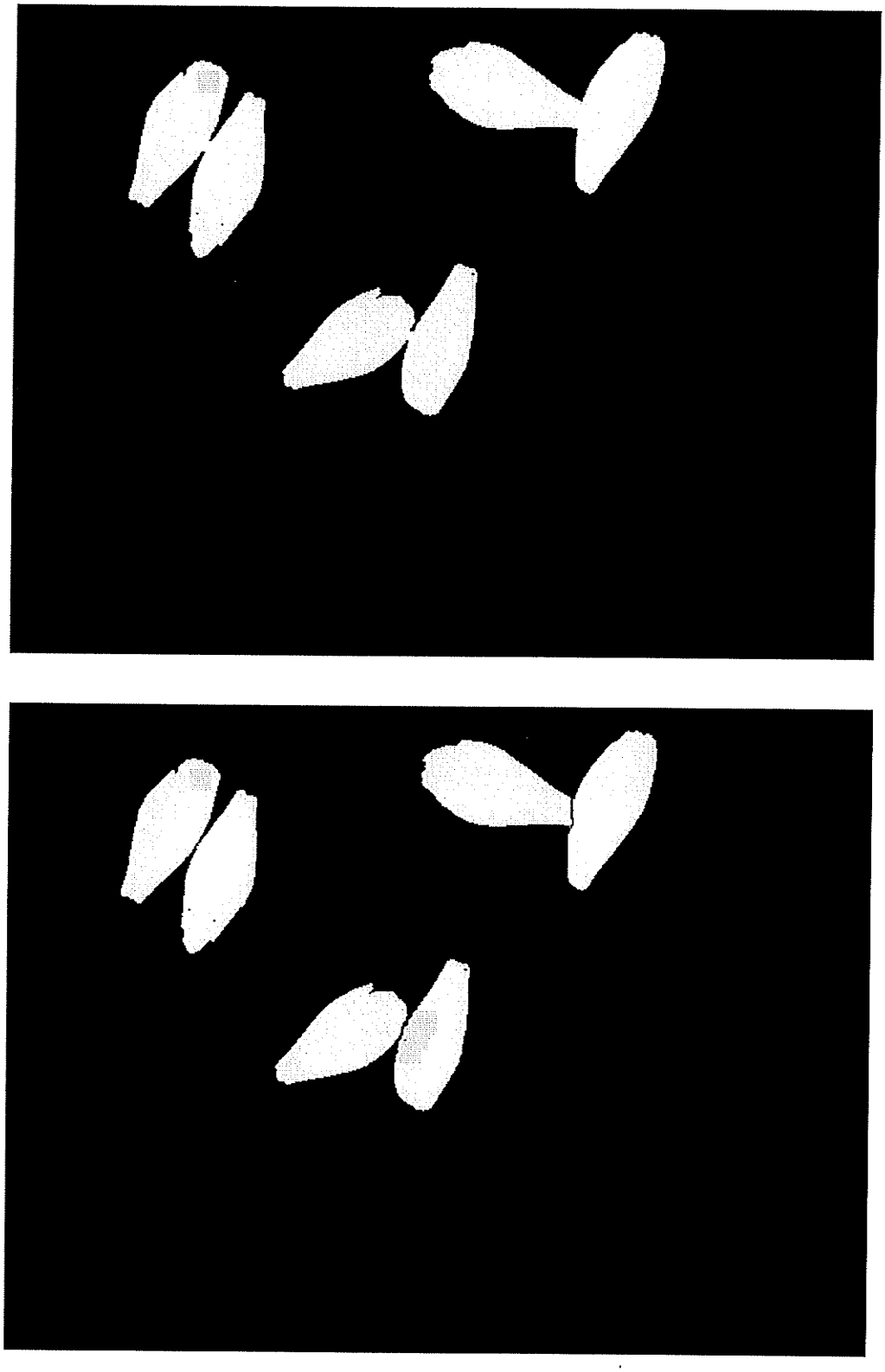

Figure A11. Example of (top) touching and (bottom) separated kernels of barley

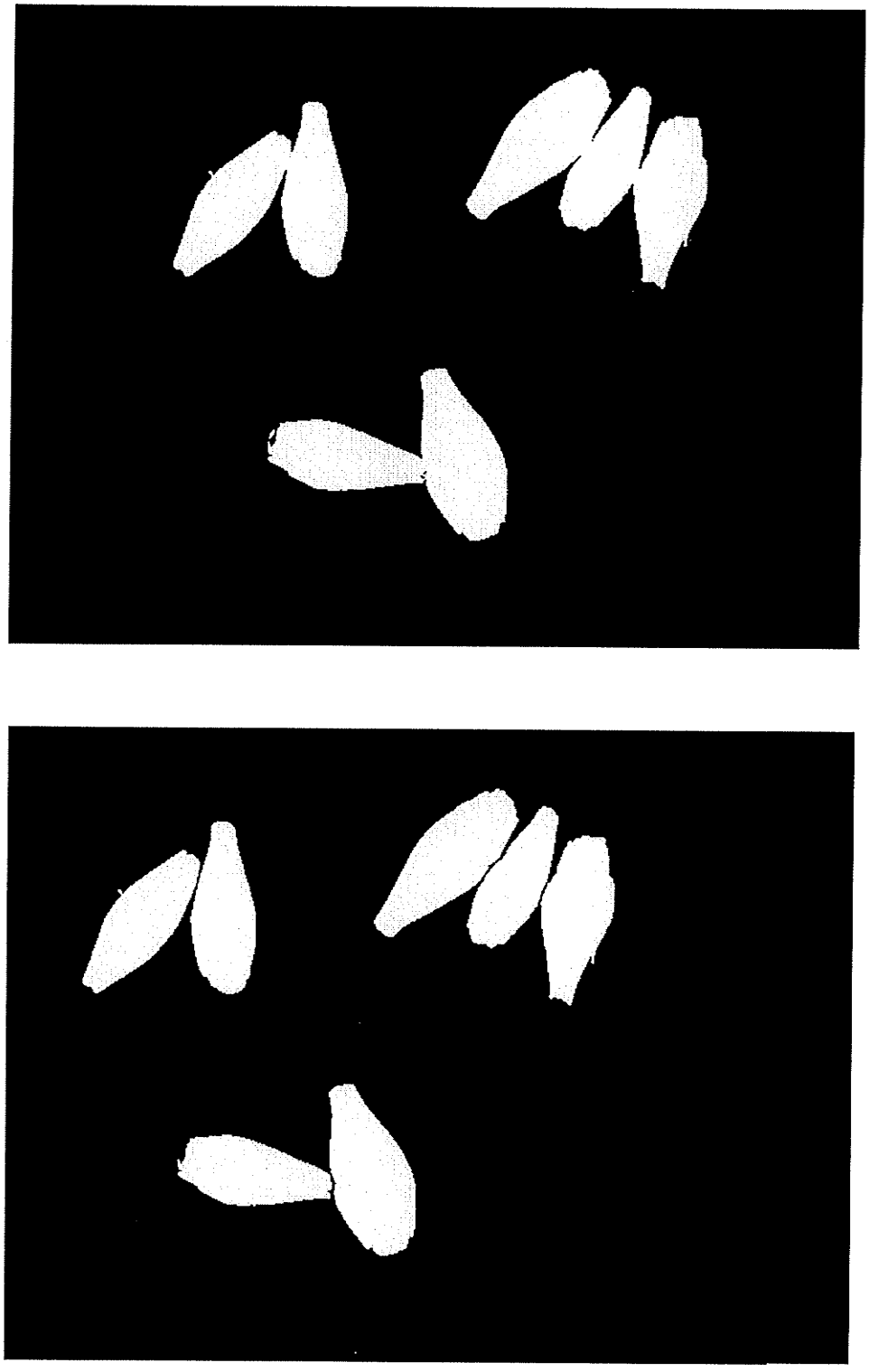

Figure A12. Example of (top) touching and (bottom) separated kernels of barley

Appendix B
CONFUSION MATRICES FOR GRAIN TYPE CLASSIFICATION WITH A NEURAL NETWORK

Table B1. Confusion matrix for grain type classification with physically separated kernels trial 1

	CWAD	Barley	Oats	CWRS
CWAD (n=1000)	959 (95.9%)	12	3	26
Barley (n=1000)	9	978 (97.8%)	6	7
Oats (n=1000)	8	14	974 (97.4%)	2
CWRS (n=1000)	9	7	3	981 (98.1%)

Table B2. Confusion matrix for grain type classification with physically separated kernels trial 2

	CWAD	Barley	Oats	CWRS
CWAD (n=1000)	952 (95.2%)	19	9	20
Barley (n=1000)	18	966 (96.6%)	5	11
Oats (n=1000)	8	15	977 (97.7%)	0
CWRS (n=1000)	9	7	1	983 (98.3%)

Table B3. Confusion matrix for grain type classification with physically separated kernels trial 3

	CWAD	Barley	Oats	CWRS
CWAD (n=1000)	954 (95.4%)	12	3	31
Barley (n=1000)	9	971 (97.1%)	4	16
Oats (n=1000)	15	12	971 (97.1%)	2
CWRS (n=1000)	6	11	5	978 (97.8%)

Table B4. Confusion matrix for grain type classification with software separated kernels trial 1

	CWAD	Barley	Oats	CWRS
CWAD (n=1000)	943 (94.3%)	16	7	34
Barley (n=1000)	15	966 (96.6%)	7	12
Oats (n=1000)	18	9	969 (96.9%)	4
CWRS (n=1000)	4	9	5	982 (98.2%)

Table B5. Confusion matrix for grain type classification with software separated kernels trial 2

	CWAD	Barley	Oats	CWRS
CWAD (n=1000)	948 (94.8%)	20	11	21
Barley (n=1000)	9	969 (96.9%)	11	11
Oats (n=1000)	10	12	975 (97.5%)	3
CWRS (n=1000)	16	6	3	975 (97.5%)

Table a6. Confusion matrix for grain type classification with software separated kernels trial 3

	CWAD	Barley	Oats	CWRS
CWAD (n=1000)	949 (94.9%)	15	6	30
Barley (n=1000)	16	969 (97.4%)	12	3
Oats (n=1000)	14	10	975 (97.2%)	1
CWRS (n=1000)	15	8	2	975 (97.3%)